Humans with inherited T cell CD28 deficiency are susceptible to skin papillomaviruses but are otherwise healthy

Vivien Béziat, Franck Rapaport, Jiafen Hu, Matthias Titeux, Mathilde Bonnet Des Claustres, Mathieu Bourgey, Heather Griffin, Élise Bandet, Cindy Ma, Roya Sherkat, et al.

HHS Public Access

Author manuscript

Cell. Author manuscript; available in PMC 2022 July 08.

Published in final edited form as:

Cell. 2021 July 08; 184(14): 3812–3828.e30. doi:10.1016/j.cell.2021.06.004.

Humans with inherited T cell CD28 deficiency are susceptible to skin papillomaviruses but are otherwise healthy

A full list of authors and affiliations appears at the end of the article.

SUMMARY

We study a patient with the human papilloma virus (HPV)-2-driven "tree-man" phenotype and two relatives with unusually severe HPV4-driven warts. The giant horns form an HPV-2-driven multifocal benign epithelial tumor overexpressing viral oncogenes in the epidermis basal layer. The patients are unexpectedly homozygous for a private *CD28* variant. They have no detectable CD28 on their T cells, with the exception of a small contingent of revertant memory $CD4^+$ T cells. T cell development is barely affected, and T cells respond to CD3 and CD2, but not CD28, costimulation. Although the patients do not display HPV-2- and HPV-4-reactive $CD4^+$ T cells *in vitro*, they make antibodies specific for both viruses *in vivo*. CD28-deficient mice are susceptible to cutaneous infections with the mouse papillomavirus MmuPV1. The control of HPV-2 and HPV-4 in keratinocytes is dependent on the T cell CD28 co-activation pathway. Surprisingly, human CD28-dependent T cell responses are largely redundant for protective immunity.

In brief

By studying a family of individuals with cutaneous protrusions and severe warts driven by human papilloma virus (HPV) infection, Beziat et al. discover that human CD28 is largely dispensable for protective immunity against most infections. Inherited CD28 deficiency only slightly impairs T cell development and function, but control of HPV in keratinocytes is dependent on the T cell CD28 co-activation pathway.

Graphical Abstract

*Correspondence vivien.beziat@inserm.fr (V.B.), casanova@rockefeller.edu (J.-L.C.).

AUTHOR CONTRIBUTIONS

V.B., M.S., and J.-L.C. designed the study and wrote the manuscript. V.B., M.T., M.B.d.C., H.G., E.B., C.S.M., O.D., T.F., G.R., N.B., M.R., R.Y., M.A., F.A.A., M. Momenilandi, J.N., S.B., M. Materna, L.M., N.V., and L.L. performed the experiments. J.H., J.L., D.S., K.B., T.A., and N.C. contributed to mouse experiments. F.R., M. Bourgey, D.M.L., R.S., H.R.-Z., M.C.-A., T.H., A.G., T.K., F.A., S.D., M.Z., and D.L. conducted genome, exome, linkage, RNA-seq, Vir-Scan, and statistical analyses. C.R., M.A.-A., M.L.-V., D.G., C.S., H.V., L.Y., A.H.S., J.U., E.C., S.S.N., D.T.W., M.J., J.R., M. Bayat, F.L., O.L., J.-L.P., S.F., N.M., T.W., and A.H. provided material from the patients and conducted clinical explorations. O.L., F.Z., P.G., G.O., L.A., S.F., M.M.D., L.D.N., N.M., T.W., D.L., J.D., A.H., E.J., S.G.T., and X.B. provided expertise and feedback. J.L.C. secured funding. All the authors critically reviewed the manuscript.

DECLARATION OF INTERESTS

L.D.N. receives compensation as Chief Editor of Frontiers in Immunology. T.W. serves on advisory boards for MSD (Merck Sharp and Dohme). J.-L.C. serves on the scientific advisory boards of ADMA Biologics Inc., Kymera Therapeutics, and Elixiron Immunotherapeutics. All other authors declare no competing interests.

SUPPLEMENTAL INFORMATION

Supplemental information can be found online at https://doi.org/10.1016/j.cell.2021.06.004.

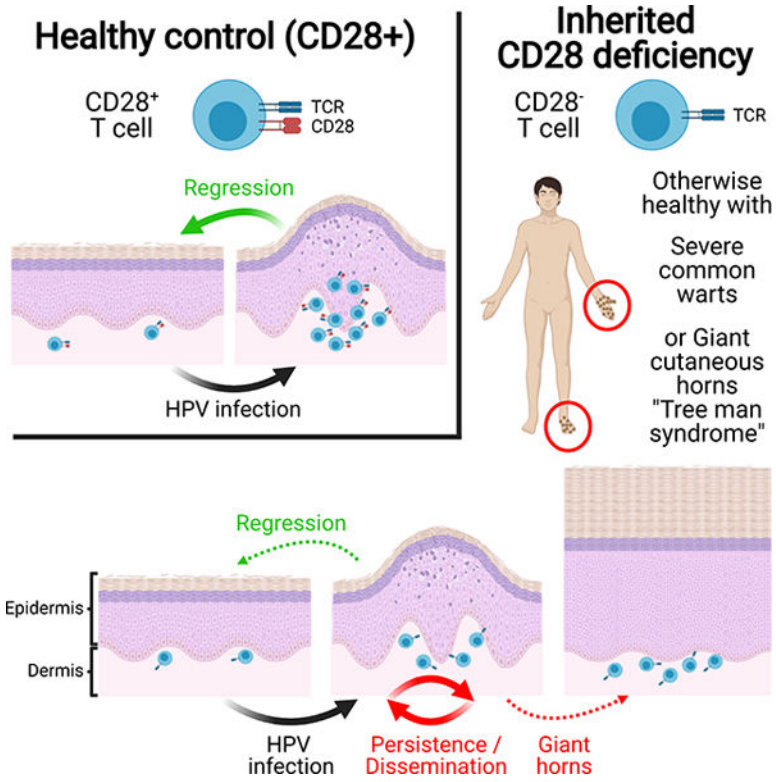

INTRODUCTION

Human papillomavirus (HPV) infections of cutaneous keratinocytes cause various types of lesions, including flat and common warts (Cubie, 2013). Common warts are typically caused by α-papillomavirus HPV-2 and γ-papillomavirus HPV-4. They are seen in the general population, in which they are typically localized and benign (Cubie, 2013). However, they can persist and spread in patients with various inherited or acquired T cell immunodeficiencies, who are also prone to a number of other infections (Béziat, 2020). “Cutaneous horns” are protrusions of keratotic material of various sizes and shapes that may arise from single common warts (Mantese et al., 2010; Yu et al., 1991). These “cutaneous horns” are often both giant and disseminated. This generalized severe hyperkeratotic cutaneous papillomatosis has been named “tree man syndrome” (TMS) (Alisjahbana et al., 2010; Uddin et al., 2018; Wang et al., 2007b). Only four unrelated TMS cases have been reported, and the α-papillomavirus HPV-2, a classic cause of common warts (Orth et al., 1977), was demonstrated to be the cause of three of these cases (Alisjahbana et al., 2010; Uddin et al., 2018; Wang et al., 2007b). These viruses have not been analyzed in depth, and the genomes of the keratinocytes in these lesions were not sequenced. Remarkably, TMS patients have severe skin lesions despite being normally resistant to other infections. TMS should not be confused with epidermodysplasia verruciformis (EV), the cutaneous warts of which are actually flat and caused by β-HPVs (de Jong et al., 2018a). The flat warts of EV often progress to non-melanoma skin cancers. “Typical” or “isolated EV” is due to biallelic null mutations of *TMC6* (encoding EVER1), *TMC8* (encoding EVER2), or *CIB1*, selectively disrupting keratinocyte-intrinsic immunity to these viruses (de Jong et al., 2018b;

Ramoz et al., 2002). Patients with “atypical” or “syndromic EV” display a number of other infections, due to various inborn errors of T cells (de Jong et al., 2018a). Consistently, T cell responses against commensal β-HPVs may protect against skin cancers in the general population (Strickley et al., 2019).

The rarity and lack of contagiousness of TMS are intriguing, given the ubiquitous and benign nature of the underlying HPV-2 infection. By analogy with EV, it is tempting to speculate that TMS may result from inborn errors of immunity to HPV-2. However, by contrast to most EV kindreds, the four reported cases of TMS were sporadic, as opposed to familial, and parental consanguinity was not reported (Alisjahbana et al., 2010; Uddin et al., 2018; Wang et al., 2007b). Nevertheless, TMS lesions are strikingly reminiscent of those caused by natural infection with Shope virus, the cottontail rabbit papillomavirus (CRPV), in wild rabbits (Breitburd et al., 1997; Giri et al., 1985). In 1933, Richard E. Shope showed that some cottontail rabbits from the US Midwest displayed giant horns caused by a filterable virus (Shope and Hurst, 1933). Peyton Rous performed experimental infections in 1934 and showed that warts resolved in less than 10% of wild cottontail rabbits (between 2–8 weeks after wart appearance), with 65% of rabbits displaying persistent warts, sometime overlaid by giant horns and 25% going on to develop malignant lesions affecting internal organs within 6–12 months (Rous and Beard, 1934). Remarkably, it was shown in 1991 that, in outbred New Zealand White rabbits, the persistence of skin lesions segregated with MHC class II genes, indicating that these CRPV-driven lesions are genetically controlled and due to inadequate $CD4^+$ T cell immunity (Han et al., 1992). The genetic and immunological basis of these lesions has not been characterized further in wild or domestic rabbits. These observations suggest that human TMS might result from an inherited immunodeficiency. Three of the TMS patients had an apparently normal T cell compartment (Wang et al., 2007a, 2007b; Uddin et al., 2018), but the fourth displayed idiopathic $CD4^+$ T cell lymphopenia (Alisjahbana et al., 2010). We thus hypothesized that TMS might result from inborn errors of immunity to HPV-2, a causal agent of common warts.

RESULTS

A rare homozygous CD28 variant segregates with severe verrucosis in three relatives

We studied a 30-year-old Iranian patient with TMS (P1) and two of his relatives with a history of disseminated common warts (P2 and P3, aged 40 and 12 years, respectively; see case reports in the STAR Methods) (Figures 1A and 1B). A detailed clinical description is provided in the STAR Methods. We performed single-nucleotide polymorphism (SNP) array-based genome-wide linkage (GWL) analysis on the three patients and 13 relatives, testing the hypothesis of an autosomal recessive (AR) trait with complete penetrance. Highly significant evidence of linkage was obtained for a single 20.5 Mb region on chromosome 2 (LOD score = 5.12) (Figure 1C). The high percentage of homozygosity in P1 (6%), P2 (5%), and P3 (10%) on microarray analysis confirmed the consanguinity of their parents (Figures 1A and S1A). We also analyzed whole-exome sequencing (WES) results for P1, P2, and P3 (Figure S1B). None of the known genes underlying Mendelian disorders carried heterozygous or homozygous rare non-synonymous or splice variants. Within the linked region, only three protein-coding genes, including *CD28*, displayed nonsynonymous or

splice variants, which were also homozygous and rare (minor allele frequency [MAF] <0.01; Figures S1B and S1C). CD28 is a major costimulatory molecule of T cells that can be engaged by CD80 or CD86 on antigen-presenting cells (Rudd et al., 2009). The private variant of *CD28* in this kindred affects the last nucleotide of exon 1 (*c.52G>A*). It is predicted to replace codon 18, encoding the glycine residue in the last position of the signal peptide, with a codon encoding arginine (p.Gly18Arg) (Figure 1D). Moreover, the c.52G>A variant is computationally predicted to disrupt the donor site for splicing located between exons 1 and 2 (Desmet et al., 2009). The c.52G>A variant has a CADD score of 13.8, above the MSC of 9.2 (Figure 1E) (Kircher et al., 2014; Itan et al., 2016). The segregation of this mutant allele is consistent with a fully penetrant AR trait (Figure 1A). Moreover, there are only five homozygous missense *CD28* variants, all with a MAF >0.00002, in public databases (gnomAD, TOPMed, ATAVDB, GME) (Figure 1E). The other two homozygous variants were predicted (KANSL1L) or shown to be neutral (USP37) (Figures S1D–S1H). Moreover, we showed $CD28^{-/-}$ mice to be vulnerable to MmuPV1 (Figure S2). Collectively, these findings suggest that AR CD28 deficiency is exceedingly rare in the general population and disease-causing in this kindred.

The c.52G>A variant greatly decreases CD28 mRNA levels in T lymphocytes

Human CD28 is a transmembrane protein expressed on the surface of T cells (Esensten et al., 2016). We investigated the impact of the c.52G>A variant on endogenous *CD28* mRNA levels, by performing reverse transcription PCR and reverse transcription qPCR on *ex vivo* PHA-expanded primary T cells. Reverse transcription qPCR with two different probes showed that *CD28* mRNA levels were 150- to 200-fold lower in PHA-driven T cell blasts from the patients than in those of the controls, whereas the levels in heterozygous cells were half those in control cells (Figure 1F). Reverse transcription PCR detected products of similar molecular weight (MW) in controls, heterozygotes, and patients (Figure S3A). The full-length product was detected in much smaller amounts by reverse transcription PCR in the patients' cells than in cells from all other individuals tested (Figure S3A). We showed, by TA cloning of the reverse transcription PCR products from a control and P1, that all mRNAs in control T cells used the canonical splicing donor site of exon 1 (Figure 1G). Only 79% of CD28 transcripts in P1's T cells used the canonical mRNA splicing donor site of exon 1 containing the missense nucleotide substitution (p.Gly18Arg) (Figure 1G). The remaining 21% of the transcripts used alternative donor splice sites corresponding to a truncated and frameshift transcript (referred to hereafter as p.Val16fs) or a transcript retaining the first nine nucleotides of intron 1 (referred to hereafter as I1-Ret). Both aberrant transcripts have a premature stop codon upstream of the segment encoding the transmembrane domain. The same aberrant splice transcripts were obtained by exon trapping (Figures S3B and S3C). These data demonstrate that the c.52G>A variant strongly decreases *CD28* mRNA levels in the primary T cells of patients, probably by nonsense-mediated decay of the two aberrant transcripts, p.Val16fs and I1-Ret.

Characterization of CD28 splice variants resulting from the c.52G>A variant

We investigated whether the novel transcripts resulting from the c.52G>A variant encoded functional CD28 isoforms. We transfected HEK293T cells with pcDNA-V3.1 expression vectors containing *CD28* cDNAs encoding the wild-type (WT), p.Gly18Arg, p.Val16fs, and

I1-Ret isoforms fused to a C-terminal V5 tag. Western blotting with an anti-V5 tag monoclonal antibody (mAb) revealed the presence of the WT and p.Gly18Arg isoforms at the expected MW (~40 kDa) (Figure 1H). No p.Val16fs or I1-Ret proteins were detected, suggesting that the translation of CD28 was not reinitiated downstream of the premature stop codons. The p.Gly18Arg mutant isoform, in which the last amino acid of the CD28 signal peptide is affected (Figure 1D), was predicted to result in a relocation of the signal peptide cleavage site without impairment of protein trafficking to the cell surface (Figure S3D). We transfected HEK293T cells with the WT, p.Gly18Arg, p.Val16fs, and I1-Ret cDNAs and monitored the extracellular expression of CD28 by flow cytometry (Figure 1I). The WT and p.Gly18Arg isoforms of CD28 were normally expressed on the cell surface, whereas the p.Val16fs and I1-Ret isoforms were not detected. Despite normal expression of p.Gly18Arg on the cell surface, the alteration to the signal peptide cleavage site may have affected the primary structure of the protein at the cell surface, and, ultimately, its function. We used a lentiviral vector to transduce Jurkat T cells, which lack CD28 expression, stably with the WT and p.Gly18Arg CD28 isoforms, to determine whether p.Gly18Arg retained the ability to induce nuclear factor κB (NF-κB) signaling upon binding to an anti-CD28 mAb (Figures 1J and S3E) (Rudd et al., 2009). CD28-mediated phosphorylation of p65 (p-p65) was observed with this variant. Stimulation with PMA was used as a positive control. These findings suggested that the homozygous *CD28* c.52G>A allele generates extremely low levels (<1% normal levels) of functional p.Gly18Arg proteins in the patients' T cells because the aberrant transcripts (p.Val16fs and I1-Ret) are degraded and their protein products are not detected.

The c.52G>A variant is loss-of-expression and loss-of-function in T lymphocytes

We assessed the expression and function of CD28, by flow cytometry, on primary $CD4^+$ and $CD8^+$ T cell populations, expanded by PHA *ex vivo* (Figure 2A). No CD28 expression was detected on PHA-driven T cell blasts from the three CD28-deficient patients, and CD28 levels on heterozygous T cells were 50% lower than those in controls. We tested the functional consequences of the lack of detection of CD28. We crosslinked CD28 and/or CD3 with specific mAbs and monitored NF-κB p65 phosphorylation (p-p65) after 30 min, with PMA stimulation used as a positive control (Figure 2B). PMA stimulation induced high levels of p-p65 in $CD4^+$ and $CD8^+$ T cells from the patients, heterozygotes, and controls. CD3 stimulation alone weakly induced the production of p-p65 in both T cell subsets in all individuals. In the heterozygotes and healthy controls, stimulation via CD28 alone induced strong p65 phosphorylation in $CD4^+$ T cells, and CD3/CD28 costimulation induced strong p65 phosphorylation in $CD8^+$ T cells (Figure 2B). The patients' $CD4^+$ and $CD8^+$ T cells displayed no detectable p65 phosphorylation following CD28 stimulation alone, and no increase in p65 phosphorylation following CD3/CD28 costimulation, relative to CD3 stimulation alone (Figure 2B). We used a lentiviral vector to express the WT *CD28* cDNA in T cells PHA blasts from P1. This rescued p65 phosphorylation in $CD4^+$ T cells upon CD28 crosslinking, and in $CD8^+$ T cells upon CD3/CD28 crosslinking (Figure 2C). Even though the c.52G>A allele generates very low levels of a *CD28* mRNA potentially encoding a functional p.Gly18Arg isoform, it is a loss-of-expression and loss-of-function allele in the homozygous primary T cells of the patients, which display complete CD28 deficiency.

CD28-dependent responses are abolished in the patients' T lymphocytes

We used RNA sequencing (RNA-seq) to analyze the induction of CD28 target genes. We sorted $CD4^+$ naive T cells from P1 and four healthy controls, and stimulated them with PMA or anti-CD2, anti-CD3, anti-CD28, anti-CD3 plus anti-CD2, or anti-CD3 plus anti-CD28 mAb-coated beads for 2 h before the extraction and sequencing of mRNA. We first compared the different stimulations with the unstimulated baseline. The patient's cells responded normally to CD3, CD3 and CD2 costimulation, and to stimulation with PMA (Figure S4A). The stimulation of CD2 or CD28 alone induced only a few genes in T cells from healthy controls relative to unstimulated cells (Figure S4A) (Riley et al., 2002). The weak response to CD28 stimulation alone was abolished in the patient. CD3 and CD28 costimulation in the patient's naive $CD4^+$ T cells was impaired relative to that in controls (Figure S4A). CD28 stimulation essentially amplifies CD3 responses (Riley et al., 2002). We compared the costimulation of CD3 and CD2, or of CD3 and CD28, with that of CD3 alone (Figure 2D; Table S1). We found that the response to CD3 and CD2 costimulation was similar in the patient and controls, while that to CD3 and CD28 costimulation was abolished in the patient. Levels of mRNA for *IL2*, a prototypic CD28 target gene (Esensten et al., 2016), displayed an induction of ~24-fold relative to CD3 stimulation alone in control cells, but not in the patient's cells, after CD3 and CD28 costimulation. We assessed the induction of the interferon (IFN)-γ, tumor necrosis factor (TNF), and interleukin (IL)-2 proteins in resting primary memory $CD4^+$ T cells, following stimulation with a combination of anti-CD3 and anti-CD28 mAbs (Figure 2E). The costimulation of CD3 and CD28 induced a greater increase in TNF and IL-2 levels, but not IFN-γ levels, than CD3 stimulation alone, in heterozygotes and controls. In $CD4^+$ memory T cells from the patients, costimulation with CD3 and CD28 did not increase the production of either cytokine. PMA plus ionomycin, used as a control, induced the production of high levels of all the cytokines tested in controls, heterozygotes, and patients. Costimulation with CD28 plus CD3 strongly increased the proliferation of control $CD4^+$ and $CD8^+$ T cells relative to CD3 stimulation alone (Figured 2F and 2G). CD28 costimulation failed to increase the CD3-mediated proliferation of the patients' $CD4^+$ and $CD8^+$ T cells. CD2 costimulation, used as a control, increased CD3-mediated proliferation similarly in $CD4^+$ and $CD8^+$ T cells from patients and controls. Consistent with the proximal signaling impairment downstream of CD28, more distal CD28-dependent responses were thus abolished in the patients' T lymphocytes.

CD28 loss has a modest impact on the homeostasis of leukocyte subsets

The global distribution of leukocyte subsets in peripheral blood was normal in the three patients (Table S2). Within the myeloid compartment, the monocyte (P1–P3) and dendritic cell (P1) subsets were normal (Figures S4B and S4C). Within the lymphoid compartment, B cell subset counts and frequencies were normal, and we detected near-normal frequencies of total and class-switched memory B cells in the patients (Figures S4D and S4E; Table S2). Natural killer (NK) cell counts were low (Table S2), but the frequencies of the immature $CD56^{bright}$ and mature $CD56^{dim}$ NK subsets were normal, with the possible exception of an unusually large proportion of $NKG2C^+$ cells, a population previously shown to expand upon CMV infection (Figures S4F–S4H) (Béziat et al., 2013). $CD8^+$ T counts were high in P1 and P3, and $CD4^+$ T cell count was high only in P3 (Table S2). The frequency of naive $CD4^+$ T cells was high, and the frequencies of central memory $CD4^+$ and $CD8^+$ T cells were low

(Figures 3A and 3B). The proliferation of T cells from P1 was normal in response to anti-CD3 antibody or PHA stimulation, weak upon tuberculin stimulation, and absent upon tetanus toxin stimulation (in the absence of a booster dose of vaccine since infancy) (Table S2). Within $CD3^+$ T cells, the frequencies of iNKT and γδ T cells were normal, whereas that of MAIT cells was low in all patients (at levels similar to that in heterozygotes) (Figure 3C). Within $CD4^+$ T cells, regulatory T (Treg) cell frequency was ~70% lower than the mean value for controls (Figure 3D), consistent with CD28 requirement and redundancy in mice for natural and induced Treg development and homeostasis, respectively (Salomon et al., 2000; Semple et al., 2011; Tai et al., 2005; Tang et al., 2003). The frequencies of Th subsets (Th1, Th2, Th1*, Th17, and Tfh) were normal (Figure 3E). We then performed single-cell RNA sequencing (scRNA-seq) on peripheral blood mononuclear cells (PBMCs) from three controls and the three patients (Figures 3F–3H and S5A). This analysis confirmed the largely normal distribution of lymphocyte subsets. It did not identify major transcriptomic abnormalities in T cell subsets, including naive and memory T cells, Tregs, and γδ T cells, other than extremely low levels of CD28 mRNA in all T cell compartments tested (Figure S5B). The TCR-Vα and Vβ repertoires of the patients' $CD28^-$ $CD4^+$ T cells displayed normal diversity (Data S1). The induction of costimulatory (OX40, CD40L, and ICOS) and coinhibitory molecules (CTLA4, PD1, Tigit, BTLA, Tim3, and LAG3), as well as CD25 and ICAM1, upon stimulation with PMA plus ionomycin was normal in patients' $CD4^+$ and $CD8^+$ T cells (Figure S6A; Data S1). The induction of OX40, CD40L, ICOS, Tim3, LAG3, CD25, and ICAM1 upon costimulation with CD2/CD3/CD28 mAb-coated beads was partially impaired in the patients, whereas that of CTLA4, PD1, Tigit, and BTLA was normal. The patients displayed no clinical signs of autoimmunity or autoinflammation. Low levels of EBV (P1, P2, and P3) and HCMV (P1-P2) replication were detected in the patients' blood, without clinical manifestations (Table S2). We detected IFN-γ^+ $CD4^+$ and $CD8^+$ T cells in P1 and P2 upon stimulation with overlapping HCMV peptides *in vitro* (Figure S6B) and IFN-γ^+ $CD4^+$ T cells in all BCG-vaccinated patients following stimulation with tuberculin (PPD) *in vitro*. Thus, the distribution and function of the various leukocyte subsets were normal or subnormal in the three patients, probably accounting for the lack of infectious phenotypes other than severe verrucosis, and, more generally, the lack of other overt immunopathological phenotypes.

Evidence of somatic mosaicism in $CD4^+$ memory T cells

We then analyzed CD28 expression in the various T cell subsets from the patients. Consistent with our findings for bulk $CD4^+$ and $CD8^+$ T cells (Figure 2A), we detected no CD28 expression on circulating naive $CD4^+$ and $CD8^+$ T cells or on memory $CD8^+$ T cells from the three patients, by flow cytometry (Figure 4A). Surprisingly, we found that 0.8%, 2.1%, and 2.9% of the memory $CD4^+$ T cells of P3 (aged 12 years), P1 (30 years), and P2 (40 years), respectively, expressed CD28, with fluorescence levels similar to those for heterozygotes, but lower than those for controls (Figure 4A). This suggested the possible reversion of one *CD28* allele in the progenitors of these patients' T cells and, possibly, the expansion of the revertant pool with age. The sorting of $CD28^+$ T cells from all three patients confirmed a reversion of one *CD28* allele to the WT form, because some cells were heterozygous for the c.52G>A variant, whereas $CD28^-$ cells were homozygous (Figures 4B and S7A). We also detected the c.52+5A>G somatic mutation (Figure 4B), which, as

predicted (Figure S7B) and confirmed by exon trapping (Figures S3B and S3C), restored normal splicing despite the presence of the original c.52G>A variant. We showed that the revertant cells were autologous, and not maternally derived, by genotyping the rare variant of *USP37* (Figures 4B and S7A). We sorted $CD4^+$ $CD28^+$ revertants from P1, P2, and P3 and found their TCR-Vα and -Vβ repertoires to be highly diverse, suggesting that the reversions occurred before T cell Vβ rearrangement in the thymus (Data S1). We also analyzed the identified TCR-Vβ sequences using the GLIPH software that clusters TCRs predicted to bind the same MHC-restricted antigenic peptide (Glanville et al., 2017). This predicted that almost all TCR-Vβ from the revertant cells share specificity with CD28-deficient $CD4^+$ cells. The vast majority of MHC-restricted peptides recognized by the $CD28^+$ revertants are also probably recognized by the patients' $CD28^-$ $CD4^+$ cells. An analysis of >12 million PBMCs from P3 showed that 0.00034% of $CD31^+CD4^+$ T cells, which are known to be recent thymic emigrants (RTEs), expressed CD28 (Figure 4C). This implies an ~1,500-fold expansion of revertant cells between RTEs and memory $CD4^+$ T cells. The revertant memory $CD4^+$ T cells were phenotypically diverse, with Treg and Th $CD4^+$ subsets present in proportions close to those observed in the $CD28^-$ compartment (Figures 4D and 4E). We then performed cellular indexing of transcriptomes and epitopes by sequencing (CITE-seq) on sorted memory $CD4^+$ T cells from one control, P1, and P2 (Figures 4F–4H, S7C, and S7D). Using stringent filtering criteria, we identified a total of 38 $CD28^+$ revertant cells from P1 or P2. Using uniform manifold approximation and projection (UMAP) for dimensions reduction, we found that the $CD28^+$ revertants and the $CD28^-$ non-revertants from the two patients were scattered all over controls' $CD4^+$ memory T cells (Figures 4G, S7C, and S7D). In line with our scRNA-seq on total PBMCs (Figure S5), this confirms that the transcriptome of patients' $CD4^+CD28^-$ non-revertant memory T cells is not significantly different from that of controls' $CD4^+$ memory cells. This also shows that the transcriptome of the $CD28^+$ revertants is not significantly biased toward a specific cluster or subset of memory $CD4^+$ T cells. The only mRNA that was significantly different between patients' $CD28^+$ revertants and $CD28^-$ memory $CD4^+$ T cells was CD28 mRNA level itself, which was, as expected, highly significantly increased in the former (Figure 4H). Overall, the revertant T cells were highly enriched in memory $CD4^+$ T cells, a compartment in which they probably increased in frequency with age (their frequency paralleling the age of the three patients). They were highly diverse in terms of their TCR and functional repertoire, and they occurred in the three patients following at least two types of somatic mutation.

CD28 loss results in a moderate impairment of humoral responses, including those against HPVs

CD28-deficient mice produce only small amounts of immunoglobulin G (IgG) antibody (Ab) in response to peptides or viruses and have low serum IgG1 levels (Shahinian et al., 1993). We investigated the humoral responses of the patients. The patients had normal serum Ig classes and IgG subclasses (Table S2), with the exception of slightly high serum IgE levels in P1, who also has food allergy and asthma. Standard immunological assays showed that the patients had detectable Abs against numerous pathogens, including Abs directed against T cell-dependent (e.g., herpesviruses and influenza A) and T cell-independent microbial antigens (pneumococcus and *Haemophilus influenzae* B) in the absence of vaccination (Table S2). We performed VirScan (Figure 5A). We compared the three CD28-

deficient patients with 20 aged-matched healthy controls and found that P1, P2, and P3 had been infected with at least 9, 6, and 7 common viruses, respectively. VirScan is a powerful tool for providing an overall picture of the virome encountered by a subject, but its resolution remains limited for infections due to some common viruses, in particular specific HPV subtypes (Isnard et al., 2019; Xu et al., 2015). In this analysis, none of the patients or controls satisfied the stringent positivity cutoff for HPV-2 and HPV-4 used, despite the reported prevalence of 5%–15% and 20%–50%, respectively, for these viruses in the general population (Antonsson et al., 2010; Waterboer et al., 2009). We performed a Luminex assay detecting antibodies against 38 different HPV L1 virus-like particles, including HPV-2, HPV-4, and all HPVs present in the nonavalent HPV vaccine Gardasil (HPV-6, HPV-11, HPV-16, HPV-18, HPV-31, HPV-33, HPV-45, HPV-52, and HPV-58) (Figures 5B and 5C). We found that P1 was seropositive for HPV-2, HPV-6, HPV-11, HPV-36, HPV-50, HPV-58, HPV-92, HPV-96, and HPV-101; P2 was seropositive for HPV-1 and HPV-4; and P3 was seropositive for HPV-2, HPV-96, and HPV-101. These Ab responses, including those for HPV-2 and HPV-4, remained stable over a period of 14–21 months (Figure 5B). The mother of P1, who lives in the same household, was seropositive for HPV-1, HPV-4, HPV-6, and HPV-80. These data suggest that the patients were exposed to different HPV subtypes and developed lasting Ab responses. However, the lack of significant anti-HPV-4 antibodies in P3 after several years of recurrent infection suggests a suboptimal anti-HPV Ab response in this patient. The presence of anti-HPV-2 Abs in P3 further suggests that the clinical penetrance of unusually severe HPV-2 disease is not complete in humans with CD28 deficiency, possibly due to the development of an effective T cell response, as demonstrated by wart regression in P2 (see case reports). Finally, we tested the T cell-dependent vaccinal response of patients to the nonavalent HPV vaccine (P1 and P3) and DPT (diphtheria, pertussis, and tetanus; P1, P2, and P3) vaccines (Figure 5C; Table S2). Other than for HPV-6 and HPV-11 in P1, who was already seropositive for these subtypes before vaccination, we detected no response in P1 and only a very weak response in P3. No response to tetanus toxin vaccination was observed in any of the three patients 5 months after recall boost (Table S2). No response, a weak response, and a normal response to diphtheria toxin vaccination were observed in P1, P2, and P3, respectively, 5 months after the recall boost (Table S2). Overall, these data suggest that CD28-deficient patients respond poorly to vaccination, but generate good T cell-dependent and -independent IgG responses to numerous pathogens, including HPVs, in natural conditions, although this Ab response is frequently quantitatively weaker than that in controls. Consistently, the patients do not suffer from any of the many clinical manifestations of patients with inborn errors of B cell and Ab immunity, including recurrent bacterial infections of the respiratory and digestive tracts (Notarangelo et al., 2020).

Anti-HPV $CD4^+$ T cell responses are not detected in the patients

We generated overlapping peptides of E6 from HPV-2 and L1 from HPV-4 for functional assessments of the T cell responses to HPVs developed by patients and controls. We incubated PBMCs from 46 healthy controls, P1, P1's mother, and P2 with overlapping HPV-2, HPV-4, or HCMV peptides for 14 days to induce the expansion of antigen-specific T cells (Bhatt et al., 2020). After 14 days, we stimulated the cells for a further 4 h with the overlapping peptides and then assessed intracellular IL-2, IL-4, IL-17A, IFN-γ, and TNF

levels in $CD4^+$ and $CD8^+$ T cells (Figures 5D and 5E and data not shown). Data were stratified on the basis of seropositivity for the three viruses. We detected no IL-2, IL-4, and IL-17A in the controls or patients in response to HPV peptides (data not shown). In response to overlapping peptides from HCMV, we observed high levels of TNF and IFN-γ production in $CD8^+$ T cells, and, to lesser extent, in $CD4^+$ T cells from controls and patients. The anti-HCMV response was correlated with positive results in serological tests for HCMV. A clear $CD4^+$ T cell response to HPV-2 and HPV-4 peptides was found in 7 and 27 controls, respectively (Figure 5D). No robust $CD8^+$ T cell response was detected in controls or patients for either of the two sets of overlapping peptides for HPV proteins (Figure 5E). A robust anti-HPV-2 $CD4^+$ T cell response in controls was associated with high anti-HPV-2 E6 serum Ab titers. The $CD4^+$ T cell anti-HPV-4 response was not correlated with anti-HPV-4 L1 Ab titers, suggesting either that the observed anti-L1-HPV-4 T cell response is not entirely specific for HPV-4, possibly due to cross-reaction with different HPV types, or the serological assay is not sensitive enough to detect all individuals infected with HPV-4. Neither P1 nor P2 presented robust T cell responses to E6-HPV-2 or L1-HPV-4 peptides. P1's mother, who lives in P1's household and was seropositive for HPV-4 but seronegative for HPV-2, presented a strong response to L1-HPV-4 peptides. These data show that anti-HPV T cell responses are detectable only in $CD4^+$ T cells in these experimental conditions. They also suggest that, despite prolonged exposure, P1 and P2 did not mount robust T cell responses to HPV-2 or HPV-4, by contrast to P1's mother, whose cells expressed CD28. This absence of a detectable T cell response to HPV-2 and HPV-4 is consistent with the verrucosis in these patients and may have contributed to their development.

Infected keratinocytes do not express CD28 ligands

We assessed the expression of CD28, CD80, and CD86 in skin biopsy specimens from the patients. We detected $CD28^+$ T cells in the dermis below the lesion in control warts. We found that the lymphocytic infiltrate in the dermis below the lesions in the three patients displayed no CD28 expression on immunohistochemistry (Data S1). This suggests that the few revertant memory $CD4^+$ T cells are not specifically recruited to lesions. Consistent with the lack of CD80 and CD86 expression on keratinocytes in healthy skin and cultured keratinocytes (Black et al., 2007; Orlik et al., 2020), we detected no CD80 and CD86 on HPV-infected keratinocytes within the lesions of the patients (Data S1). We detected CD80 expression only in a few $CD207^-$ cells in the dermis. Within the epidermis, we detected only a few $CD86^+$ cells, all co-expressing CD207, a Langerhans cells marker. Most $CD86^+$ cells were within the dermis, below the lesions, and did not co-express CD207, suggesting that CD86 was expressed on $CD207^-$ dermal antigen-presenting cells. This analysis suggests that impaired interaction between the rare epidermal T cells and keratinocytes does not underlie HPV-2- and HPV-4-driven lesions in patients with CD28 deficiency. The lesions are more likely to result from impaired interactions between T cells and antigen-presenting cells in the epidermis, dermis, or draining lymph nodes.

The histology of TMS lesions is not typical of viral papillomas

CD28 deficiency explains the susceptibility to HPVs common to these three patients, but it cannot account for their different phenotypes, with TMS in P1 and severe warts in P2 and P3. Because HPV-2 has been detected in all TMS patients tested (Wang et al., 2007b;

Alisjahbana et al., 2010), one plausible explanation is that persistent HPV-2 infection is a prerequisite for the development of TMS. According to this hypothesis, HPV-2 infection in P1 drove the formation of common warts, which subsequently progressed to TMS, whereas HPV-4 infection in P2 and P3 drove the formation of common warts with no potential to develop into TMS. We analyzed the skin lesions of the patients. The warts of P2 and P3 had histological features typical of lesions caused by HPV-4 (Figure 6A; Data S1) (Jablonska et al., 1985); three separate HPV-2^+ cutaneous horns from P1 displayed an unusual viral papilloma structure different from that of a control HPV-2^+ wart (Figure 6A; Data S1). They presented no parakeratosis or vacuolated cells with pyknotic nuclei (koilocytes) (Figure 6A; Data S1). They were not stained with pan-HPV L1 antibody on immunohistochemistry, unlike the lesions of P2, P3, and a control HPV-2^+ common wart (Figure 6A; Data S1). We detected strong E4 and minichromosome maintenance (MCM) staining in the HPV-4^+ lesions of P2 and P3, and in a control HPV-2^+ wart (Data S1). There was no E4 or MCM staining in the lesion of P1, except for a restricted area at the periphery of the lesion (Data S1). Vacuolated cells, expressing L1, MCM, and E4, normally accompany the production of infectious viral particles, suggesting that HPV-2 infection may be non-productive in the lesions of P1. Non-productive infection is reminiscent of cutaneous CRPV infections in rabbit (Breitburd et al., 1997) and cervical intraepithelial neoplasia (CIN) in humans (Doorbar, 2006; Schiffman et al., 2016), although CIN is typically characterized by cytonuclear abnormalities.

HPV-2 is episomal in TMS lesions

We performed whole-genome sequencing (WGS) on two separate skin lesions and blood from each patient (P1, P2, and P3). We detected no copy number variations (duplications or deletions) in the genomic DNA (gDNA) from P1's lesions relative to the blood. We detected 545 and 1,581 somatic substitutions in the two biopsy samples relative to the blood sample (Figure 6B). None of these substitutions was an obvious candidate driver (data not shown). As reported for the somatic mutations detected in the common warts of P2 and P3 (Data S1), only a few mutations were common to the two lesions of P1, suggesting that these lesions did not arise from a common ancestor clone. We obtained 0.5–2.0 million HPV-2 (P1) or HPV-4 (P2 and P3) reads by WGS on the patients' lesions, none of which was detected in the blood (Figure 6C). No other HPVs and no insertion of HPV-2 into the patient's genome were detected. These data suggest that episomal and non-productive HPV-2 drive the benign, multifocal TMS lesions of P1, as for other HPVs in many cases of human cervical intra-epithelial neoplasia (CIN) and squamous cell carcinoma (SCC) (Arias-Pulido et al., 2006; Gray et al., 2010; Vinokurova et al., 2008), and in rabbit CRPV-induced horns (Breitburd et al., 1997). The detection of E4 and MCM staining in the periphery of the lesions of P1 suggests that some areas remain productive, perhaps contributing to the spread of TMS lesions in the patient.

Virological studies reveal viral oncogene overexpression in TMS lesions

We analyzed the viruses found in the lesions in greater detail. The HPV-2 strain of P1 was the same in both lesions tested, and 30 variants relative to the reference sequence were detected, 29 of which were also found in a set of 24 HPV-2 strains from conventional HPV-2^+ common warts (Table S3). The remaining variant (c.1828G>A) was a synonymous

mutation in E1, and was not reported in viruses from two other TMS patients (Wang et al., 2007b). We nevertheless tested the hypothesis that the HPV-2 viral life cycle was abnormal in TMS lesions, by performing RNA-seq on two separate lesions from P1 and comparing the results with RNA-seq results for three separate HPV-2$^+$ common warts from two unrelated donors with severe warts (Figure 6D). We determined the relative abundance of virus transcripts and, consistent with the lack of detection of L1 on immunohistology (Figure 6A), we found that L1 and L2 transcript levels were lower than in the control warts ($p < 10^{-51}$ and $p < 10^{-10}$, respectively). Transcripts for the E6 and E7 oncogenes were present at higher levels ($p < 10^{-4}$ and $p = 10^{-2}$, respectively). Other transcripts assessed (E1, E2, and E5β) were present in similar amounts in the lesions of P1 and control warts. The splicing junctions identified within the HPV-2 mRNA occurred at the same position in the TMS and common wart lesions. Consistent with the very low levels of L1 and L2 transcripts, splicing involving late transcripts were absent or barely detectable (Table S3). We performed *in situ* hybridization, with the staining of HPV-2$^+$ lesions from a control and P1 for the E6/E7 mRNA, to assess the potential spatiotemporal deregulation of viral oncogenes (Figure 6E; Data S1). E6/E7 expression in the control HPV-2$^+$ common wart was maximal in the late epidermis. In the lesions of P1, E6/E7 was strongly overexpressed in the basal and parabasal layers of the epidermis. The peripheral area of the lesion from P1 displaying normal MCM and E4 expression also displayed normal E6/E7 expression in the late epidermis, supporting the notion that some areas of TMS lesions may remain productive. Our data demonstrate that the TMS observed in P1 is a slowly spreading, multifocal, benign epithelial tumor driven by a regular episomal HPV-2 strain lacking late transcripts but overexpressing the E6 and E7 oncogenes in the basal and parabasal epidermis in a context of CD28 deficiency impairing the T cell-mediated clearance of HPV-2-infected keratinocytes.

DISCUSSION

We report AR CD28 deficiency in three patients with isolated susceptibility to cutaneous α- and γ-HPVs. One patient (P1) had giant horns and TMS resulting from long-term HPV-2 infection, whereas the other two had disseminated common warts caused by HPV-4. CD28 has been studied since its initial description, in 1985, as a surface receptor specifically activating T cells upon stimulation with a mAb in the presence of phorbol esters (Hara et al., 1985). The human *CD28* cDNA was isolated in 1987 (Aruffo and Seed, 1987). The first CD28-deficient mouse was produced in 1993, confirming the major costimulatory role of CD28 in TCR signaling (Shahinian et al., 1993). These mice had normal CD4$^+$ and CD8$^+$ T cell numbers, suggesting that CD28 was not required for the development and maintenance of these subsets *in vivo*. T cells from CD28-deficient mice became anergic and proliferated poorly in response to transient stimulation with viral peptide antigens or a virus displaying abortive replication, but repeated antigen stimulation or sustained viral infection bypassed the requirement for CD28 (Kündig et al., 1996). Nevertheless, these mice were found to be vulnerable to multiple pathogens, including *Listeria monocytogenes*, *Salmonella typhimurium*, and *Trypanosoma cruzi* (Martins et al., 2004; Mittrücker et al., 1999, 2001). Here, more than 30 years after the discovery of CD28, we report CD28-deficient humans. Surprisingly, these three patients are highly susceptible to cutaneous HPV-2 and HPV-4, but they are otherwise healthy (Casanova and Abel, 2018). They did not even display other HPV

infections, despite being seropositive for many other HPVs, including HPV-1 and HPV-6, two skin-tropic HPVs driving plantar warts and condyloma (Doorbar et al., 2015). P1 and P2 are adult men aged 30 and 40 years that have been exposed to, and infected with, various microorganisms. It is unknown whether P3, the only adolescent and the only female CD28-deficient patient described here, will be prone to HPV-driven uterine lesions, including CIN, despite vaccination with Gardasil 9, which did not improve her skin lesions or those of P1.

Causality between CD28 deficiency and skin HPV-2 and HPV-4 lesions in the patients was established by genetic, biochemical, and immunological means. It was replicated in CD28-deficient mice, which were susceptible to skin infections with MmuPV1. The selective expansion of CD28-expressing "revertant" memory $CD4^+$ T cells, following at least two reversion events in each of the three patients studied here, attests to the selective advantage conferred by CD28 on this T cell subset. Somatic reversions in patients with inherited T cell disorders can underlie milder clinical presentations (Pillay et al., 2021). The revertants identified in the CD28-deficient patients are unlikely to have made a major contribution to the control of a broad range of infectious agents. Their TCR repertoire is predicted by GLIPH to largely overlap with that of CD28-deficient memory $CD4^+$ T cells. Furthermore, the patients have very few $CD28^+CD4^+$ revertant T cells (1–10 cells/mm^3 of blood). Patients with acquired immunodeficiency syndrome (AIDS) develop multiple, severe, opportunistic infections, including severe skin HPV infections, when their $CD4^+$ T cell levels fall below 200 $CD4^+$ T cells/mm^3 of blood (Deeks et al., 2015). These findings strongly suggest that human CD28 is largely redundant for host defense (Casanova and Abel, 2018). The many infections of patients with CARMIL2 deficiency (Wang et al., 2016; Schober et al., 2017), whose T cells do not respond to CD28 stimulation, suggests that CARMIL2 plays a broader role in immunity.

The TMS phenotype in P1 manifested after a decade of HPV-2-driven disseminated common warts. All TMS lesions in this and other patients tested were positive for HPV-2, suggesting that common warts induced by this virus have a unique potential to progress to TMS lesions (Wang et al., 2007b; Alisjahbana et al., 2010). We also found that E6 and E7, two potent oncogenes, were overexpressed in a lesion from P1. This phenotype is reminiscent of high-grade cervical lesions and cancers (Schiffman et al., 2016). This deregulation could not be explained by viral integration into the patient's genome, or mutations of the HPV-2 episomal genome. For instance, the 63T>A variant in the upstream regulatory region (URR), which was previously described in another TMS patient and associated with promoter activity three times stronger than that of the reference promoter (Lei et al., 2007), is present in 81% of the "normal" common warts tested. Only one variant identified in the HPV-2 present in the TMS lesions of P1 was private but it was synonymous and not found in other HPV-2 strains from TMS patients. It is thus unlikely that P1 and other patients with TMS were infected with a specific HPV-2 strain. Surprisingly, E6/E7 overexpression in TMS lesions was restricted to the basal layer of the epidermis. To our knowledge, such a pattern of deregulation has never been reported before and may account for the giant cutaneous horns in the patients. The event driving this deregulation remains unclear but may involve modifier genes in P1 not present in patients with other inborn errors underlying severe HPV-2^+ warts without giant horns. However, TMS lesions usually appear in early adulthood, after several years of persistent infection leading to "normal" common warts. The hypothesis of modifier genes

thus seems unlikely, and we detected no candidate modifier genes in our patient. The TMS phenotype may, thus, result from the AR CD28 deficiency itself. The initial persistence of warts preceding TMS probably requires a specific T cell defect, of CD28 in P1, but probably other as yet undiscovered inborn errors in other patients (Alisjahbana et al., 2010; Wang et al., 2007b; Uddin et al., 2018).

Finally, our findings provide new insight into the general context of host-PV interaction. They confirm and extend the report of MHC-II-dependence for κ-papillomavirus CRPV-driven warts and tumors in rabbits (Han et al., 1992). Individual rabbits and humans prone to CRPV- and HPV-driven skin warts, respectively, carry genetic variants that weaken adaptive immunity. It would be of interest to determine whether the warts, horns, and tumors that develop in rabbits are dependent on CD28. Generating and testing CD28-deficient rabbits, genetically or with a neutralizing Ab, would answer one of the questions raised by Shope and Rous nearly 100 years ago. In humans, AR EVER1, EVER2, and CIB1 deficiencies underlie isolated EV, which is characterized by flat warts and non-melanoma skin cancer caused by β-HPVs in otherwise healthy individuals (de Jong et al., 2018b; Ramoz et al., 2002), through the disruption of keratinocyte-intrinsic immunity to β-HPVs. By contrast, inborn errors of T cells cause atypical forms of EV (de Jong et al., 2018a). The affected patients are not selectively prone to EV and display a number of other infectious diseases. Their T cell deficits do not impair the CD28 response pathway. There are also many other inherited T cell deficits that underlie severe common warts (Béziat, 2020). These two groups overlap, with some patients having both flat and common warts. It is intriguing that AR CD28 deficiency underlies a selective susceptibility to common warts caused by α- and γ-HPVs in otherwise healthy individuals, through an exclusive and specific impairment of T cell adaptive immunity. The selective susceptibility to α- and γ-HPVs of CD28-deficient patients mirrors the susceptibility to β-HPVs of CIB1-EVER-deficient patients. The cellular basis of these two disorders differs, because CIB1-EVER-dependent keratinocyte-intrinsic immunity to β-HPVs is disrupted in EV patients with disseminated flat warts and skin cancer, whereas CD28-dependent T cell adaptive immunity to α/γ-HPVs is disrupted in patients with disseminated common warts or giant horns.

Limitations of the study

One limitation of our study is that we only studied three relatives living in Iran. Another limitation is that we did not study them from infancy onward.

STAR★METHODS

RESOURCE AVAILABILITY

Lead contact—Further information and requests for resources and reagents should be directed to and will be fulfilled by the Lead Contact, Jean-Laurent Casanova (casanova@mail.rockefeller.edu).

Materials availability—All unique/stable reagents generated in this study are available from the Lead Contact with a completed Materials Transfer Agreement with Inserm or the Rockefeller University.

Data and code availability—The whole-exome sequencing and whole genome sequencing datasets generated during this study are available at the Sequence Read Archive (SRA: PRJNA715377). The scRNA-seq and CITE-seq datasets generated during this study are available at the EGA European Genome-Phenome Archive (EGA: EGAS00001004837). High-throughput sequencing (HTS) of T cell receptor β (TRB) and T cell receptor α (TRA) dataset are available from Adaptive Biotechnologies (http://clients.adaptivebiotech.com/login; Email: beziat-review@adaptivebiotech.com; Password: beziat2021review). Primary CD4+ naive T cell RNA-Seq datasets generated during this study are available at the gene expression omnibus: GEO: GSE139299. Lesions RNA-Seq datasets generated during this study are available at the GEO: GSE139259. The assembled genomes are available from GenBank under the accession numbers GenBank: MN605988 and MN605989 for HPV-2 (from P1) and HPV-4 (from P2 and P3), respectively. This study did not generate any unique code. Any other piece of data will be available upon reasonable request.

EXPERIMENTAL MODEL AND SUBJECT DETAILS

P1 is a 30-year-old Iranian man with TMS. He was born to Iranian first cousins and he lives in Iran. His medical history until the age of eight years was unremarkable. From the age of eight years, he progressively developed common warts, which eventually entirely covered his hands and feet. At the age of 22 years, large cutaneous horns began to develop over the warts over a period of a few months, despite the application of several topical treatments and the removal of some of the larger warts (Figure 1B). P1 worked as a driver until this time. He weighed more than 60 kg until he was 24 years old. He began losing weight when he was 24, after starting regular opium inhalation. He currently weighs 45 kg. With the exception of a cousin (P2) and his daughter (P3), none of the other members of his family have reported susceptibility to warts. The patient has a family history of atopic dermatitis and diabetes mellitus in his mother, and allergic rhinitis in some sisters and brothers. Dermatological examination showed an extension of multiple horns over the entire body, including the scalp, particularly at the extremities, which were distorted by giant cutaneous horns without normal skin. Histological analysis of two separate skin biopsies revealed a papilloma without parakeratosis or vacuolated cells (Data S1). Multiplex PCR showed HPV-2 to be the only cutaneous HPV present in the warts and common to both biopsy specimens; traces of HPV-3 and HPV-4 were found in one sample each. The presence of HPV-2 in both the lesions of P1 studied was confirmed by sequencing the whole viral genome and by whole-genome DNA sequencing for two separate lesions. No mucosal damage or extension to the bones (Figure 1B), lymph nodes and deep organs from large warts was observed on X-ray. P1 also suffered from food allergies and asthma, with bronchial hyperactivity and superinfections (about one to two per year). A computed tomography scan revealed the presence of kidney stones, and the patient suffered two episodes of renal colic. Standard blood tests were normal, with the exception of high IgE levels (514 kU/L) and vitamin D deficiency. Viremia without clinical manifestations was documented for EBV (4.3 log cp/mL (< 2.0)) and CMV (3.5 log copies/mL (< 2.7)).

P2 is a 40-year-old cousin of P1. He developed his first warts at the age of 10 years. The warts slowly spread until they entirely covered his hands and feet. Unlike P1, P2 did not develop cutaneous horns. At the age of 20 years, the warts suddenly started to regress

without therapeutic intervention. Within two years, they had almost completely disappeared, leaving dyspigmentation of the affected skin area. Only two residual warts remained, and these warts were surgically removed for analysis. Histological analyses of these two lesions showed them to have the typical features of common warts (Data S1). Multiplex PCR showed HPV-4 to be the only cutaneous HPV implicated in warts common to two biopsy samples; traces of HPV-2 were found in only one sample. The presence of HPV-4 in both the lesions of P2 was confirmed by whole-viral genome sequencing. P2 suffers from asthma and reported frequent ear infections (several times per year), but has no marked susceptibility to other infections, and has never been hospitalized. Viremia for EBV (3.4 log cp/mL (< 2.0)) and CMV (3.2 log copies/mL (< 2.7)) was documented, without clinical manifestations.

P3 is the 12-year-old daughter of P2. She began to develop common warts at the age of eight years and she currently has 15 warts on her hands. Histological analyses of two lesions showed them to have the typical features of common warts (Data S1). Multiplex PCR showed HPV-4 to be the only cutaneous HPV implicated in warts common to the two biopsy samples. The presence of HPV-4 in both the lesions of P3 was confirmed by whole-viral genome sequencing. P2 and P3 have the same HPV-4 viral strain, suggesting intrafamilial infection. So far, like P2, P3 has not developed the TMS phenotype. She displays no particular susceptibility to other infections, has no allergies or asthma, and has never been hospitalized. EBV (3.2 log cp/mL (< 2.0)) viremia, without clinical manifestations, was documented.

The three patients were otherwise healthy, and normally resistant to other common microorganisms. In particular, they had no other mucocutaneous and/or viral infections, including flat warts, molluscum contagiosum, and laryngeal or anogenital warts.

METHOD DETAILS

Linkage analysis, whole-exome sequencing, whole genome sequencing—We extracted genomic DNA from blood samples collected from the patients, their parents and siblings, with the iPrep PureLink gDNA Blood Kit and iPrep Instruments from Life Technologies. We used the Genome-Wide Human SNP Array 6.0 (Thermo Fisher scientific) for linkage analysis. Multipoint LOD scores were calculated with MERLIN software (Abecasis et al., 2002), assuming that the gene responsible for the defect displayed AR inheritance and complete penetrance. WES was performed for P1, P2 and P3. Exome capture was performed with the SureSelect Human All Exon 71 Mb kit (Agilent Technologies). Paired-end sequencing was performed on a HiSeq 2500 machine (Illumina) generating 100-base reads. We aligned the sequences with the GRCh37 reference build of the human genome, using the BWA (Li and Durbin, 2010). Downstream processing and variant calling were performed with the Genome Analysis Toolkit (McKenna et al., 2010), SAMtools (Li et al., 2009), and Picard tools. Substitution and InDel calls were made with the GATK UnifiedGenotyper. All variants were annotated with an annotation software system developed in-house (Adzhubei et al., 2010; Kircher et al., 2014; Ng and Henikoff, 2001). WGS for P1 (whole blood and warts) were performed as part of the Qatar Genome Programme (QGP). sequencing libraries were generated from whole blood-derived fragmented DNA using the TruSeq DNA Nano kit (Illumina, Inc., San Diego, USA) and

sequence reads were generated using a HiSeq X Ten1 system (Illumina, Inc., San Diego, USA). We obtained on average 409×10^6 (standard deviation: 24.8×10^6) 2 × 100-bp paired-end reads. We performed WGS for P2 and P3 (whole blood and warts) at Macrogen. Sequencing libraries were generated from whole blood-derived fragmented DNA using the TruSeq DNA PCR-Free kit (Illumina) and sequenced with an Illumina NovaSeq6000 S4. We obtained on average 439×10^6 (standard deviation: 55.8×10^6) 2 × 100-bp paired-end reads.

Estimation of homozygosity rate—Homozygosity rate was estimated as previously described (Belkadi et al., 2016). Genomic measurements of individual homozygosity were compared with those for ethnically matched controls with and without consanguinity (self-declared) from our in-house WES database.

Detection and study of somatic mutations in lesions—We used BWA-MEM to align the WGS reads to the GRCh37 reference genome (Li, 2013). For the calling of somatic substitutions in the warts, we used Samtools 1.6 for pileups and then applied Varscan v2.4.3 to the pileups, first with the somatic option, then with the somatic filter with default parameter options (Koboldt et al., 2012; Li et al., 2009). We retained variants for which fewer than two reads were obtained for the blood sample and at least three reads were obtained for one of the warts. Finally, we removed all the substitutions that were present in at least three reads and had a VAF > 0.1 in at least one of 20 private cancer-free whole-genome sequencing samples. We used R v.3.5.2 and the muts.to.sigs.input and whichSignatures functions from the SomaticSignatures package (retrieved from the Bioconductor 3.8 release) to extract the COSMIC signatures (Gehring et al., 2015).

Genomic copy number variation—We identified copy number variations in WGS data by calculating coverage as the number of reads for each 10 kb bin in the genome for the warts and the blood sample. We used Varscan v.2.4.3 to extract log-ratios, which we segmented with the smoothDNA function of the DNACopy package (retrieved from the Bioconductor 3.8 release) (Olshen et al., 2004). We considered each segment with a log-ratio of amplitude greater than 0.2 (i.e., a gain or loss of more than 15%) to constitute a copy number event.

HPV detection and insertion—We quantified HPV viruses in WGS data for the 143 types of HPV from the Papillomavirus Episteme (PaVE) (Van Doorslaer et al., 2013), using HPVDetector v.1.0 (Chandrani et al., 2015) in QuickDetect mode according to the recommendations of the authors who designed this method. We used HPVDetector v.1.0 in Integration mode to search for integration sites, and we removed every integration site present in fewer than five reads.

HPV whole-genome sequencing—The HPV-2 genome was fully sequenced from two separate lesions from P1 (from the leg and back). The HPV-4 genome was fully sequenced from the two separate hand lesions from P2 and P3. The HPV-2 and HPV-4 genomes were amplified with the CloneAmp Hifi premix (Takara), using nine and twelve pairs of primers, respectively (See Key resources table), seven of which have been described before (Wang et al., 2007b). The amplicons were subjected to electrophoresis in agarose gels, and Sanger-sequenced as described in the Sanger sequencing section. Sequences were aligned with the

HPV-2 and HPV-4 reference sequences (Papillomavirus Episteme database, PaVE) (Van Doorslaer et al., 2013). The HPV-2 sequence from P1 was compared to the HPV-2 sequence of 24 normal HPV-2^+ common warts (non TMS) sampled in the United Kingdom (n = 22) and Iran (n = 2).

HPV typing by multiplex PCR—HPV genotyping was performed with type-specific PCR bead-based multiplex genotyping assays, as previously described (Schmitt et al., 2006; Smelov et al., 2018). Briefly, after DNA extraction from wart lesions, multiplex PCRs were run with specific primers for the detection of: 46 βHPVs (HPV-5, 8, 9, 12, 14, 15, 17, 19, 20, 21, 22, 23, 24, 25, 36, 37, 38, 47, 49, 75, 76, 80, 92, 93, 96, 98, 99, 100, 104, 105, 107, 110, 111, 113, 115, 118, 120, 122, 124, 143, 145, 150, 151, 152, 159, 174); 7 wart-specific HPVs (HPV-1, 2, 3, 4, 10, 27, 57); and 52 γHPVs (HPV-4, 48, 50, 60, 65, 88, 95, 101, 103, 108, 109, 112, 116, 119, 121, 123, 126, 127, 128, 129, 130, 131, 132, 133, 134, 148, 149, 156, SD, 161, 162, 163, 164, 165, 166, 167, 168, 169, 170, 171, 172, 173, 175, 178, 179, 180, 184, 197, 199, 200, 201, 202). As a positive control, to assess DNA quality, we also included primers for the amplification of β-globin in each assay. Multiplex PCR was performed with 5 μl of DNA sample mixed with MasterMix from the QIAGEN Multiplex PCR Kit (QIAGEN) according to the manufacturer's instructions. We used 10 μL of the PCR products for bead-based genotyping on a Luminex 200 machine (Schmitt et al., 2006).

Sanger sequencing—Genomic DNA was obtained from whole blood or from $CD28^+$ or $CD28^-$ $CD4^+$ T cells obtained from patients by FACS (purity > 98%). The *CD28* mutation was amplified from genomic DNA by PCR; the PCR products were purified by centrifugation through Sephadex G-50 Superfine resin (Merck) and sequenced with the BigDye Terminator Cycle Sequencing Kit (Applied Biosystems). Sequencing products were purified by centrifugation through Sephadex G-50 Superfine resin, and sequences were analyzed with an ABI Prism 3500 apparatus (Applied Biosystems). The sequences obtained were aligned with the genomic sequence of *CD28* (Ensembl), with Serial Cloner 2.6 software.

Cell culture—Peripheral blood mononuclear cells (PBMCs) were isolated by Ficoll-Hypaque centrifugation (Merck) from cytopheresis or whole-blood samples obtained from healthy volunteers and patients, respectively. PHA blasts were generated by culturing PBMCs in RPMI-1640 medium supplemented with 10% FCS, 1 μg/mL PHA (Sigma) and 10 ng/mL rIL-2 (Thermo Fisher Scientific). We added rIL-2 to the culture medium every 48 to 72 hours. The Jurkat and P815 cell lines were cultured in RPMI-1640 medium supplemented with 10% FCS. HEK293T cells were cultured in DMEM supplemented with 10% FCS.

mRNA purification, RT-PCR and RT-qPCR—Total RNA was extracted from the indicated cells with the RNeasy Extraction Kit (QIAGEN). RNA was reverse-transcribed with oligo-dT primers (Thermo Fisher Scientific) and SuperScript II reverse transcriptase (Thermo Fisher Scientific). The cDNA for the CD28 transcript was amplified with a recombinant *Taq* polymerase (Thermo Fisher Scientific) and the following primers binding to the UTRs: forward primer: 5′-TGGAACCCTAGCCCATCGTCA-3′, reverse primer: 5′-

AGCCGGCTGGCTTCTGGATA-3′. The *ACTB* transcript cDNA, used as a positive control, was amplified with the following primers: forward primer 5′-CCTTCCTGGGCATGGAGTCCT-3′, reverse primer: 5′-AATCTCATCTTGTTTTCTGCG-3′. RT-qPCR was performed with the Applied Biosystems Assays-on-Demand probes/primers specific for CD28-FAM (Hs00174796_m1 and Hs01007422_m1), and 13-glucuronidase-VIC (GUS; 4326320E), which was used for normalization. Data are displayed as $2^{-\Delta Ct}$ after normalization relative to *GUS* (endogenous control) expression (ΔCt).

Identification of CD28 mRNA splice variants by TA cloning—Bulk CD28 splice variants were amplified from PHA blast cDNA with recombinant *Taq* polymerase (Thermo Fisher Scientific) and primers binding to the UTRs, as described in the "mRNA purification, RT-PCR and RT-qPCR" section. PCR products were cloned with the TOPO TA cloning kit (Thermo Fisher Scientific), and used for the one-shot transformation of TOP10 chemically competent *E. coli* cells (Thermo Fisher Scientific), which were then spread on LB-agar plates containing X-gal and ampicillin. CD28 splice variants were amplified from individual colonies with the M13 forward and reverse primers from the TA cloning kit. We subjected the PCR products to Sanger sequencing, as described in the Sanger sequencing section, and then aligned the sequences with that of the *CD28* cDNA (NM_001243077), using SnapGene software to identify alternative splicing variants.

Exon trapping—We cloned *CD28* gDNA from P1 and a control, as described in Figure S3B. Briefly, *CD28* gDNA containing exon 1 and the first 998 nucleotides of intron 1 gDNA was amplified with CloneAmp Hifi premix (Takara), the forward primer 5′-CGAGGAGATCTGCCGCCGCGGCGTCTTTCAGTTCCCCTCAC-3′, and the reverse primer 5′- TTATCTCTCTCTGCCACCTGTACATCCTTGG-3′. Similarly, *CD28* gDNA containing the last 954 nucleotides of intron 1 and exon 2 was amplified with the forward primer 5′- CAGGTGGCAGAGAGAGATAACTCCCCTCTGGAGTC-3′ and the reverse primer 5′- CTCGAGCGGCCGCGTACGCGTTTCACATGGATAATGGTTCCATTG −3′. The Infusion Cloning kit (Clontech) was used to insert both PCR products into the pCMV6 entry vector (Origene) between the ASIS1 and *Mlu*1 cloning sites by homologous recombination. The c.52+5A>G mutation was inserted by mutagenesis. The exon-trapping plasmid obtained was used to transfect HEK293T cells, from which mRNA was purified after 24 hours, and reverse-transcribed as described in the "mRNA purification, RT-PCR and RT-qPCR" section. Variants for splicing between exons 1 and 2 were amplified with a recombinant *Taq* polymerase (Thermo Fisher Scientific), the forward primer 5′-TGGAACCCTAGCCCATCGTCA-3′, and the reverse primer 5′-CATTTGCTGCCAGATCCTCTT-3′. PCR products were subsequently cloned with the TOPO TA cloning kit (Thermo Fisher Scientific) and analyzed as described in the "Identification of CD28 mRNA splice variants by TA cloning" section.

Plasmids and transient transfection—The C-terminal Myc/DDK-tagged pCMV6 empty vector and the human *CD28* (NM_006139), *KANSL1L* (NM_152519) and *USP37* (NM_020935) expression vectors were purchased from Origene. Constructs carrying mutant alleles were generated by direct mutagenesis with the QuikChange II XL Site-Directed

Mutagenesis Kit (Agilent Technologies), according to the manufacturer's instructions. The full-length wild-type and mutant human *CD28* cDNAs were inserted into the V5/His-tagged pcDNA3.1 plasmid, with the directional TOPO expression kit (Thermo Fisher Scientific). HEK293T cells were transiently transfected with the various constructs, with a calcium phosphate kit (Thermo Fisher Scientific) or in the presence of X-tremeGENE 9 DNA Transfection Reagent (Roche), according to the manufacturers' instructions.

Cell lysis and immunoblotting—Total protein extracts were prepared by mixing cells with lysis buffer (50 mM Tris pH7.4, 150 mM NaCl, 2 mM EDTA, 0.5% Triton X-100) and incubating for 30 minutes at 4°C. The cells were centrifuged for 10 minutes at 16000 x *g*, and the supernatant was collected for immunoblotting. A mixture of protease and phosphatase inhibitors was added to the buffers immediately before use: aprotinin (Sigma, 10 μg/mL), PMSF (Sigma, 1 mM), leupeptin (Sigma, 10 μg/mL), phosSTOP (Sigma, 1x) di-isopropylfluorophosphate (DFP, Sigma, 5 mM). The proteins were separated by SDS-PAGE and immunoblotting was performed with Abs against the V5 tag (R962–25, Thermo Fisher Scientific) and GAPDH (FL335, Santa Cruz).

Flow cytometry—Immunophenotyping was performed by flow cytometry, with mAbs against CCR7 (G043H7, Biolegend), CD1c (L161, Biolegend), CD3 (7D6, Thermo Fisher Scientific; UCHT1, BD), CD4 (RPA-T4, BD), CD8 (RPA-T8, BD), CD11c (S-HCL-3, BD), CD14 (M5E2, BD), CD15 (HI98, BD), CD16 (3G8, BD), CD19 (HIB19 and 4G7, BD), CD20 (LT20, Miltenyi Biotec), CD25 (MA-251, BD), CD27 (O323, Sony; L128, BD), CD28 (15E8, Miltenyi Biotec; CD28.2, BD), CD31 (WM-59, BD), CD45RA (Hl100, BD), CD54 (HA58, BD), CD56 (B159, BD; NCAM16.2, BD), CD123 (6H6, Biolegend), CD134 (L106, BD) CD141 (1A4, BD), CD152 (BNI3, BD), CD154 (24–31, Biolegend), CD161 (DX12, BD), CD183 (REA232, Miltenyi Biotec), CD185 (REA103, Miltenyi Biotec), CD194 (REA279, Miltenyi Biotec), CD196 (REA190, Miltenyi Biotec), CD223 (3DS223H, Thermo Fisher Scientific), CD272 (MIH26, Thermo Fisher Scientific), CD278 (C398.4A, Biolegend), CD279 (MIH4, Thermo Fisher Scientific), CD366 (F38–2E2, Thermo Fisher Scientific), FOXP3 (259D/C7, BD), IFN-γ (B27, BD), IgA (IS11–8E10, Miltenyi Biotec), IgG (G18–145, BD), IgM (PJ2–22H3, Miltenyi Biotec), KIR2DL1/S1 (EB6, Beckman Coulter) KIR2DL2/S2/L3 (GL183, Beckman Coulter), KIR3DL1 (DX9, Biolegend), NKG2A (REA110, Miltenyi Biotec), NKG2C (REA205, Miltenyi Biotec), TCR-iNKT (6B11, BD), TCR-γδ (11F2, Miltenyi Biotec), and TCR-Vα7.2 (REA179, Miltenyi Biotec), TIGIT (MBSA43, Thermo Fisher Scientific). Cells were also stained with the Aqua Live/Dead Cell Stain Kit (Thermo Fisher Scientific). When required, cells were fixed and permeabilized with a fixation/permeabilization kit (eBioscience) after extracellular staining, for intracellular staining. Alternatively, cells were fixed with Fix Buffer 1 (BD) and permeabilized with Perm buffer III (BD) after extracellular staining, for intracellular staining. Samples were analyzed with a FACS Aria II cytometer or a Fortessa X20 (BD) or Gallios (Beckman Coulter) machine, depending on the experiment. Data were then analyzed with FlowJo 10.1r5 software. The terminal differentiation profile of the $CD56^{dim}$ compartment was assessed by determining the distribution of NKG2A and KIR (Béziat et al., 2010; Björkström et al., 2010). T cell subsets were defined as naive ($CD45RA^{+}CCR7^{+}$), central memory ($CD45RA^{-}CCR7^{+}$), effector memory ($CD45RA^{-}CCR7^{-}$) and T_{EMRA}

(CD45RA$^+$CCR7$^-$) cells among the CD4$^+$ and CD8$^+$ T cells. γδ T cells (CD3$^+$TCR-γδ$^+$), MAIT (CD3$^+$CD161$^+$TCR-vα7.2$^+$) and iNKT (CD3$^+$TCR-iNKT$^+$) were defined among the total CD3$^+$ T cells. Treg (CD3$^+$CD4$^+$CD25^{hi}FoxP3$^+$) were defined among the CD4$^+$ T cell compartment. T-helper (Th) subsets within the CD4$^+$ memory compartments were defined as follows: Tfh (CXCR5$^+$), Th1 (CXCR5$^-$CXCR3$^+$CCR4$^-$CCR6$^-$), Th2 (CXCR5$^-$CXCR3$^-$CCR4$^+$CCR6$^-$), Th1* (CXCR5$^-$CXCR3$^+$CCR4$^-$CCR6$^+$) and Th17 (CXCR5$^-$CXCR3$^-$CCR4$^+$CCR6$^+$).

Lentivirus production and transduction—Lentiviruses were produced as follows. Two days before transduction, 0.5–1.0×10^6 HEK293T cells were used to seed a six-well plate. Patient and control PBMCs were thawed and cultured in RPMI supplemented with 10% FCS with PHA (Sigma, 1 μg/mL). The following day, HEK293T cells were transfected with pCMV-VSV-G (0.2 μg) (Stewart et al., 2003), pHXB2-env (0.2 μg; NIH-AIDS Reagent Program; #1069), psPAX2 (1 μg; gift from Didier Trono; Addgene plasmid # 12260), pLVX-CD28_WT-IRES-mCherry (1.6 μg) or pLVX-CD28_Gly18Arg-IRES-mCherry (1.6 μg) or pLVX-EF1α-IRES-mCherry (1.6 μg) (empty vector; Takara) in the presence of X-tremeGENE HP (Sigma Aldrich), in accordance with the manufacturer's protocol. The medium was replaced after 8 hours of incubation. In parallel, PHA blasts were used to seed 96-well round-bottomed plates at a density of 2×10^5 cells/well and were stimulated with beads coated with antibodies against CD2 and CD3 (T cell activation/expansion kit, Miltenyi Biotec). Anti-CD28 antibodies were omitted from the bead coating. On day 0, 24 hours after the HEK293T cell medium was changed, the viral supernatant was recovered and passed through a filter with 0.2 μm pores. Protamine sulfate (8 μg/mL) was added to the viral supernatant, which was then added to the activated T cells or Jurkat cell line (immediately after seeding), which were spinoculated for 2 hours at 1200 x *g* and 25°C. After spinoculation, cells were cultured for 48 hours at 37°C under an atmosphere containing 5% CO_2. On day +2, the cells were transferred to a 24-well plate containing RPMI supplemented with 2% human serum AB (Sigma), penicillin/streptomycin (1/1000) and r-IL2 (10 ng/mL, Thermo Fisher Scientific) for primary T cells and RPMI supplemented with 10% FCS for Jurkat cells. The medium was replaced on day +5 and the p-p65 experiment was performed on day +6.

Histological analysis and immunohistochemistry—Formalin-treated paraffin-embedded sections of each specimen were stained with hematoxylin and eosin for histological analysis. Immunohistochemistry (IHC) studies were carried out on 3 μm-thick sections of formalin-fixed, paraffin-embedded tissue, with standard techniques. Pan HPV detection was performed with the K1H8 antibody (Thermo Fisher Scientific), which recognizes the highly conserved L1 protein of the viral capsid. The slides were developed with the Bond Polymer Refine Detection kit (Menarini/Leica).

Immunohistofluorescence analyses—Paraffin-embedded 5 μm-thick skin sections were processed for immunohistofluorescence analyses after heat-induced epitope retrieval in citrate buffer pH 6. Sections were blocked by incubation for 1 h in 5% FCS in PBS and incubated with primary antibodies overnight at 4°C. The following primary antibodies were diluted in 5% FCS in PBS and used at the appropriate dilution: rat monoclonal anti-CD3

(1:100, ab11089, Abcam), rabbit polyclonal anti-CD28 (1:100, HPA070003, Sigma), rabbit monoclonal anti-CD86 (1:50, 91882S, CST), mouse monoclonal anti-CD80 (1:50, MAB140, R&D Systems), mouse monoclonal anti-CD207 (1:50, NCL-L-Langerin, Novocastra) when used with antibodies against CD3 and CD86 or rabbit polyclonal anti-CD207 (1:50, HPA011216, Sigma) when used with anti-CD80 antibody.

The sections were washed in 5% FCS in PBS and incubated for 1 h at room temperature with the appropriate secondary antibody: CD3 was detected with Cy3-conjugated goat anti-rat IgG (H+L) (112–165-003, Jackson Immunoresearch) when used with CD28 or with Alexa Fluor® 488-conjugated goat anti-rat IgG (H+L) (A11006, Life Technologies) when used with CD86 and CD207; CD28 was detected with Alexa Fluor® 488-conjugated goat anti-rabbit IgG (H+L) (A11008, Life Technologies); CD80 was detected with Alexa Fluor® 488-conjugated goat anti-mouse IgG1 (A21121, Life Technologies). Mouse CD207 was detected with Alexa Fluor® 647-conjugated donkey anti-mouse IgG (H+L) (715–605-150, Jackson Immunoresearch) and rabbit CD207 and CD86 were detected with Alexa Fluor® 594-conjugated donkey anti-rabbit IgG (H+L) (711–585-152, Jackson Immunoresearch). Slides were mounted in Fluoromount-G® (Clinisciences) supplemented with DAPI (1:1000, Cell Signaling). Laser scanning confocal microscopy was performed with a LEICA SP8 SMD microscope with a 40 x Plan-Apochromat objective and a magnification of 1 x or 0.75 x. Stacks of images were processed with Fiji software (Schindelin et al., 2012). Purified HPV-2 E1Ê4-MBP (maltose binding protein) fusion protein was immunized into rabbits as described previously (Doorbar et al., 1989; Peh et al., 2002). The detection of the E4 and MCM biomarkers was performed as previously described (Middleton et al., 2003 J Virol), with rabbit polyclonal anti-HPV-2 or −4 E4 serum at a 250-fold dilution. Detection was performed with Alexa Fluor 594-conjugated goat anti-rabbit igG (H+L) (Thermo Fisher Scientific) diluted 150-fold. The MCM7 antibody (47DC141, Thermo Fisher Scientific) was incubated with the slides at a 200-fold dilution for 1 hour at room temperature, and the slides were then stained by incubation for 1 hour at room temperature with the ImmPRESS horse anti-mouse IgG HRP polymer (Vector Laboratories). The slides were developed with a 500-fold dilution of Tyramide-488 (Cambridge BioScience), and the nuclei were counterstained with DAPI. Immunofluorescence was recorded by scanning with a Pannoramic digital slide scanner (3DHISTECH, Budapest, Hungary).

In situ* hybridization assay for HPV-2 E6/E7—In situ* hybridization for HPV-2-specific RNA was performed manually with the RNAscope 2.5 HD detection assay kit (Bio-Techne) – Brown with an HPV-2 E6/E7 probe (Cat. No 806601), according to the manufacturer's instructions. Sections were lightly counterstained with Carazzi's hematoxylin and were then classified as positive or negative. Positive sections displayed brown granular cytoplasmic and/or nuclear staining stronger than the signal obtained for the negative control slide. RNA integrity was confirmed with the PPIB control probe (Cat. No 313901). An HPV-2 positive wart was used as a positive control for E6/E7 mRNA levels, with HPV-negative normal skin used as a negative control.

Assays of redirected T cell function—Thawed PBMCs were rested overnight in complete medium and dispensed, at a final concentration of 5×10^6 cells/mL, into 96-well

round-bottomed plates. P815 murine mastocytoma target cells were added to PBMCs at a final concentration of 2.5×10^6 cells/mL. Anti-CD3-PE (7D6, 1/100), and/or anti-CD28 (CD28.2, 5 μg/mL) antibodies were added alone or in combination to the indicated wells. PMA (40 ng/mL) and ionomycin (10^{-5}M) were used to stimulate the cells in separate wells, as a positive control. The cells were incubated for 6 hours (37°C, 5% CO_2) after the addition of monensin (GolgiStop, BD Biosciences, 1/1500 final concentration), and brefeldin A (GolgiPlug, BD Biosciences, 1/1000 final concentration). The cells were washed and stained for CD3, CD4, CD8, CCR7, CD45RA and with a viability stain. They were then permeabilized (fixation/permeabilization buffer, eBioscience) and stained for intracellular TNF (cA2, Miltenyi Biotec), IL-2 (MQ1–17H12, Sony) and IFN-γ (B27, BD) before flow cytometry.

Phospho-NF-κB p65 in PHA blasts—PHA blasts were stained by incubation for 10 minutes at 37°C with the Aqua Live/Dead kit (Thermo Fisher Scientific). We dispensed 10^6 PHA blasts into each well of a 96-well V-bottomed plate, and incubated them on ice for 10 minutes with anti-CD28 (CD28.2, eBioscience) or anti-CD3 (OKT3, eBioscience) mAb, as indicated (5 μg/mL each). Cells were washed twice with cold medium and a polyclonal goat anti-mouse Ig (BD Biosciences) was added to each well (5 μg/mL) to crosslink activating receptors. PMA (40 ng/mL) was used, in separate wells, as a positive control. After 20 minutes of incubation at 37°C, cells were fixed by incubation for 10 minutes at 37°C with Fix buffer I (BD Biosciences) and stained by incubation for 30 minutes with mAb against CD3 (BW264/56, Miltenyi Biotec), CD4 (M-T321, Miltenyi Biotec) and CD8 (BW135/80, Miltenyi Biotec). The cells were permeabilized by incubation for 20 minutes at room temperature with Perm buffer III (BD Biosciences) and stained by incubation for three hours at room temperature with an anti-NF-κB p65-(pS259)-PE antibody (BD Biosciences). Cells were then acquired on a FACS Gallios (Beckman Coulter) flow cytometer and analyzed with FlowJo v10.

Induction of costimulation and coinhibitory molecules—Freshly thawed PBMCs were cultured in complete medium (RPMI, glutamine, 10% FCS) supplemented with 2% human serum (Sigma), at a final concentration of 2×10^6 cells/mL in a 24-well plate. Cells were left unstimulated or were stimulated with CD2/CD3/CD28 mAb-coated beads (Miltenyi Biotec) or PMA (40 ng/mL) and ionomycin (10^{-5}M). After 72 hours of incubation (37°C, 5% CO_2), the cells were stained for extracellular receptors and with the Aqua Live/Dead Cell Stain Kit (Thermo Fisher Scientific), and analyzed by flow cytometry on a FACS Gallios machine. For CTLA4 analysis, cells were fixed and permeabilized (Fixation/permeabilization buffer, eBioscience), stained for intracellular CTLA4 and analyzed by flow cytometry on a FACS Gallios machine.

***Ex vivo* CFSE proliferation assay—**Freshly thawed PBMCs were stained with CFSE (Thermo Fisher Scientific) and cultured in complete medium (RPMI, glutamine, 10% FCS) supplemented with 2% human serum (Sigma), at a final concentration of 2×10^6 cells/mL in a 24-well plate. Cells were left unstimulated or were stimulated with CD3 antibody-coated, CD3/CD2 antibody-coated, CD3/CD28 antibody-coated or CD2/CD3/CD28 antibody-coated beads (Miltenyi Biotec). After 5 days of incubation (37°C, 5% CO_2), the cells were

stained for extracellular receptors (CD3, CD4 and CD8) and with the Aqua Live/Dead Cell Stain Kit (Thermo Fisher Scientific), and analyzed by flow cytometry on a FACS Gallios machine.

Short-term stimulation with overlapping peptides or tuberculin—Freshly thawed PBMCs were cultured in complete medium (RPMI, glutamine, 10% FCS) at a final concentration of 5×10^6 cells/mL in a 96-well U-bottomed plate. Cells were left unstimulated or were stimulated with overlapping CMV^{pp65} peptides (JPT Technology, 1 μg/mL final concentration for each peptide), tuberculin PPD (5 μg/mL final concentration; Statens Serum Institut) or CD2/CD3/CD28 mAb-coated beads (Miltenyi Biotec) in the presence of brefeldin A (GolgiPlug, BD Biosciences, 1/1000 final concentration). After 16 hours of incubation (37°C, 5% CO_2), the cells were stained for extracellular receptors and with the Aqua Live/Dead Cell Stain Kit (Thermo Fisher Scientific), permeabilized (fixation/permeabilization buffer, eBioscience), stained for intracellular IFN-γ-AF700 (B27) and analyzed by flow cytometry on a FACS Gallios machine.

Long-term stimulation with overlapping peptides—Freshly thawed PBMCs from controls and patients were cultured in complete medium (RPMI, glutamine, 10% FCS) at a final density of $2–4\times10^6$ cells/mL. Cells were left unstimulated or were stimulated by incubation for one hour with overlapping CMV^{pp65}, HPV-2^{E6} or HPV-4^{L1} peptides (all from JPT Technology, 1 μg/mL final concentration for each peptide), washed and transferred to a 24-well plate. After 24 hours, IL-2 was added to each well (100 IU, Proleukin, Novartis). The medium and IL-2 were renewed every two to three days. After 14 days of culture, overlapping peptides were added to each well at a final concentration of 1 μg/mL for each peptide, and the cells were incubated for four hours. The cells were then washed, stained for extracellular epitopes (CD3, CD4, CD8) and with the Aqua Live/Dead Cell Stain Kit (Thermo Fisher Scientific), permeabilized (fixation/permeabilization buffer, eBioscience), stained for intracellular IFN-γ-AF700 (B27) and TNF-APC (cA2) and analyzed by flow cytometry on a FACS LSR-Fortessa machine.

Single-cell RNA-seq—Single-cell RNA-seq was performed on PBMCs obtained from the three patients, and from three wild-type controls. The frozen PBMCs were quickly thawed at 37°C and gently resuspended by serial additions of DMEM + 10% heat-inactivated FBS, to obtain a final volume of 14 mL. The cells were collected by centrifugation for 5 minutes at 300 x *g*, cells and were washed twice with 5 mL DMEM + 10% HI-FBS to remove cell debris. Cells were counted and viability was assessed with the LIVE/DEAD Viability kit (Thermo Fisher Scientific), according to the kit manufacturer's guidelines. The cell preparation was enriched in viable cells, by resuspending one million cells in 200 μL of 1 x PBS, 2% HI-FBS 1 mM $CaCl_2$, passing the resulting suspension through a strainer with 40 μm pores and removing the dead cells with the EasySep Dead Cell Removal Kit (Stem Cell Technologies). The cells were collected by centrifugation for five minutes at 300 x *g* and resuspended at a concentration of 1000 cells/μL in 0.04% BSA in PBS. Cell viability was ≥ 80% for all samples. The samples were loaded onto a 10X Genomics Chromium chip for single-cell capture. Reverse transcription and library preparation were performed with Chromium Single Cell 3′ Reagent Kits (v3.1), in accordance with the manufacturer's

guidelines, and library quality was assessed with a Bioanalyzer DNA chip. The libraries were sequenced on one lane (S4 flowcell) of an Illumina NovaSeq 6000 sequencer.

Sequence read quality in individual sequencing lanes was assessed with BVAtools. Cell Ranger v3.0.1 was used for mapping reads to the hg38 human reference genome assembly, filtering, and counting barcodes and UMIs, resulting in a list of UMI counts for every gene in every cell. Based on these counts, we extracted the summary statistics for the number of genes expressed per cell and for the number of UMIs per cell. Cells with > 20% mitochondrial genes were excluded. Low-quality cells and doublets were filtered out by excluding cells falling outside the [−1 SD;+2.5 SD] interval for UMI and gene count distributions. The DoubletFinder package was used to identify and filter out the remaining cell doublets (McGinnis et al., 2019). Once dead cells and doublets had been removed, the CD28-deficient patient and control samples were analyzed jointly with the Seurat v3 R package (Stuart et al., 2019) and cell clustering was performed by the uniform manifold approximation and projection dimension reduction method (Becht et al., 2018) with the most variable genes, but excluding mitochondrial and ribosomal protein genes. This analysis identified 10 distinct clusters of lymphoid cells, based on the marker genes for each cluster determined by the MAST approach (Finak et al., 2015). A pseudobulk differential gene expression analysis was performed by extracting the sum of UMI counts for each cluster in each sample, followed by normalization against the total number of counts per cluster and per sample, and quantile normalization. The patients and controls were then compared for each CD28-expressing cluster, with the edgeR package (Robinson and Oshlack, 2010). Genes displaying a two-fold difference in expression, with a Benjamini-Hochberg adjusted $p\text{-}value < 10^{-3}$ were considered to display significant differential expression. For the figures, cluster annotations and expression values for the genes of interest were projected onto the UMAP clustering.

Primary CD4$^+$ naive T cell RNA-Seq analysis—Total RNA from primary naive CD4$^+$ T cells was extracted with the RNeasy Plus Micro Kit (QIAGEN), according to the manufacturer's instructions. We generated cDNA with the SMART-Seq RNA kit (Takara Bio) for low-input RNA and DNA library preparation, and used the Nextera XT DNA Library Preparation Kit (Illumina) and the Nextera XT Index Kit v2 set A (Illumina), respectively, for indexing with low DNA input requirements. The RSeQC package was used for quality evaluation of the raw high throughput sequence data (Wang et al., 2012). Raw RNA-seq reads were aligned with UCSC human genome assembly version hg38, with STAR aligner (Dobin et al., 2013). HTseq-count (Anders et al., 2015) was used to count the reads mapping to each gene feature. Downstream analysis and heatmap generation were performed with an in-house script in R (R: A language and environment for statistical computing. R Foundation for Statistical Computing, Vienna, Austria. URL https://www.R-project.org/), with DESEq2 (Love et al., 2014), and ComplexHeatmap (Gu et al., 2016). In brief, differentially expressed genes (DEGs) were identified in controls by performing Student's t tests to compare four non-stimulated and stimulated control samples for each of the conditions, with a *p-value* cutoff of 0.01, and then filtering to select genes displaying at least a two-fold up- or downregulation in at least three of the four controls. The residual responses for the CD28–deficient patient were evaluated by determining the number of

responsive genes passing the above filter in healthy controls, as follows: The total count of responsive genes in a subject for a particular set of *in vitro* stimulation conditions and time point was divided by the mean number of responsive genes in all healthy controls and multiplied by 100. Alternatively, fold-changes in expression after costimulation with CD2+CD3 or CD3+CD28 were calculated relative to stimulation with CD3 alone in certain conditions, as indicated in the figure legends.

High-throughput sequencing (HTS) of T cell receptor β (TRB) and T cell receptor α (TRA)—$CD4^+CD28^-$ and $CD4^+CD28^+$ (revertants) T cells from P1, P2 and P3, and $CD4^+CD28^+$ T cells from a control were sorted with a FACSAria cell sorter (Becton Dickinson, San Jose, CA). The TCRβ (*TRB*) and TCRα (*TRA*) rearranged genomic products were amplified by multiplex PCR, with DNA from these cells as the template (Adaptive Biotechnologies Seattle, WA). We ensured that all possible VDJ combinations were amplified, by using an adequate set of forward primers for the *TRBV* and *TRAV* gene segments and reverse primers for the *TRBJ* and *TRAJ* gene segments. Adaptive Biotechnologies use assay-based and computational techniques to minimize PCR amplification bias. The assay is quantitative, and the frequency of a given *TRB* or *TRA* sequence is representative of the frequency of that clonotype in the original sample. The PCR products were sequenced on an Illumina HiSeq platform. Custom algorithms were used to filter the raw sequences for errors and to align the sequences with reference genome sequences. The data were then analyzed with ImmunoSeqTM online tools. The frequency of productive and non-productive *TRB* and *TRA* rearrangements was analyzed within both unique and total *TRB* or *TRA* sequences obtained from sorted T cell subsets. The frequency distributions for individual clonotypes (including *TRBV* to *TRBJ* pairing and *TRAV* to *TRAJ* pairing) were analyzed within unique sequences. Heatmap representations of the frequencies of individual *TRAV* to *TRAJ* gene pairs and *TRBV* to *TRBJ* gene pairs were produced with R software version 3.6.3 (2020–02-29). TCR-Vβ sequence of the revertants and CD28- CD4+ T cells from P1, P2 and P3 were also analyzed using the GLIPH software that clusters TCRs that are predicted to bind the same MHC-restricted peptide antigen (Glanville et al., 2017).

CITE-Seq Analysis—PBMCs from P1, P2 and one control were thawed and cultured overnight in X-Vivo 20 (Lonza). Dead cells were removed using the dead cell removal kit (Miltenyi Biotec). $CD4^+$ memory T cells were negatively sorted using the Memory CD4+ T cell isolation kit (Miltenyi Biotec). Purity and cell viability were measure by flow cytometry and were above 90% and 95%, respectively. Cells were stained for CD3 (C0049), CD4 (C0072), CD45RA (C0063) and CD28 (C0386) using Total-seq C antibodies for CITE-seq from Biolegend. Cell suspensions were used for single cell isolation using 10X Genomics Single cell protocols. 5′ expression and TCR Libraries were generated using Chromium Single Cell 5′ Library & Gel Bead kit Version 1 (10x genomics # 1000014). Hashtag libraries were generated using Chromium Single Cell 5′ Feature Barcode Library Kit (# 1000080). Standard protocol from 10X genomics was followed to generate the libraries. After QC, Three expression libraries were pooled together and sequenced on Novaseq using 100 cycle SP flowcell, the TCR and hashtag libraries were pooled together and sequenced on Nextseq. Sequence reads quality of individual sequencing library was assessed using

BVAtools (https://bitbucket.org/mugqic/bvatools). Cell Ranger v5.0.1 was used to map the reads to the hg38 human reference genome assembly and detect antibody feature barcodes, perform filtering, and count barcodes and UMIs; resulting in two list of UMI counts: one for every gene in every cell and one for the antibody detection. Based on these counts, we filtered out cells which were not detected in both scRNA and antibody analyses. We extracted the summary statistics for the number of expressed genes per cell along with the summary statistics for the number UMI per cell. Cells with > 20% of mitochondrial genes were excluded. To filter out low quality cells and doublets, cells falling outside the [−1SD; +2.5SD] interval for the UMI and gene count distribution were excluded. Further, the DoubletFinder package was used to identify and filter out remaining cell doublets (McGinnis et al., 2019). After dead cells and doublet removal, the CD28 patient (P1 and P2) and control samples were jointly analyzed using the Seurat v4 R package (Stuart et al., 2019) and cell clustering was performed using the Uniform Manifold Approximation and Projection dimension reduction method (Becht et al., 2018) using the most variable genes, but excluding mitochondrial and ribosomal protein genes. This analysis identified sixteen distinct clusters of cells, based on the marker genes for each cluster determined using the MAST approach (Finak et al., 2015). We identified 12 different CD4+ memory cell populations, and four small additional cluster corresponding to remaining activated T cells, Treg, gdT and NKT, and CD8+ T cells; these four non-CD4 memory cell clusters were excluded from further analyses. We looked at the level of CD28 antibody in controls and determine the standard antibody detection for cell expressing normal CD28 genes expression correspond to a signal between 0.5 and 2. By combining the antibody signal and the gene expression signal, we annotated cells carrying the CD28 mutation if no expression of the gene CD28 is detected and if the antibody signal is lower than 0.25. We annotated the CD28 revertant cells if the expression of the CD28 gene is detected and the signal of antibody is measured between 0.5 and 2 as observed in controls. We thus identify 1438 cells CD28 mutant and 38 revertant cells for P1 and P2 together. A differential gene expression analysis was performed comparing CD28 revertants to mutants using the MAST approach in the twelve CD4+ memory populations. For the figures, cluster annotations, the expression of genes of interest and the antibody signal were projected on the UMAP clustering.

RNA-Seq analysis of the lesions of P1 and control common warts—Two TMS lesions from P1, and three HPV-2^{+} common warts immersed in RNA-Later were snap-frozen in liquid nitrogen and crushed with a tissue pulverizer kit (Cell Crusher) according to the manufacturer's instructions. Total RNA was extracted with the RNeasy Fibrous Tissue Mini Kit (QIAGEN), according to the manufacturer's instructions. The procedure included a DNase digestion step or an additional column to remove contaminating DNA. The concentration and purity of the total RNA extracted were measured by spectrometry with an Xpose (Trinean). RNA integrity was evaluated by capillary electrophoresis with a Tape Station (Agilent). The Ovation Universal RNA-Seq System from NUGEN was used to prepare the RNA-seq libraries from 100 ng of total RNA, as recommended by the manufacturer. This type of RNaseq kit is less sensitive to total RNA degradation (the RNA integrity number (RIN) of the two samples from P1 was quite low: 3.9 for one sample and 5 for the other; for the common warts, all the RIN were > 8). This kit constructs strand-specific RNA-Seq libraries from 10 to 100 ng of total RNA and uses Insert-Dependent

Adaptor Cleavage (InDA-C) technology to remove the ribosomal RNA transcripts. The RNA is subjected to reverse transcription, the second strand is synthesized, and a fragmentation step is then performed before Illumina-compatible indexed adaptator ligation. This ligation is followed by a strand-selection enzymatic reaction to provide information about the orientation of the transcripts. Insert-dependent adaptor cleavage (InDA-C)-specific primers were then used for the targeted depletion of human ribosomal RNA sequencing transcripts before PCR enrichment. We ensured that no excess amplification occurred during the final PCR step, by evaluating the number of PCR cycles to be applied to each sample in a preliminary Q-PCR test with EvaGreen. An equimolar pool of the final indexed RNA-Seq libraries was sequenced on an Illumina NovaSeq6000 (paired-end reads, 100 bases + 100 bases) and ~50 million paired-end reads per library were produced. We used STAR 2.7.2b (Dobin et al., 2013) with standard parameters to align RNA-seq reads with a chimeric genome of concatenated GRCH37.87 and HPV-2 downloaded from the PAVE website (Van Doorslaer et al., 2013) (http://pave.niaid.nih.gov). We used IGV 2.4.19 (Robinson et al., 2011) to extract the splicing junction track from the aligned reads.

Animals and MmuPV1 infection—All work on mice was approved by the Institutional Animal Care and Use Committee of Pennsylvania State University's College of Medicine (COM) and all procedures were performed in accordance with guidelines and regulations. Infectious mouse papillomavirus (MmuPV1) was isolated from lesions on the tails of mice from our previous studies (Cladel et al., 2015, 2019b). In brief, papillomas scraped from the tails of the mice were homogenized in phosphate-buffered saline (1 × PBS) with a Polytron homogenizer (Brinkman PT10–35) at maximum speed for three minutes, with chilling in an ice bath. The homogenate was spun in a bench centrifuge at 10,000 rpm and the supernatant was decanted into Eppendorf tubes for storage at −20°C. For these experiments, the suspension of the mouse papillomavirus was stored at −80°C in glycerol (1:1,V/V). We obtained 27 C57BL/6, six Rag1 KO mice, and 26 female $Cd28^{-/-}$ (6–8 weeks old) mice from Jackson Laboratories. All mice were housed (2–3 mice/cage) in sterile cages within sterile filter hoods and were fed sterilized food and water in the COM BL2 animal core facility. Mice were sedated i.p. with 0.1 mL/10 g body weight of a ketamine/xylazine mixture (100 mg/10 mg in 10 mL double-distilled H_2O). The muzzle and tail skin sites were wounded with a scalpel blade. Twenty-four hours after wounding, the mice were again anesthetized and challenged with infectious virus (containing 1×10^9 viral DNA genomes) at the pre-wounded muzzle and tail sites, with a TB needle used to scrape the pre-wounded inoculation sites superficially. Infection of the muzzle and tail was monitored weekly, with a photographic documentation of progression for each animal (Cladel et al., 2013). $Cd28^{-/-}$ mice were killed in weeks 2, 3, 4 and 5 after viral infection. C57BL/6 and Rag1 KO mice were killed in week 6 post infection. The infected tissues were harvested for additional analyses.

Detection of MmuPV1 by *in situ* hybridization (ISH), RNA *in situ* hybridization (RNA-ISH), and immunohistochemistry—Biopsy specimens were fixed in 10% neutral buffered formalin and embedded in paraffin. Adjacent sequential sections were cut for hematoxylin and eosin (H&E), *in situ* hybridization (ISH), RNA *in situ* hybridization (RNA-ISH), and immunohistochemistry (IHC), as described in previous studies (Cladel et

al., 2016, 2017; Hu et al., 2015). For ISH, a biotin-labeled 3913 bp *Eco*RV/ *Bam*H1 subgenomic fragment of MmuPV1 was used as an *in situ* hybridization probe for the detection of MmuPV1 DNA in tissues (Cladel et al., 2015). Access to target DNA was obtained by incubation with 0.2 mg/mL pepsin in 0.1 N HCl at 37°C for 8 min. The sections were thoroughly washed and the biotinylated probe was added. The sections were heated at 95°C for 5 min to dissociate the target and probe DNA. Re-annealing was allowed to occur for 2 hours at 37°C. Target-bound biotin was detected by incubation with a streptavidin AP conjugate followed by colorimetric development in BCIP/NBT. ISH, counterstaining was performed with Nuclear Fast Red (American MasterTech, Inc.). Viral RNA was detected in formalin-fixed, paraffin-embedded (FFPE) tissues with RNAscope technology (Advanced Cell Diagnostics, Inc.), using custom probes mapping within the second exon of the E1Ê4 ORF (nt 3139–3419), according to the manufacturer's protocol. After hybridization, the bound probes were detected by colorimetric staining in the RNAscope 2.5 HD Assay - BROWN. For IHC, an in-house anti-MmuPV1 E4 polyclonal antibody (from Dr. John Doorbar) or anti-MmuPV1 L1 antibody (MPV.B9, in-house) was used on FFPE sections. Before mounting, the sections were counterstained with 50% hematoxylin Gill's No. 1 solution (Sigma-Aldrich) and 0.02% ammonium hydroxide solution (Sigma-Aldrich) (Cladel et al., 2017).

MmuPV1 viral load assessment by RT-qPCR—We collected tail tissues from the mice killed at different time points after infection. Total RNA was extracted from these tissues and reverse-transcribed to generate cDNA for quantitative PCR analysis. Copy numbers were assessed with 200 ng RNA from each sample (Viral RNA E1Ê4 transcripts were quantified with the primers 5′-TAGCTTTGTCTGCCCGCACT-3′ and 5′-GTCAGTGGTGTCGGTGGGAA-3′ and probe 5′FAM-CGGCCCGAAGACAACACCGCCACG-3′TAMRA. We reverse-transcribed 200 ng of RNA with the RevertAid First-Strand cDNA synthesis kit (Thermo-Fisher) and used 1 μL of the resulting cDNA for Q-PCR analysis. We used 500 nM of each primer and 250 nM probe with the Brilliant III Q-PCR kit (Agilent), under the following qPCR conditions: 95°C for 3 min, followed by 50 cycles of 95°C for 5 s and 60°C for 10 s on an Agilent AriaMx Q-PCR machine.

Anti-MmuPV1 antibody detection by ELISA—Serum was collected from the mice at the end of the experiment. MmuPV1 VLP and KLH-conjugated MmuPV1 E4 peptide (PKTTPPRRELFPPTPLTQPP) were used as antigens for ELISA. MPV.A4 was used as the positive control for VLP. Serum from naive animals was used as the negative control. ELISA was performed as previously described (Cladel et al., 2019b).

USP37 *in vitro* deubiquitination assays—HEK293T cells were transfected with a plasmid encoding the WT or Glu459Lys USP37, with polyethylenimine (Linear, Molecular Weight 25,000) (Polysciences, Warrington, PA, USA). We mixed 10 μg plasmid with 30 μL polyethylenimine solution (1 mg/mL) in 1 mL Opti-MEM (Life Technologies). The mixture was incubated for 15 minutes and added to subconfluent cells in 100 mm dishes (in 10 mL of 10% FBS-DMEM). Two days later, cells were lysed in ice-cold lysis buffer [50 mM Tris-HCl pH 7.4, 150 mM NaCl, 1 mM NaF, 1 mM EDTA, 1 mM EGTA, 1% Triton X-100, 1

mM DTT, protease inhibitor cocktail (Sigma-Aldrich, #P8340)]. The lysates were centrifuged at 15,000 x *g* for 10 min at 4°C. The supernatants were subjected to immunoprecipitation with anti-FLAG M2 antibody-conjugated agarose beads (Sigma-Aldrich), followed by elution with FLAG peptide (Sigma-Aldrich), according to the protocols recommended by the manufacturer. Immunopurified USP37 proteins (wild-type or mutant, 50 ng) were incubated with 0.4 μg of Lys48-linked polyubiquitin chains (2–7-mer, Boston Biochem) in 20 μL of 5 mM $MgCl_2$ and 2 mM DTT in TBS at 37°C, for 0, 10, 30, or 120 min. Reaction products were separated by SDS-PAGE and detected by silver staining.

VirScan - phage immunoprecipitation-sequencing (PhIP-Seq)—Antibody profiling by phage immunoprecipitation-sequencing (PhIP-Seq) was performed on plasma samples from patients and controls using an expanded version of the original VirScan library, and the data were analyzed as previously described (Drutman et al., 2020; Kerner et al., 2020; Mina et al., 2019; Mohan et al., 2019), but with the following modifications. We calculated species-specific significance cutoff values to estimate the minimum number of enriched, non-homologous peptides required to consider a sample seropositive, as previously described with an in-house dataset and a generalized linear model (Hasan et al., 2021; Khan et al., 2021). For each sample, we calculated virus-specific scores, by dividing the counts of enriched, non-homologous peptides by the estimated score cutoff. These adjusted virus scores were further depicted in heatmap plots. We randomly selected an age-matched subset of 19 individuals from a larger cohort of 800 individuals of Arab ancestry (representing general adult population) from our inhouse database, for comparison with the patients and initial controls. Pooled human plasma used for IVIg (Privigen® CSL Behring AG), and human IgG- depleted serum (Molecular Innovations, Inc.) were used as additional controls. All research on human subjects was performed with informed written consent, and the procedures were approved by the Institutional Research Ethics Boards of Sidra Medicine and Qatar Biobank.

Antibody profiling by phage immunoprecipitation-sequencing (PhIP-Seq) (Xu et al., 2015) was performed on plasma samples from patients and controls, and the data were analyzed as previously described (Drutman et al., 2020; Kerner et al., 2020), but with the following modifications. We calculated species-specific significance cutoff values to estimate the minimum number of enriched, non-homologous peptides required to consider a sample seropositive, as previously described with an in-house dataset and a generalized linear model (Xu et al., 2015). For each sample, we calculated virus-specific scores, by dividing the counts of enriched, nonhomologous peptides by the estimated score cutoff. These adjusted virus scores were further depicted in heatmap plots. We randomly selected an age-matched subset of 19 individuals from a larger cohort of 800 individuals of Arab ancestry (representing general adult population) from our in-house database, for comparison with the patients and initial controls. Pooled human plasma used for IVIg (Privigen® CSL Behring AG), and human IgG-depleted serum (Molecular Innovations, Inc.) were used as additional controls. All research on human subjects was performed with informed written consent, and the procedures were approved by the Institutional Research Ethics Boards of Sidra Medicine and Qatar Biobank.

Anti-HPV Luminex serological tests—Plasma samples were sent to the German Cancer Research Center (DKFZ, Heidelberg, Germany) on dry ice for serological analysis. Antibodies against L1 antigens of HPV types 1, 2, 4, 5, 6, 8, 9, 10, 11, 12, 15, 16, 17, 18, 21, 22, 23, 24, 27b, 31, 33, 36, 38, 41, 45, 48, 50, 52, 58, 60, 75, 80, 88, 92, 93, 96, 101 and 103 were analyzed simultaneously with Luminex-based multiplex serological tests, as previously described (Waterboer et al., 2005). In brief, HPV L1 antigens were expressed as recombinant glutathione S-transferase (GST) fusions proteins, loaded onto polystyrene beads and simultaneously presented to primary serum antibodies. The immunocomplexes formed were detected with a biotinylated secondary antibody and streptavidin-R-phycoerythrin as a reporter dye. Sera were tested at a dilution of 1:100 and antigen-specific seropositivity was determined on the basis of predefined cutoff values (Clifford et al., 2007; Michael et al., 2008; Sankaranarayanan et al., 2016).

QUANTIFICATION AND STATISTICAL ANALYSIS

Two-tailed Mann-Whitney tests tests were used for single comparisons of independent groups. Wilcoxon tests were used for single comparisons of paired groups. Kruskal-Wallis tests were used for multiple comparisons of independent groups. In the relevant figures, n.s. indicates not significant; ***$p < 0.001$; **$p < 0.01$; and *$p < 0.05$. Analyses were performed with GraphPad software.

Supplementary Material

Refer to Web version on PubMed Central for supplementary material.

Authors

Vivien Béziat[1,2,*], Franck Rapaport[2,30], Jiafen Hu[3,30], Matthias Titeux[1,30], Mathilde Bonnet des Claustres[1,30], Mathieu Bourgey[4,30], Heather Griffin[5,30], Élise Bandet[1,30], Cindy S. Ma[6,7,30], Roya Sherkat[8,30], Hassan Rokni-Zadeh[9,30], David M. Louis[10,30], Majid Changi-Ashtiani[11,31], Ottavia M. Delmonte[12,31], Toshiaki Fukushima[13,31], Tanwir Habib[14,31], Andrea Guennoun[14,31], Taushif Khan[14,31], Noemi Bender[15,31], Mahbuba Rahman[14,31], Frédégonde About[1,31], Rui Yang[2,31], Geetha Rao[6,7,31], Claire Rouzaud[1,16,31], Jingwei Li[3,31], Debra Shearer[3,31], Karla Balogh[3,31], Fatima Al Ali[14,31], Manar Ata[14,31], Soroosh Dabiri[17], Mana Momenilandi[18], Justine Nammour[1], Marie-Alexandra Alyanakian[16], Marianne Leruez-Ville[16], David Guenat[19], Marie Materna[1], Léa Marcot[1], Natasha Vladikine[1], Christine Soret[19], Hassan Vahidnezhad[20], Leila Youssefian[20], Amir Hossein Saeidian[20], Jouni Uitto[20], Émilie Catherinot[21], Shadi Sadat Navabi[22], Mohammed Zarhrate[1], David T. Woodley[23], Mohamed Jeljeli[24], Thomas Abraham[3], Serkan Belkaya[2], Lazaro Lorenzo[1], Jérémie Rosain[1,16], Mousa Bayat[17], Fanny Lanternier[1,16], Olivier Lortholary[1,16], Faramarz Zakavi[25], Philippe Gros[4,26], Gérard Orth[27], Laurent Abel[1,2], Jean-Luc Prétet[19,32], Sylvie Fraitag[16,32], Emmanuelle Jouanguy[1,2,32], Mark M. Davis[28,32], Stuart G. Tangye[6,7,32], Luigi D. Notarangelo[12,32], Nico Marr[14,32], Tim Waterboer[15,32], David Langlais[4,26,32], John Doorbar[5,32], Alain Hovnanian[1,16,32], Neil Christensen[3,33], Xavier Bossuyt[18,33], Mohammad Shahrooei[18,22,34], Jean-Laurent Casanova[1,2,29,34,35,*]

Affiliations

[1]University of Paris, Imagine Institute, INSERM U1163, 75015 Paris, France

[2]The Rockefeller University, New York, NY 10065, USA

[3]Pennsylvania State University College of Medicine, Hershey, PA 17033, USA

[4]McGill University, Montreal, QC H3A 0G1, Canada

[5]University of Cambridge, Cambridge CB2 1QP, UK

[6]Garvan Institute of Medical Research, Darlinghurst, NSW 2010, Australia

[7]St. Vincent's Clinical School, UNSW Sydney, Sydney, NSW 2052, Australia

[8]Isfahan University of Medical Sciences, AIRC, Isfahan 81746-73461, Iran

[9]Zanjan University of Medical Sciences, Zanjan 45139-56184, Iran

[10]Stanford University Medical School, Stanford, CA 94305, USA

[11]Institute for Research in Fundamental Sciences (IPM), Tehran 19395-5746, Iran

[12]National Institute of Allergy and Infectious Diseases, NIH, Bethesda, MD 20892, USA

[13]Institute of Innovative Research, Tokyo Institute of Technology, Yokohama 226-8501, Japan

[14]Sidra Medicine, Doha, Qatar

[15]German Cancer Research Center, 69120 Heidelberg, Germany

[16]Necker Hospital for Sick Children, AP-HP, 75015 Paris, France

[17]Zahedan University of Medical Sciences, 054 Zahedan, Iran

[18]University of Leuven, 3000 Leuven, Belgium

[19]Papillomavirus National Reference Center, Besançon Hospital, 25030 Besançon, France

[20]Thomas Jefferson University, Philadelphia, PA 19107, USA

[21]Foch Hospital, 92150 Suresnes, France

[22]Dr. Shahrooei Lab, Ahvaz, Iran

[23]University of Southern California, Los Angeles, CA 90033, USA

[24]Cochin University Hospital, AP-HP, 75014 Paris, France

[25]Ahvaz Jundishapur University of Medical Sciences, 061 Ahvaz, Iran

[26]McGill Research Centre on Complex Traits, Montreal, QC H3G 0B1, Canada

[27]Pasteur Institute, 75015 Paris, France

[28]HHMI, Stanford University Medical School, Stanford, CA 94305, USA

[29]HHMI, New York, NY 10065, USA

[30]These authors contributed equally

[31]These authors contributed equally

[32]These authors contributed equally

[33]These authors contributed equally

[34]These authors contributed equally

[35]Lead contact

ACKNOWLEDGMENTS

We thank patients and families, members of the laboratory, Stephen Elledge, Genomics Core of Sidra Medicine, Primary Immunodeficiency Foundation of Sedigheh Tahereh, regional Tumor Bank of Franche-Comté (TRFC; BB-0033-00024), Integrative Biology of Emerging Infectious Diseases Laboratory of Excellence (ANR-10-LABX-62-IBEID and ANR-11-LABX-0021), French National Agency for Research (ANR-10-IAHU-01 and NKIR-ANR-13-PDOC-0025-01), ITMO Cancer of Aviesan and INCa within the framework of the 2021-2030 Cancer Control Strategy, Qatar National Research Fund (NPRP9-251-3-045), Sidra Medicine, American Association for the Study of Liver Diseases, National Health and Medical Research Council of Australia, Office of Health and Medical Research of the New South Wales State Government, National Center for Advancing Translational Sciences, National Institutes of Health Clinical and Translational Science Award program, National Institute of Dental and Craniofacial Research program, NIH, The Jake Gittlen Memorial Golf Tournament, The Gittlen Laboratories for Cancer Research, the Research Fund of Pathology Department and Cancer Institute of Penn State University College of Medicine, and JSPS KAKENHI (19H05289).

REFERENCES

Abecasis GR, Cherny SS, Cookson WO, and Cardon LR (2002). Merlin–rapid analysis of dense genetic maps using sparse gene flow trees. Nat. Genet 30, 97–101. [PubMed: 11731797]

Adzhubei IA, Schmidt S, Peshkin L, Ramensky VE, Gerasimova A, Bork P, Kondrashov AS, and Sunyaev SR (2010). A method and server for predicting damaging missense mutations. Nat. Methods 7, 248–249. [PubMed: 20354512]

Alisjahbana B, Dinata R, Sutedja E, Suryahudaya I, Soedjana H, Hidajat NN, Soetikno RD, Oktaliansah E, Deng A, Rady P, et al. (2010). Disfiguring generalized verrucosis in an indonesian man with idiopathic CD4 lymphopenia. Arch. Dermatol 146, 69–73. [PubMed: 20083696]

Anders S, Pyl PT, and Huber W (2015). HTSeq–a Python framework to work with high-throughput sequencing data. Bioinformatics 31, 166–169. [PubMed: 25260700]

Antonsson A, Green AC, Mallitt KA, O'Rourke PK, Pandeya N, Pawlita M, Waterboer T, and Neale RE (2010). Prevalence and stability of antibodies to 37 human papillomavirus types–a population-based longitudinal study. Virology 407, 26–32. [PubMed: 20723959]

Arias-Pulido H, Peyton CL, Joste NE, Vargas H, and Wheeler CM (2006). Human papillomavirus type 16 integration in cervical carcinoma in situ and in invasive cervical cancer. J. Clin. Microbiol 44, 1755–1762. [PubMed: 16672403]

Aruffo A, and Seed B (1987). Molecular cloning of a CD28 cDNA by a high-efficiency COS cell expression system. Proc. Natl. Acad. Sci. USA 84, 8573–8577. [PubMed: 2825196]

Becht E, McInnes L, Healy J, Dutertre C-A, Kwok IWH, Ng LG, Ginhoux F, and Newell EW (2018). Dimensionality reduction for visualizing single-cell data using UMAP. Nat. Biotechnol 37, 38–44.

Belkadi A, Pedergnana V, Cobat A, Itan Y, Vincent QB, Abhyankar A, Shang L, El Baghdadi J, Bousfiha A, Alcais A, et al.; Exome/Array Consortium (2016). Whole-exome sequencing to analyze population structure, parental inbreeding, and familial linkage. Proc. Natl. Acad. Sci. USA 113, 6713–6718. [PubMed: 27247391]

Béziat V (2020). Human genetic dissection of papillomavirus-driven diseases: new insight into their pathogenesis. Hum. Genet 139, 919–939. [PubMed: 32435828]

Béziat V, Descours B, Parizot C, Debré P, and Vieillard V (2010). NK cell terminal differentiation: correlated stepwise decrease of NKG2A and acquisition of KIRs. PLoS ONE 5, e11966. [PubMed: 20700504]

Béziat V, Liu LL, Malmberg JA, Ivarsson MA, Sohlberg E, Björklund AT, Retière C, Sverremark-Ekström E, Traherne J, Ljungman P, et al. (2013). NK cell responses to cytomegalovirus infection lead to stable imprints in the human KIR repertoire and involve activating KIRs. Blood 121, 2678–2688. [PubMed: 23325834]

Bhatla N, Nene BM, Joshi S, Esmy PO, Poli URR, Joshi G, Verma Y, Zomawia E, Pimple S, Prabhu PR, et al.; Indian HPV vaccine study group (2018). Are two doses of human papillomavirus vaccine sufficient for girls aged 15–18 years? Results from a cohort study in India. Papillomavirus Res. 5, 163–171. [PubMed: 29578097]

Bhatt KH, Neller MA, Srihari S, Crooks P, Lekieffre L, Aftab BT, Liu H, Smith C, Kenny L, Porceddu S, and Khanna R (2020). Profiling HPV-16-specific T cell responses reveals broad antigen reactivities in oropharyngeal cancer patients. J. Exp. Med 217, e20200389. [PubMed: 32716518]

Björkström NK, Riese P, Heuts F, Andersson S, Fauriat C, Ivarsson MA, Björklund AT, Flodström-Tullberg M, Michaëlsson J, Rottenberg ME, et al. (2010). Expression patterns of NKG2A, KIR, and CD57 define a process of CD56dim NK-cell differentiation uncoupled from NK-cell education. Blood 116, 3853–3864. [PubMed: 20696944]

Black APB, Ardern-Jones MR, Kasprowicz V, Bowness P, Jones L, Bailey AS, and Ogg GS (2007). Human keratinocyte induction of rapid effector function in antigen-specific memory CD4+ and CD8+ T cells. Eur. J. Immunol 37, 1485–1493. [PubMed: 17506032]

Breitburd F, Salmon J, and Orth G (1997). The rabbit viral skin papillomas and carcinomas: a model for the immunogenetics of HPV-associated carcinogenesis. Clin. Dermatol 15, 237–247. [PubMed: 9167908]

Casanova J-L, and Abel L (2018). Human genetics of infectious diseases: Unique insights into immunological redundancy. Semin. Immunol 36, 1–12. [PubMed: 29254755]

Chandrani P, Kulkarni V, Iyer P, Upadhyay P, Chaubal R, Das P, Mulherkar R, Singh R, and Dutt A (2015). NGS-based approach to determine the presence of HPV and their sites of integration in human cancer genome. Br. J. Cancer 112, 1958–1965. [PubMed: 25973533]

Cladel NM, Budgeon LR, Cooper TK, Balogh KK, Hu J, and Christensen ND (2013). Secondary infections, expanded tissue tropism, and evidence for malignant potential in immunocompromised mice infected with Mus musculus papillomavirus 1 DNA and virus. J. Virol 87, 9391–9395. [PubMed: 23785210]

Cladel NM, Budgeon LR, Balogh KK, Cooper TK, Hu J, and Christensen ND (2015). A novel pre-clinical murine model to study the life cycle and progression of cervical and anal papillomavirus infections. PLoS ONE 10, e0120128. [PubMed: 25803616]

Cladel NM, Budgeon LR, Balogh KK, Cooper TK, Hu J, and Christensen ND (2016). Mouse papillomavirus MmuPV1 infects oral mucosa and preferentially targets the base of the tongue. Virology 488, 73–80. [PubMed: 26609937]

Cladel NM, Budgeon LR, Cooper TK, Balogh KK, Christensen ND, Myers R, Majerciak V, Gotte D, Zheng Z-M, and Hu J (2017). Mouse papillomavirus infections spread to cutaneous sites with progression to malignancy. J. Gen. Virol 98, 2520–2529. [PubMed: 28942760]

Cladel NM, Peng X, Christensen N, and Hu J (2019a). The rabbit papillomavirus model: a valuable tool to study viral-host interactions. Philos. Trans. R. Soc. Lond. B Biol. Sci 374, 20180294. [PubMed: 30955485]

Cladel NM, Jiang P, Li JJ, Peng X, Cooper TK, Majerciak V, Balogh KK, Meyer TJ, Brendle SA, Budgeon LR, et al. (2019b). Papillomavirus can be transmitted through the blood and produce infections in blood recipients: Evidence from two animal models. Emerg. Microbes Infect 8, 1108–1121. [PubMed: 31340720]

Clifford GM, Shin H-R, Oh J-K, Waterboer T, Ju Y-H, Vaccarella S, Quint W, Pawlita M, and Franceschi S (2007). Serologic response to oncogenic human papillomavirus types in male and female university students in Busan, South Korea. Cancer Epidemiol. Biomarkers Prev. 16, 1874–1879. [PubMed: 17855708]

Cubie HA (2013). Diseases associated with human papillomavirus infection. Virology 445, 21–34. [PubMed: 23932731]

de Jong SJ, Imahorn E, Itin P, Uitto J, Orth G, Jouanguy E, Casanova J-L, and Burger B (2018a). Epidermodysplasia Verruciformis: Inborn Errors of Immunity to Human Beta-Papillomaviruses. Front. Microbiol 9, 1222. [PubMed: 29946305]

de Jong SJ, Créquer A, Matos I, Hum D, Gunasekharan V, Lorenzo L, Jabot-Hanin F, Imahorn E, Arias AA, Vahidnezhad H, et al. (2018b). The human CIB1-EVER1-EVER2 complex governs keratinocyte-intrinsic immunity to β-papillomaviruses. J. Exp. Med 215, 2289–2310. [PubMed: 30068544]

Deeks SG, Overbaugh J, Phillips A, and Buchbinder S (2015). HIV infection. Nat. Rev. Dis. Primers 1, 15035. [PubMed: 27188527]

Desmet F-O, Hamroun D, Lalande M, Collod-Béroud G, Claustres M, and Béroud C (2009). Human Splicing Finder: an online bioinformatics tool to predict splicing signals. Nucleic Acids Res 37, e67. [PubMed: 19339519]

Dobin A, Davis CA, Schlesinger F, Drenkow J, Zaleski C, Jha S, Batut P, Chaisson M, and Gingeras TR (2013). STAR: ultrafast universal RNA-seq aligner. Bioinformatics 29, 15–21. [PubMed: 23104886]

Doorbar J (2006). Molecular biology of human papillomavirus infection and cervical cancer. Clin. Sci. (Lond.) 110, 525–541. [PubMed: 16597322]

Doorbar J, Coneron I, and Gallimore PH (1989). Sequence divergence yet conserved physical characteristics among the E4 proteins of cutaneous human papillomaviruses. Virology 172, 51–62. [PubMed: 2549722]

Doorbar J, Egawa N, Griffin H, Kranjec C, and Murakami I (2015). Human papillomavirus molecular biology and disease association. Rev. Med. Virol 25 (Suppl 1), 2–23. [PubMed: 25752814]

Drutman SB, Mansouri D, Mahdaviani SA, Neehus A-L, Hum D, Bryk R, Hernandez N, Belkaya S, Rapaport F, Bigio B, et al. (2020). Fatal Cytomegalovirus Infection in an Adult with Inherited NOS2 Deficiency. N. Engl. J. Med 382, 437–445. [PubMed: 31995689]

Esensten JH, Helou YA, Chopra G, Weiss A, and Bluestone JA (2016). CD28 costimulation: from mechanism to therapy. Immunity 44, 973–988. [PubMed: 27192564]

Finak G, McDavid A, Yajima M, Deng J, Gersuk V, Shalek AK, Slichter CK, Miller HW, McElrath MJ, Prlic M, et al. (2015). MAST: a flexible statistical framework for assessing transcriptional changes and characterizing heterogeneity in single-cell RNA sequencing data. Genome Biol. 16, 278. [PubMed: 26653891]

Gehring JS, Fischer B, Lawrence M, and Huber W (2015). SomaticSignatures: inferring mutational signatures from single-nucleotide variants. Bioinformatics 31, 3673–3675. [PubMed: 26163694]

Giri I, Danos O, and Yaniv M (1985). Genomic structure of the cottontail rabbit (Shope) papillomavirus. Proc. Natl. Acad. Sci. USA 82, 1580–1584. [PubMed: 2984661]

Glanville J, Huang H, Nau A, Hatton O, Wagar LE, Rubelt F, Ji X, Han A, Krams SM, Pettus C, et al. (2017). Identifying specificity groups in the T cell receptor repertoire. Nature 547, 94–98. [PubMed: 28636589]

Gray E, Pett MR, Ward D, Winder DM, Stanley MA, Roberts I, Scarpini CG, and Coleman N (2010). In vitro progression of human papillomavirus 16 episome-associated cervical neoplasia displays fundamental similarities to integrant-associated carcinogenesis. Cancer Res. 70, 4081–4091. [PubMed: 20442284]

Gu Z, Eils R, and Schlesner M (2016). Complex heatmaps reveal patterns and correlations in multidimensional genomic data. Bioinformatics 32, 2847–2849. [PubMed: 27207943]

Han R, Breitburd F, Marche PN, and Orth G (1992). Linkage of regression and malignant conversion of rabbit viral papillomas to MHC class II genes. Nature 356, 66–68. [PubMed: 1347151]

Handisurya A, Day PM, Thompson CD, Bonelli M, Lowy DR, and Schiller JT (2014). Strain-specific properties and T cells regulate the susceptibility to papilloma induction by Mus musculus papillomavirus 1. PLoS Pathog. 10, e1004314. [PubMed: 25121947]

Hara T, Fu SM, and Hansen JA (1985). Human T cell activation. II. A new activation pathway used by a major T cell population via a disulfide-bonded dimer of a 44 kilodalton polypeptide (9.3 antigen). J. Exp. Med 161, 1513–1524. [PubMed: 3159820]

Hasan MR, Rahman M, Khan T, Saeed A, Sundararaju S, Flores A, Hawken P, Rawat A, Elkum N, Hussain K, et al. (2021). Virome-wide serological profiling reveals association of herpesviruses with obesity. Sci. Rep 11, 2562. [PubMed: 33510449]

Hu J, Budgeon LR, Cladel NM, Balogh K, Myers R, Cooper TK, and Christensen ND (2015). Tracking vaginal, anal and oral infection in a mouse papillomavirus infection model. J. Gen. Virol 96, 3554–3565. [PubMed: 26399579]

Hu J, Cladel NM, Budgeon LR, Balogh KK, and Christensen ND (2017). The Mouse Papillomavirus Infection Model. Viruses 9, 246.

Huang X, Summers MK, Pham V, Lill JR, Liu J, Lee G, Kirkpatrick DS, Jackson PK, Fang G, and Dixit VM (2011). Deubiquitinase USP37 is activated by CDK2 to antagonize APC(CDH1) and promote S phase entry. Mol. Cell 42, 511–523. [PubMed: 21596315]

Ingle A, Ghim S, Joh J, Chepkoech I, Bennett Jenson A, and Sundberg JP (2011). Novel laboratory mouse papillomavirus (MusPV) infection. Vet. Pathol 48, 500–505. [PubMed: 20685915]

Isnard P, Kula T, Avettand Fenoel V, Anglicheau D, Terzi F, Legendre C, Elledge SJ, and Canaud G (2019). Temporal virus serological profiling of kidney graft recipients using VirScan. Proc. Natl. Acad. Sci. USA 116, 10899–10904. [PubMed: 31085644]

Itan Y, Shang L, Boisson B, Ciancanelli MJ, Markle JG, Martinez-Barricarte R, Scott E, Shah I, Stenson PD, Gleeson J, et al. (2016). The mutation significance cutoff: gene-level thresholds for variant predictions. Nat. Methods 13, 109–110. [PubMed: 26820543]

Jablonska S, Orth G, Obalek S, and Croissant O (1985). Cutaneous warts. Clinical, histologic, and virologic correlations. Clin. Dermatol 3, 71–82. [PubMed: 2850861]

Kerner G, Rosain J, Guérin A, Al-Khabaz A, Oleaga-Quintas C, Rapaport F, Massaad MJ, Ding J-Y, Khan T, Ali FA, et al. (2020). Inherited human IFN-γ deficiency underlies mycobacterial disease. J. Clin. Invest 130, 3158–3171. [PubMed: 32163377]

Khan T, Rahman M, Ali FA, Huang SSY, Ata M, Zhang Q, Bastard P, Liu Z, Jouanguy E, Béziat V, et al. (2021). Distinct antibody repertoires against endemic human coronaviruses in children and adults. JCI Insight 6, e144499.

Kircher M, Witten DM, Jain P, O'Roak BJ, Cooper GM, and Shendure J (2014). A general framework for estimating the relative pathogenicity of human genetic variants. Nat. Genet 46, 310–315. [PubMed: 24487276]

Koboldt DC, Zhang Q, Larson DE, Shen D, McLellan MD, Lin L, Miller CA, Mardis ER, Ding L, and Wilson RK (2012). VarScan 2: somatic mutation and copy number alteration discovery in cancer by exome sequencing. Genome Res. 22, 568–576. [PubMed: 22300766]

Kündig TM, Shahinian A, Kawai K, Mittrücker H-W, Sebzda E, Bachmann MF, Mak TW, and Ohashi PS (1996). Duration of TCR stimulation determines costimulatory requirement of T cells. Immunity 5, 41–52. [PubMed: 8758893]

Lei Y-J, Wang C, Gao C, Jiang H-Y, Chen J-M, Han J, Yuan Y-K, and Dong X-P (2007). HPV-2 isolates from patients with huge verrucae vulgaris possess stronger promoter activities. Intervirology 50, 353–360. [PubMed: 17728546]

Li H (2013). Aligning sequence reads, clone sequences and assembly contigs with BWA-MEM. arXiv, arXiv:1303.3997.

Li H, and Durbin R (2010). Fast and accurate long-read alignment with Burrows-Wheeler transform. Bioinformatics 26, 589–595. [PubMed: 20080505]

Li H, Handsaker B, Wysoker A, Fennell T, Ruan J, Homer N, Marth G, Abecasis G, and Durbin R; 1000 Genome Project Data Processing Subgroup (2009). The Sequence Alignment/Map format and SAMtools. Bioinformatics 25, 2078–2079. [PubMed: 19505943]

Love MI, Huber W, and Anders S (2014). Moderated estimation of fold change and dispersion for RNA-seq data with DESeq2. Genome Biol. 15, 550. [PubMed: 25516281]

MacArthur H, and Walter G (1984). Monoclonal antibodies specific for the carboxy terminus of simian virus 40 large T antigen. J. Virol. 52, 483–491. 10.1128/jvi.52.2.483-491.1984. [PubMed: 6208378]

Mantese SA de O, Diogo PM, Rocha A, Berbert ALCV, Ferreira AKM, and Ferreira TC (2010). Cutaneous horn: a retrospective histopathological study of 222 cases. An. Bras. Dermatol 85, 157–163. [PubMed: 20520930]

Martins GA, Campanelli AP, Silva RB, Tadokoro CE, Russo M, Cunha FQ, Rizzo LV, and Silva JS (2004). CD28 is required for T cell activation and IFN-gamma production by CD4+ and CD8+ T cells in response to Trypanosoma cruzi infection. Microbes Infect. 6, 1133–1144. [PubMed: 15488732]

McGinnis CS, Murrow LM, and Gartner ZJ (2019). DoubletFinder: Doublet Detection in Single-Cell RNA Sequencing Data Using Artificial Nearest Neighbors. Cell Syst. 8, 329–337.e4. [PubMed: 30954475]

McKenna A, Hanna M, Banks E, Sivachenko A, Cibulskis K, Kernytsky A, Garimella K, Altshuler D, Gabriel S, Daly M, and DePristo MA (2010). The Genome Analysis Toolkit: a MapReduce framework for analyzing next-generation DNA sequencing data. Genome Res. 20, 1297–1303. [PubMed: 20644199]

Michael KM, Waterboer T, Sehr P, Rother A, Reidel U, Boeing H, Bravo IG, Schlehofer J, Gärtner BC, and Pawlita M (2008). Seroprevalence of 34 human papillomavirus types in the German general population. PLoS Pathog. 4, e1000091. [PubMed: 18566657]

Mina MJ, Kula T, Leng Y, Li M, de Vries RD, Knip M, Siljander H, Rewers M, Choy DF, Wilson MS, et al. (2019). Measles virus infection diminishes preexisting antibodies that offer protection from other pathogens. Science 366, 599–606. [PubMed: 31672891]

Mittrücker H-W, Köhler A, Mak TW, and Kaufmann SHE (1999). Critical role of CD28 in protective immunity against Salmonella typhimurium. J. Immunol 163, 6769–6776. [PubMed: 10586076]

Mittrücker H-W, Kursar M, Köhler A, Hurwitz R, and Kaufmann SHE (2001). Role of CD28 for the generation and expansion of antigen-specific CD8(+) T lymphocytes during infection with Listeria monocytogenes. J. Immunol 167, 5620–5627. [PubMed: 11698433]

Mohan D, Wansley DL, Sie BM, Noon MS, Baer AN, Laserson U, and Larman HB (2019). Publisher Correction: PhIP-Seq characterization of serum antibodies using oligonucleotide-encoded peptidomes. Nat. Protoc 14, 2596.

Ng PC, and Henikoff S (2001). Predicting deleterious amino acid substitutions. Genome Res. 11, 863–874. [PubMed: 11337480]

Notarangelo LD, Bacchetta R, Casanova J-L, and Su HC (2020). Human inborn errors of immunity: An expanding universe. Sci. Immunol 5, eabb1662. [PubMed: 32651211]

Olshen AB, Venkatraman ES, Lucito R, and Wigler M (2004). Circular binary segmentation for the analysis of array-based DNA copy number data. Biostatistics 5, 557–572. [PubMed: 15475419]

Orlik C, Deibel D, Küblbeck J, Balta E, Ganskih S, Habicht J, Niesler B, Schröder-Braunstein J, Schäkel K, Wabnitz G, and Samstag Y (2020). Keratinocytes costimulate naive human T cells via CD2: a potential target to prevent the development of proinflammatory Th1 cells in the skin. Cell. Mol. Immunol 17, 380–394. [PubMed: 31324882]

Orth G, Favre M, and Croissant O (1977). Characterization of a new type of human papillomavirus that causes skin warts. J. Virol 24, 108–120. [PubMed: 198572]

Peh WL, Middleton K, Christensen N, Nicholls P, Egawa K, Sotlar K, Brandsma J, Percival A, Lewis J, Liu WJ, and Doorbar J (2002). Life cycle heterogeneity in animal models of human papillomavirus-associated disease. J. Virol 76, 10401–10416. [PubMed: 12239317]

Petersen TN, Brunak S, von Heijne G, and Nielsen H (2011). SignalP 4.0: discriminating signal peptides from transmembrane regions. Nat. Methods 8, 785–786. [PubMed: 21959131]

Pillay BA, Fusaro M, Gray PE, Statham AL, Burnett L, Bezrodnik L, Kane A, Tong WWY, Abdo C, Winter S, et al. (2021). Somatic reversion of pathogenic DOCK8 variants alters lymphocyte differentiation and function to effectively cure DOCK8 deficiency. J. Clin. Invest 131, 142434. [PubMed: 33290277]

Ramoz N, Rueda L-A, Bouadjar B, Montoya L-S, Orth G, and Favre M (2002). Mutations in two adjacent novel genes are associated with epidermodysplasia verruciformis. Nat. Genet 32, 579–581. [PubMed: 12426567]

Riley JL, Mao M, Kobayashi S, Biery M, Burchard J, Cavet G, Gregson BP, June CH, and Linsley PS (2002). Modulation of TCR-induced transcriptional profiles by ligation of CD28, ICOS, and CTLA-4 receptors. Proc. Natl. Acad. Sci. USA 99, 11790–11795. [PubMed: 12195015]

Robinson MD, and Oshlack A (2010). A scaling normalization method for differential expression analysis of RNA-seq data. Genome Biol. 11, R25. [PubMed: 20196867]

Robinson JT, Thorvaldsdóttir H, Winckler W, Guttman M, Lander ES, Getz G, and Mesirov JP (2011). Integrative genomics viewer. Nat. Biotechnol 29, 24–26. [PubMed: 21221095]

Rous P, and Beard JW (1934). A Virus-Induced Mammalian Growth with the Characters of a Tumor (the Shope Rabbit Papilloma): I. the Growth on Implantation Within Favorable Hosts. J. Exp. Med 60, 701–722. [PubMed: 19870333]

Rudd CE, Taylor A, and Schneider H (2009). CD28 and CTLA-4 coreceptor expression and signal transduction. Immunol. Rev 229, 12–26. [PubMed: 19426212]

Salomon B, Lenschow DJ, Rhee L, Ashourian N, Singh B, Sharpe A, and Bluestone JA (2000). B7/CD28 costimulation is essential for the homeostasis of the CD4+CD25+ immunoregulatory T cells that control autoimmune diabetes. Immunity 12, 431–440. [PubMed: 10795741]

Sankaranarayanan R, Prabhu PR, Pawlita M, Gheit T, Bhatla N, Muwonge R, Nene BM, Esmy PO, Joshi S, Poli URR, et al.; Indian HPV Vaccine Study Group (2016). Immunogenicity and HPV infection after one, two, and three doses of quadrivalent HPV vaccine in girls in India: a multicentre prospective cohort study. Lancet Oncol. 17, 67–77. [PubMed: 26652797]

Schiffman M, Doorbar J, Wentzensen N, de Sanjosé S, Fakhry C, Monk BJ, Stanley MA, and Franceschi S (2016). Carcinogenic human papillomavirus infection. Nat. Rev. Dis. Primers 2, 16086. [PubMed: 27905473]

Schindelin J, Arganda-Carreras I, Frise E, Kaynig V, Longair M, Pietzsch T, Preibisch S, Rueden C, Saalfeld S, Schmid B, et al. (2012). Fiji: an open-source platform for biological-image analysis. Nat. Methods 9, 676–682. [PubMed: 22743772]

Schmitt M, Bravo IG, Snijders PJF, Gissmann L, Pawlita M, and Waterboer T (2006). Bead-based multiplex genotyping of human papillomaviruses. J. Clin. Microbiol 44, 504–512. [PubMed: 16455905]

Schober T, Magg T, Laschinger M, Rohlfs M, Linhares ND, Puchalka J, Weisser T, Fehlner K, Mautner J, Walz C, et al. (2017). A human immunodeficiency syndrome caused by mutations in CARMIL2. Nat. Commun 8, 14209. [PubMed: 28112205]

Sehr P, Zumbach K, and Pawlita M (2001). A generic capture ELISA for recombinant proteins fused to glutathione S-transferase: validation for HPV serology. J. Immunol. Methods 253, 153–162. [PubMed: 11384677]

Semple K, Nguyen A, Yu Y, Wang H, Anasetti C, and Yu X-Z (2011). Strong CD28 costimulation suppresses induction of regulatory T cells from naive precursors through Lck signaling. Blood 117, 3096–3103. [PubMed: 21245484]

Shahinian A, Pfeffer K, Lee KP, Kündig TM, Kishihara K, Wakeham A, Kawai K, Ohashi PS, Thompson CB, and Mak TW (1993). Differential T cell costimulatory requirements in CD28-deficient mice. Science 261, 609–612. [PubMed: 7688139]

Shope RE, and Hurst EW (1933). Infectious Papillomatosis of Rabbits: With a Note on the Histopathology. J. Exp. Med 58, 607–624. [PubMed: 19870219]

Smelov V, Muwonge R, Sokolova O, McKay-Chopin S, Eklund C, Komyakov B, and Gheit T (2018). Beta and gamma human papillomaviruses in anal and genital sites among men: prevalence and determinants. Sci. Rep 8, 8241. [PubMed: 29844517]

Stewart SA, Dykxhoorn DM, Palliser D, Mizuno H, Yu EY, An DS, Sabatini DM, Chen ISY, Hahn WC, Sharp PA, et al. (2003). Lentivirusdelivered stable gene silencing by RNAi in primary cells. RNA 9, 493–501. [PubMed: 12649500]

Strickley JD, Messerschmidt JL, Awad ME, Li T, Hasegawa T, Ha DT, Nabeta HW, Bevins PA, Ngo KH, Asgari MM, et al. (2019). Immunity to commensal papillomaviruses protects against skin cancer. Nature 575, 519–522. [PubMed: 31666702]

Stuart T, Butler A, Hoffman P, Hafemeister C, Papalexi E, Mauck WM 3rd, Hao Y, Stoeckius M, Smibert P, and Satija R (2019). Comprehensive Integration of Single-Cell Data. Cell 177, 1888–1902.e21. [PubMed: 31178118]

Tai X, Cowan M, Feigenbaum L, and Singer A (2005). CD28 costimulation of developing thymocytes induces Foxp3 expression and regulatory T cell differentiation independently of interleukin 2. Nat. Immunol 6, 152–162. [PubMed: 15640801]

Tang Q, Henriksen KJ, Boden EK, Tooley AJ, Ye J, Subudhi SK, Zheng XX, Strom TB, and Bluestone JA (2003). Cutting edge: CD28 controls peripheral homeostasis of CD4+CD25+ regulatory T cells. J. Immunol 171, 3348–3352. [PubMed: 14500627]

Tanno H, Shigematsu T, Nishikawa S, Hayakawa A, Denda K, Tanaka T, and Komada M (2014). Ubiquitin-interacting motifs confer full catalytic activity, but not ubiquitin chain substrate specificity, to deubiquitinating enzyme USP37. J. Biol. Chem 289, 2415–2423. [PubMed: 24324262]

Typas D, Luijsterburg MS, Wiegant WW, Diakatou M, Helfricht A, Thijssen PE, van den Broek B, Mullenders LH, and van Attikum H (2015). The de-ubiquitylating enzymes USP26 and USP37 regulate homologous recombination by counteracting RAP80. Nucleic Acids Res. 43, 6919–6933. [PubMed: 26101254]

Uddin KMF, Amin R, Majumder SN, Aleem MA, Rahaman A, Dity NJ, Baqui MDA, Akter H, Rahman MM, Woodbury-Smith M, et al. (2018). An ANKRD26 nonsense somatic mutation in a female with epidermodysplasia verruciformis (Tree Man Syndrome). Clin. Case Rep. 6, 1426–1430. [PubMed: 30147876]

Van Doorslaer K, Tan Q, Xirasagar S, Bandaru S, Gopalan V, Mohamoud Y, Huyen Y, and McBride AA (2013). The Papillomavirus Episteme: a central resource for papillomavirus sequence data and analysis. Nucleic Acids Res. 41, D571–D578. [PubMed: 23093593]

Vinokurova S, Wentzensen N, Kraus I, Klaes R, Driesch C, Melsheimer P, Kisseljov F, Dürst M, Schneider A, and von Knebel Doeberitz M (2008). Type-dependent integration frequency of human papillomavirus genomes in cervical lesions. Cancer Res. 68, 307–313. [PubMed: 18172324]

Wang C, Wang W, Lei YJ, Wang JY, Dong XP, Wang J, Sheng RH, Pan ZA, Zhu WY, You LP, et al. (2007a). Multiple huge cutaneous horns overlying verrucae vulgaris induced by human papillomavirus type 2: a case report. Br. J. Dermatol 156, 760–762. [PubMed: 17493077]

Wang W, Wang C, Xu S, Chen C, Tong X, Liang Y, Dong X, Lei Y, Zheng X, Yu J, and Wang J (2007b). Detection of HPV-2 and identification of novel mutations by whole genome sequencing from biopsies of two patients with multiple cutaneous horns. J. Clin. Virol 39, 34–42. [PubMed: 17368088]

Wang L, Wang S, and Li W (2012). RSeQC: quality control of RNA-seq experiments. Bioinformatics 28, 2184–2185. [PubMed: 22743226]

Wang JW, Jiang R, Peng S, Chang Y-N, Hung C-F, and Roden RBS (2015). Immunologic Control of Mus musculus Papillomavirus Type 1. PLoS Pathog. 11, e1005243. [PubMed: 26495972]

Wang Y, Ma CS, Ling Y, Bousfiha A, Camcioglu Y, Jacquot S, Payne K, Crestani E, Roncagalli R, Belkadi A, et al. (2016). Dual T cell- and B cell-intrinsic deficiency in humans with biallelic RLTPR mutations. J. Exp. Med 213, 2413–2435. [PubMed: 27647349]

Waterboer T, Sehr P, Michael KM, Franceschi S, Nieland JD, Joos TO, Templin MF, and Pawlita M (2005). Multiplex human papillomavirus serology based on in situ-purified glutathione s-transferase fusion proteins. Clin. Chem 51, 1845–1853. [PubMed: 16099939]

Waterboer T, Neale R, Michael KM, Sehr P, de Koning MNC, Weißenborn SJ, Sampogna F, Abeni D, Green AC, Bouwes Bavinck JN, and Pawlita M; The Epi-Hpv-Uv-Ca Group (2009). Antibody responses to 26 skin human papillomavirus types in the Netherlands, Italy and Australia. J. Gen. Virol 90, 1986–1998. [PubMed: 19386782]

Xu GJ, Kula T, Xu Q, Li MZ, Vernon SD, Ndung'u T, Ruxrungtham K, Sanchez J, Brander C, Chung RT, et al. (2015). Viral immunology. Comprehensive serological profiling of human populations using a synthetic human virome. Science 348, aaa0698. [PubMed: 26045439]

Yu RCH, Pryce DW, Macfarlane AW, and Stewart TW (1991). A histopathological study of 643 cutaneous horns. Br. J. Dermatol 124, 449–452. [PubMed: 2039721]

Highlights

- Inherited human CD28 deficiency underlies severe HPV-2 and HPV-4 skin lesions
- Human CD28 is otherwise largely redundant in protective immunity to infection
- Inherited CD28 deficiency only slightly impairs T cell development and function
- HPV-2 giant horns overexpress HPV oncogenes in the basal layer of the epidermis

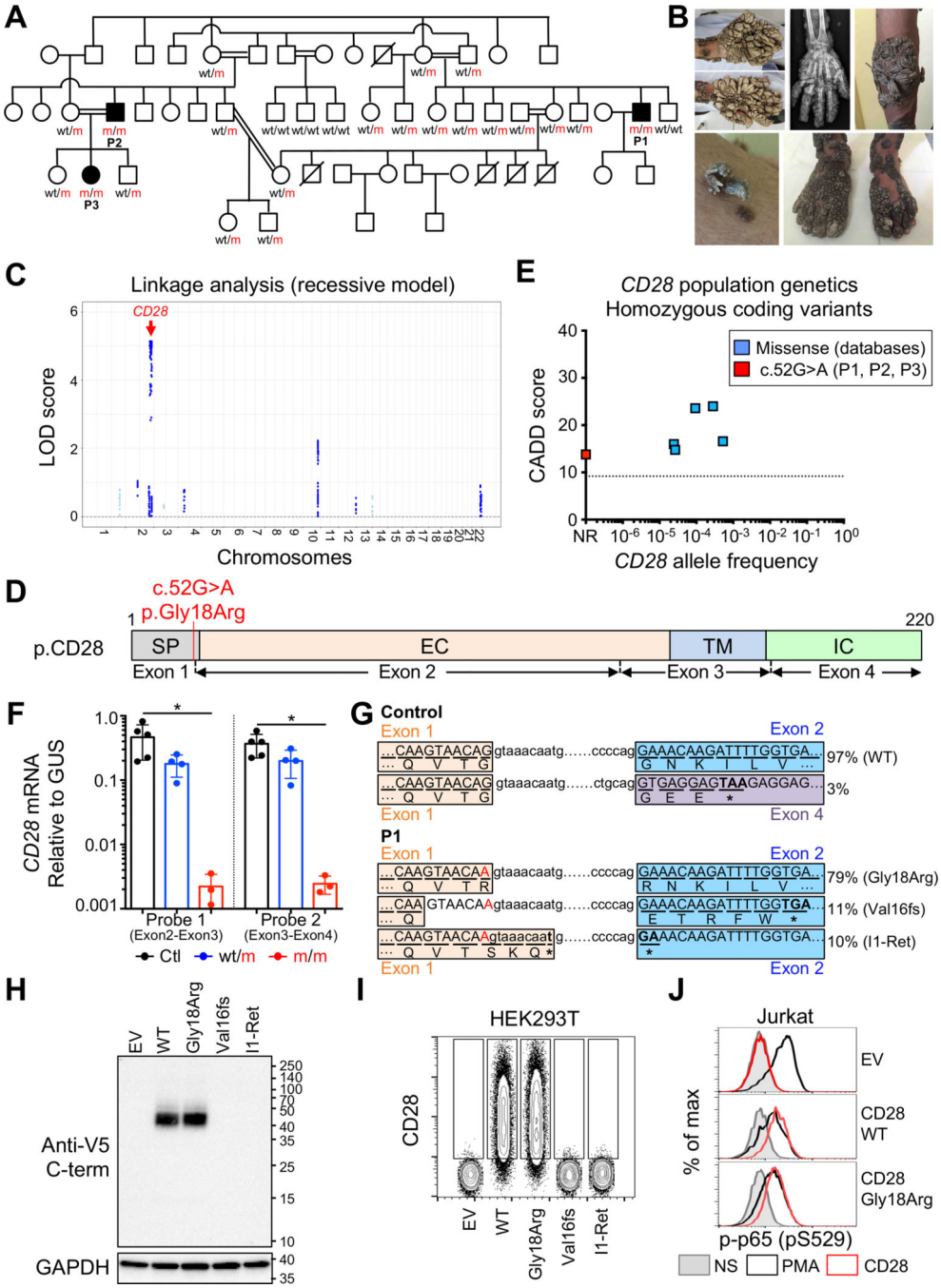

Figure 1. Autosomal recessive CD28 deficiency and "tree man" syndrome

(A) Pedigree showing familial segregation of the *c.52G>A* mutant *CD28* allele.

(B) Images of the TMS phenotype of P1 and X-ray of the right hand of P1 showing that the lesions have not extended to the bones.

(C) Genome-wide linkage analysis on DNA from 16 members of the kindred, assuming AR mode of inheritance, with complete penetrance. The linkage region with the highest LOD score was on chromosome 2 and contained *CD28* (red arrow).

(D) Schematic representation of CD28 protein. SP, signal peptide; EC, extracellular domain; TM, transmembrane domain; IC, intracellular domain. Exons and exon boundaries are depicted below. The mutation is indicated with a red line.
(E) Frequency and CADD score for all *CD28* variants reported homozygous in the public databases. The dotted line corresponds to the MSC. NR, not reported. The private c.52G>A mutation appears in red.
(F) Reverse transcription qPCR for total *CD28* with two different probes representative of three independent experiments. Bars represent the mean and the SD. Mann-Whitney tests were used for comparisons.
(G) Reverse transcription PCR from PHA blasts from one control and P1 was performed to amplify the sequence between the 5′ and 3′ UTRs of the *CD28* cDNA for insertion into a vector. We sequenced 190 colonies for the control and 106 for P1. The splice variants involving the splice donor site of exon 1, and their respective frequencies are shown. The amino acid sequence encoded by each transcript is shown below the nucleotide sequence.
(H and I) HEK293T cells were transfected with an empty vector (EV) or with vectors encoding the indicated CD28 transcripts. (H) Immunoblotting with a monoclonal antibody against the V5 tag and GAPDH. (I) Cell surface CD28 levels.
(J) Jurkat cells were transduced with an EV or a plasmid encoding the indicated CD28 cDNA. Phospho-p65 (p-p65) was detected by flow cytometry after the crosslinking of CD28 or PMA stimulation. (H–J) Data representative of three independent experiments.
See also Figures S1, S2, and S3 and Data S1.

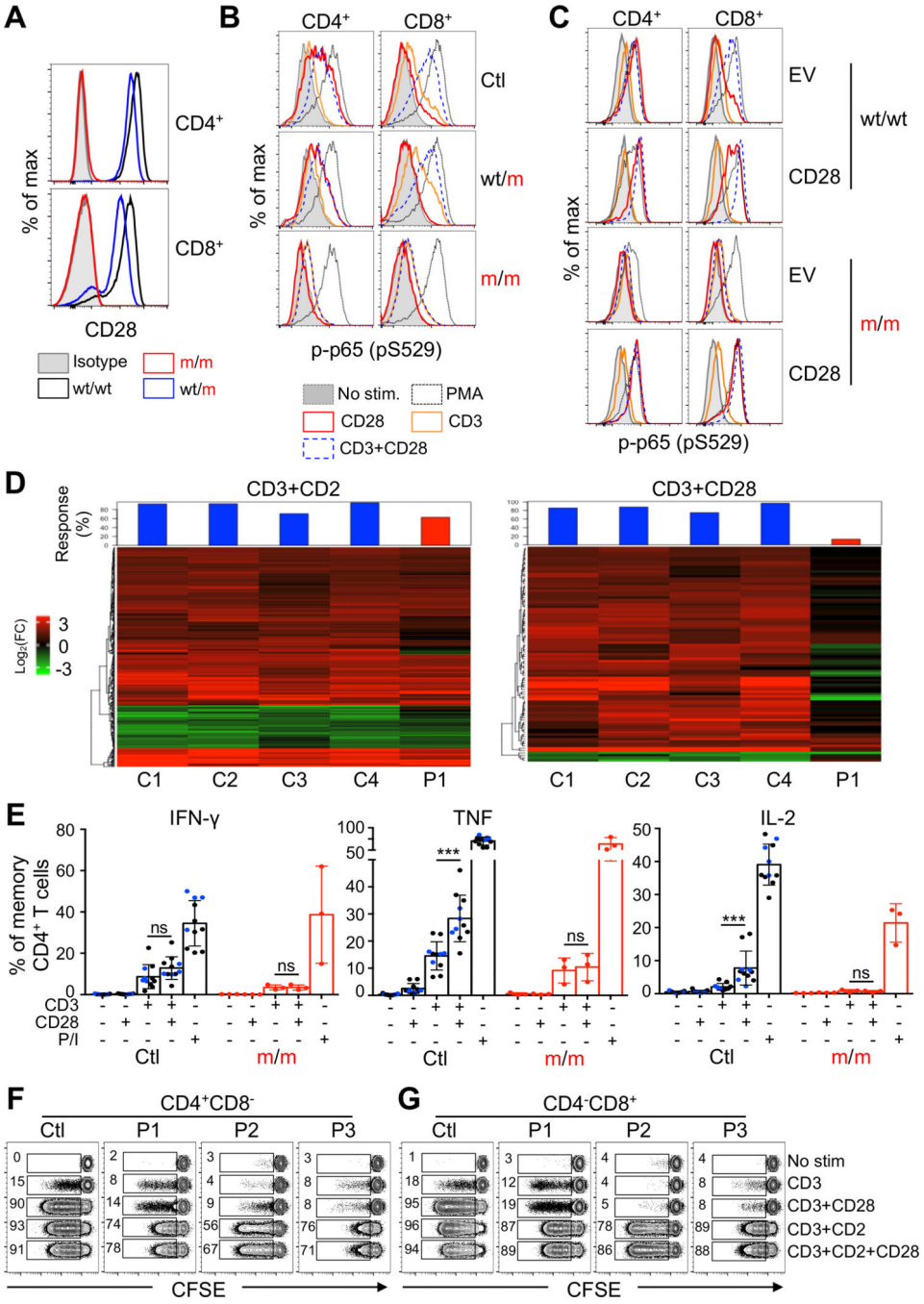

Figure 2. Abolished CD28 response in the patients' primary T cells

(A) Representative fluorescence-activated cell sorting (FACS) plots showing CD28 expression on PHA blasts from patients, heterozygotes, and controls.

(B) Phospho-p65 (p-p65) detection in $CD4^+$ (left) and $CD8^+$ (right) PHA blasts from P1 (m/m), a heterozygote (wt/m) and a healthy control (wt/wt), after crosslinking of the indicated cell surface receptors. Representative of two independent experiments.

(C) PHA blasts from one control (top) and P1 (bottom) were transduced with an empty vector (EV) or a vector encoding the wild-type CD28. Phospho-p65 (p-p65) detection by

flow cytometry in $CD4^+mCherry^+$ (left) and $CD8^+mCherry^+$ (right) PHA blasts after crosslinking of the indicated cell surface receptors. (B and C) PMA stimulation was used as a positive control.

(D) RNA-seq analysis of primary $CD4^+$ T cells. Compared to CD3 stimulation alone, 368 and 91 genes were significantly up- or downregulated in control's cell stimulated by CD3+CD2 (left) or CD3+CD28 (right), respectively. The residual responses of the CD28-deficient patient are shown as percentage in the red bar charts for each condition.

(E) Frequency of indicated cytokine in $CD4^+$ memory T cells from healthy controls and patients after stimulation with PMA and ionomycin, or P815 cells in the presence of anti-CD3 and/or anti-CD28 mAbs. Graphs show the mean ± SD. Wilcoxon tests were used for comparisons.

(F and G) CFSE dilution of $CD4^+$ (F) and $CD8^+$ (G) T cells from a control, P1, P2, and P3 after 5 day stimulation with beads coated with the indicated combination of CD2, CD3, and CD28 mAbs. Numbers indicate frequencies of proliferating cells in each condition. Data representative of 2–3 independent experiments.

See also Figure S4 and Table S1.

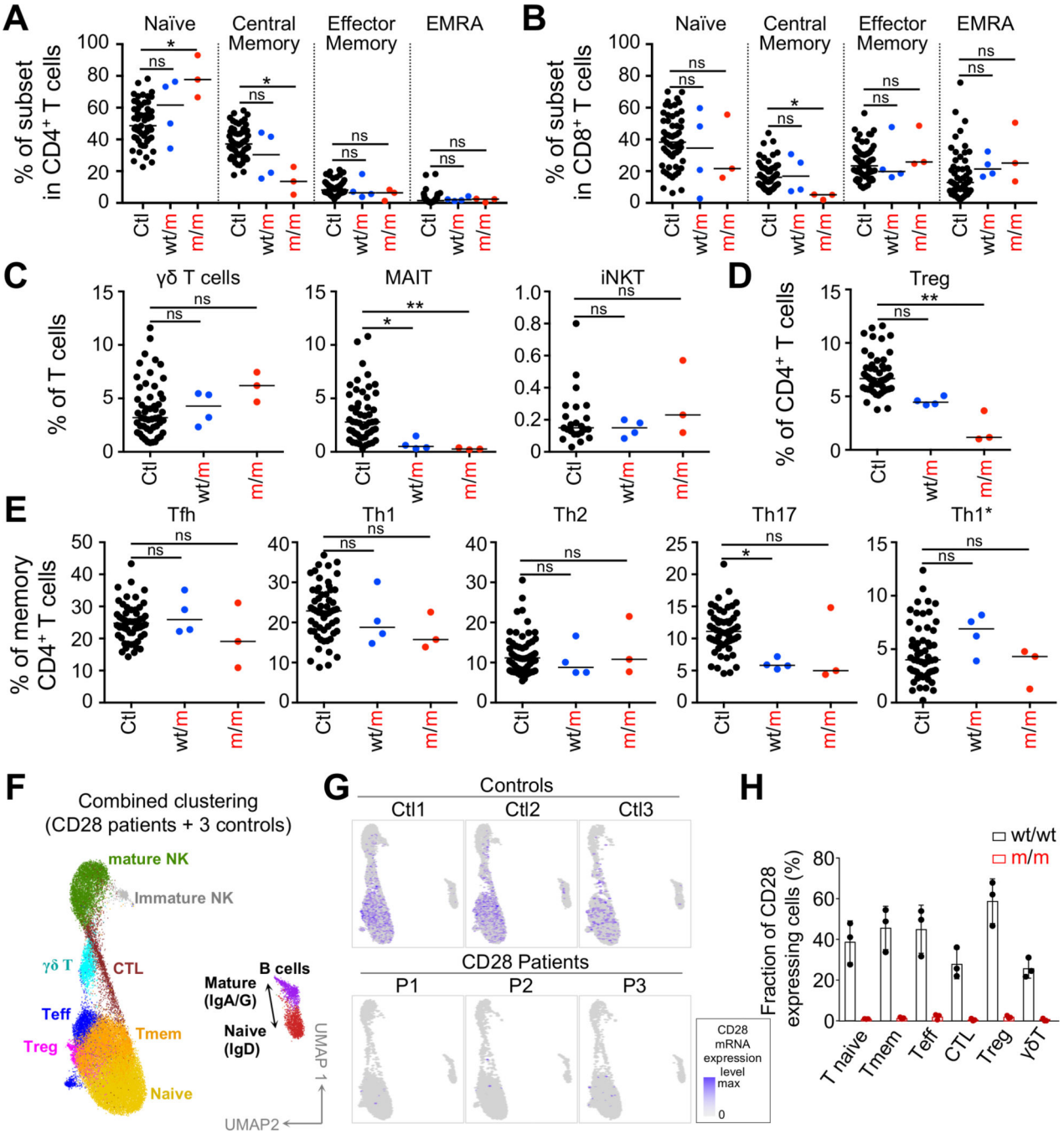

Figure 3. CD28 deficiency has a mild impact on lymphocyte subset development

(A–E) Frequency of indicated T cell subsets of controls (n = 23–57), heterozygotes (n = 4), and patients (n = 3). Kruskal-Wallis tests were used for all comparisons. The bars represent the median.

(F) scRNA-seq UMAP clustering of PBMC from 3 *CD28* homozygous patients together with a set of 3 controls. CTL, cytotoxic T cells; Teff, effector T cells; Tmem, memory T cells.

(G) CD28 expression level superimposed on the scRNA-seq UMAP clustering.

(H) Fraction of $CD28^+$ cells in T cell subsets indicated and as defined by single-cell RNA-seq UMAP clustering. Graphs show the mean ± SD.
See also Figures S4, S5, and S6, Table S2, and Data S1.

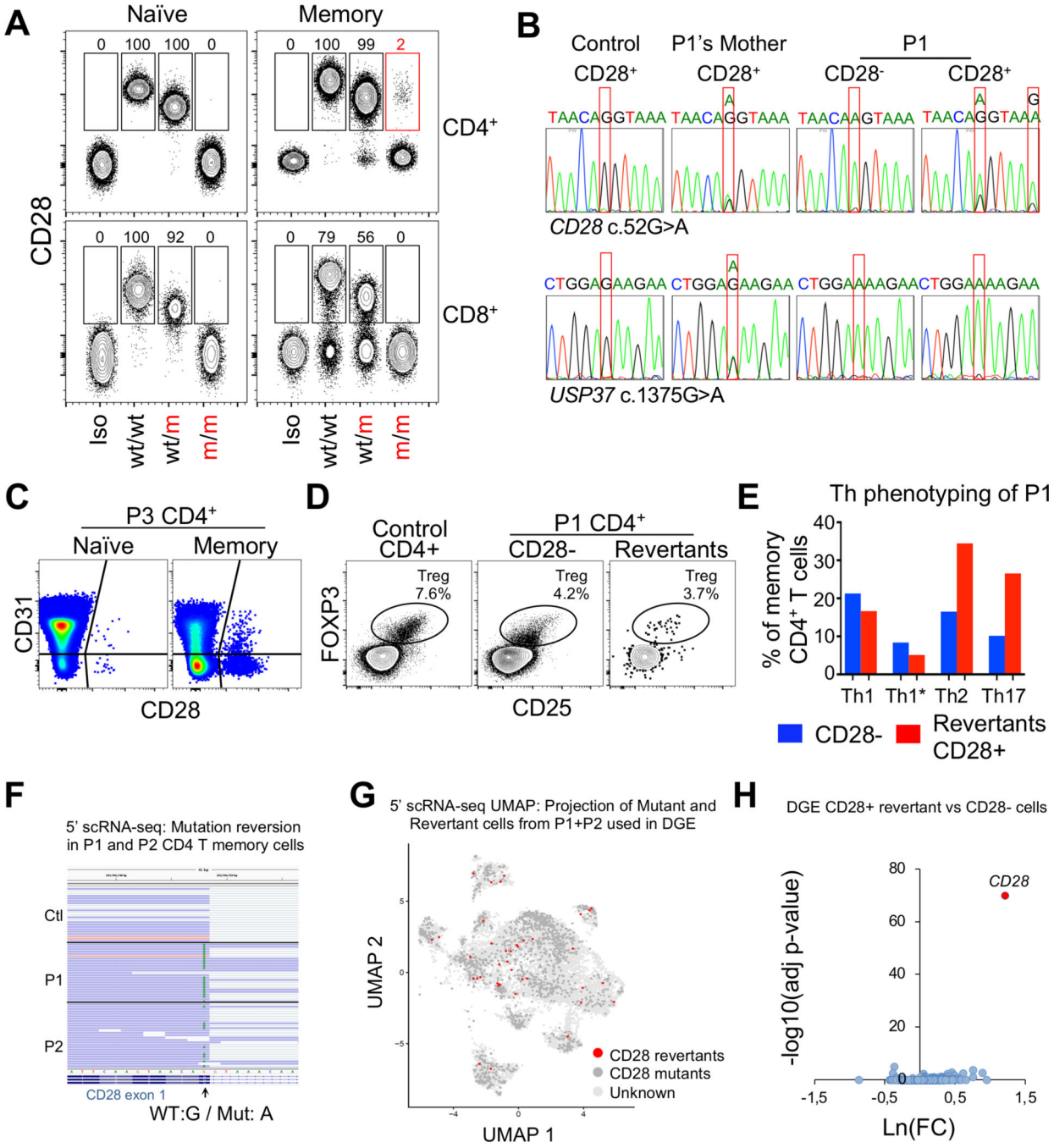

Figure 4. Evidence for somatic mosaicism in the patients' memory CD4$^+$ T cells

(A) CD28 expression on the indicated T cell subsets from P1 (m/m), a heterozygote (wt/m), and a healthy control (wt/wt). Isotype control (Iso) was used as a negative control. Representative data from the 3 patients and 4 heterozygotes. Numbers are frequencies of CD28$^+$ cells in the indicated subset of each donor.

(B) Sanger sequencing chromatograms of the c.52G>A mutation in gDNA from a control, P1's mother, and CD28$^-$ and CD28$^+$ CD4$^+$ memory T cells from P1 (upper line). A rare

mutation of *USP37* (c.1375G>A) was used to demonstrate that the $CD28^+CD4^+$ memory T cells sorted from P1 were not of maternal origin (bottom line).

(C) FACS plots of CD28 expression on recent thymic emigrants ($CD31^+CD4^+$ T cells).

(D) FACS plots showing Tregs in $CD4^+$ T cells of one control or $CD28^-$ or $CD28^+$ (revertant) $CD4^+$ T cells from P1.

(E) Comparison of Th subset frequencies in $CD28^-$ and $CD28^+$ (revertant) memory $CD4^+$ T cells from P1.

(F–H) CITE-seq analysis of CD4 memory T cells from a control, P1, and P2.

(F) Sequence reads showing the presence or absence of the reversion in RNA from P1 and P2 cells.

(G) UMAP clustering of patients' CD4 memory T cells with a projection of CD28 revertant identified using strict selection criteria. Cells with no detectable CD28 RNA or protein were considered mutants (dark gray).

(H) Volcano plot for a differential gene expression (DGE) analysis comparing CD28 revertant with $CD28^-$ cells, as shown in (G).

See also Figure S7 and Data S1.

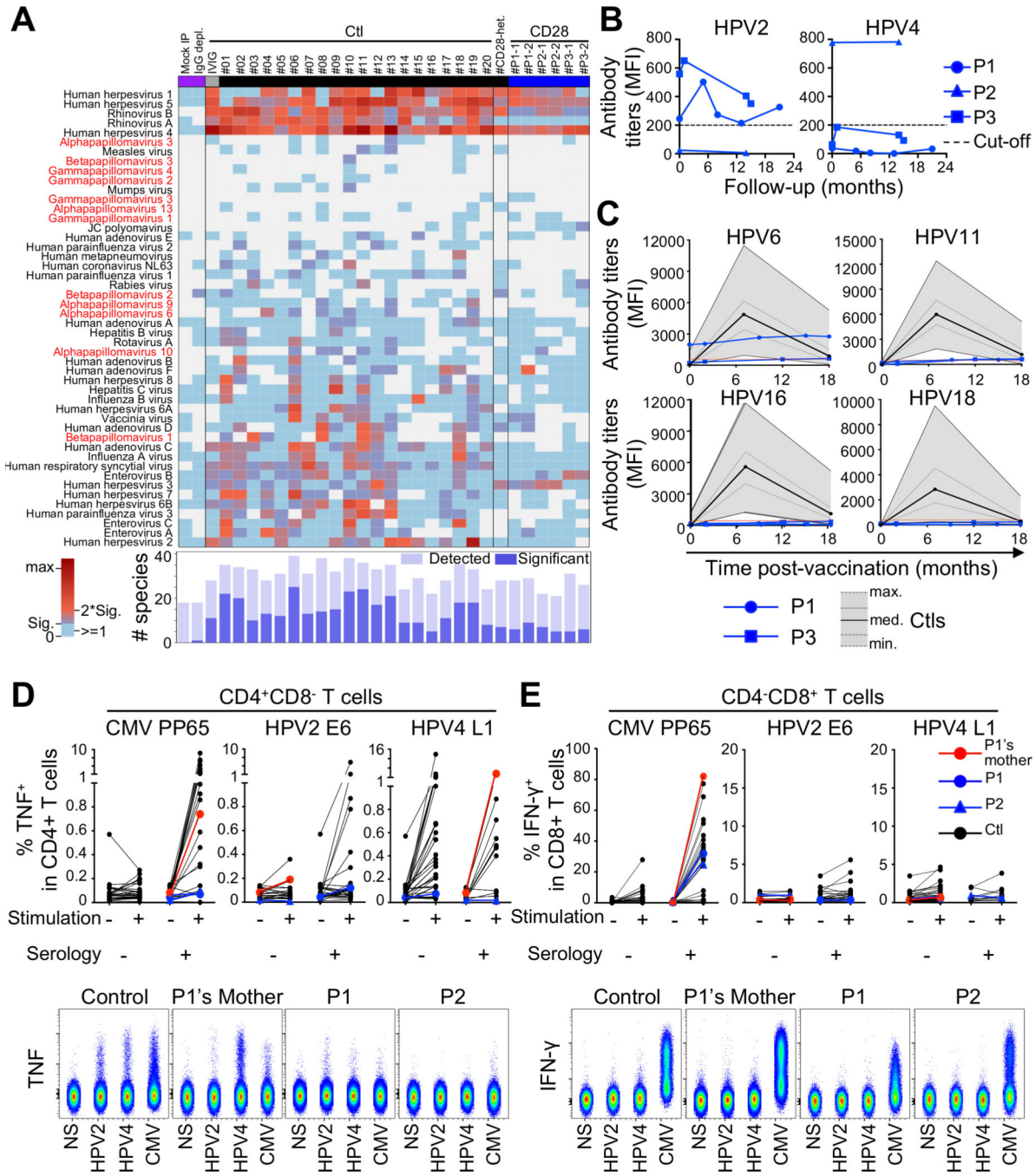

Figure 5. Anti-HPV B and T cell responses

(A) Virscan. Adjusted virus scores for indicated samples from patients, a heterozygote and controls, mock immunoprecipitate (IP) samples and-IgG depleted serum, and IVIg. Shown are virus species for which we found at least one sample to be seropositive. The heatmap shows adjusted virus score values for each sample as a color gradient from blue if antibodies were detected but below our significance cutoff values, through purple to red if the adjusted virus score values were above our significance cutoff values. The bar plot (bottom) illustrates the size of the Ab repertoire for a given sample, indicating the precise number of

different species for which peptides were enriched (light blue) and the number of different species for which the adjusted virus score values exceeded the cutoff values for significance (dark blue).

(B) Ab titers against HPV-2 and HPV-4 in patients at multiple time points; sensitivity threshold is indicated by a dashed line.

(C) Titers of antibodies against indicated HPVs in P1 and P3 pre and post Gardasil 9 vaccination (blue lines). The sensitivity threshold is indicated by a red dotted line. The black line represents the median value for a published control group (Bhatla et al., 2018). The gray area and the gray lines indicate the minimum, interquartile range and maximum responses of the control group.

(D and E) PBMCs were stimulated for 14 days with overlapping peptides from pp65 (HCMV), E6 (HPV-2), or L1 (HPV-4). Intracellular production of TNF and IFN-γ was measured in $CD4^+$ (D) and $CD8^+$ (E) T cells, respectively. Controls (n = 46), heterozygote, and patients were categorized on the basis of seropositivity for HCMV, HPV-2, and HPV-4 (top panels). Representative images are shown in the lower panels.

See also Figure S7 and Data S1.

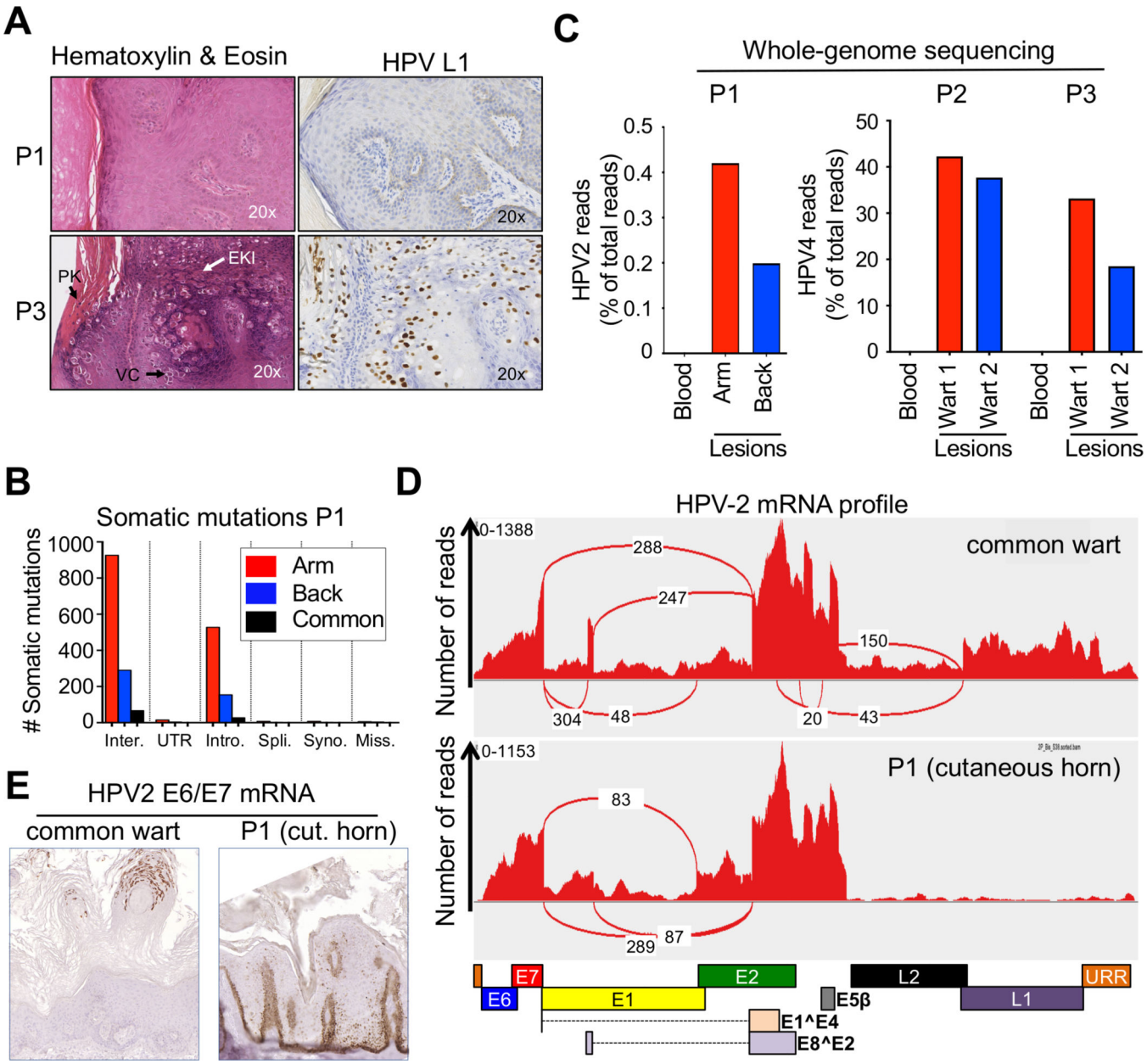

Figure 6. Histological and virological studies of TMS lesions reveal an atypical papilloma

(A) H&E staining (left), immunohistochemical staining of the L1 protein of HPV (right) in a skin lesion from P1 (top) and a common wart from P3 (bottom). Vacuolated cells (VC), parakeratosis (PK), and large eosinophilic keratohyalin inclusions (EKI), suggesting productive viral replication is not found in P1's lesions.

(B) Bar graph summarizing the number of somatic mutations in P1's lesions, sorted by mutation type: intergenic (inter.), untranslated region (UTR), intronic (intro.), splicing region (spli.), synonymous (syno.), and missense (miss.). The numbers of somatic mutations common to the 2 skin lesions are shown for each type of mutation.

(C) Bar graph showing HPV-2 (P1) and HPV-4 (P2 and P3) read counts normalized to total read counts extracted from WGS data for two separate lesions (arm and back) and the blood of the patients.
(D) Representative RNA sequencing profiles for a control wart (top) and one TMS lesion from P1 (bottom). The graph shows the number of reads detected for each position. The red connecting lines indicate the most frequent splice events detected; the number of detected reads is indicated. Boxes below the graph indicate the position of the main HPV-2 open reading frames.
(E) *In situ* hybridization showing E6/E7 mRNA levels in an HPV-2^+ common wart and a cutaneous horn from P1.
See also Table S3 and Data S1.

KEY RESOURCES TABLE

REAGENT or RESOURCE	SOURCE	IDENTIFIER
Antibodies		
TotalSeq-C0072 anti-human CD4 Antibody	Biolegend	Cat# 300567; RRID:AB_2800725
TotalSeq-C0386 anti-human CD28 Antibody	Biolegend	Cat# 302963; RRID:AB_2800751
TotalSeq-C0063 anti-human CD45RA Antibody	Biolegend	Cat# 304163; RRID:AB_2800764
TotalSeq-C0049 anti-human CD3 Antibody	Biolegend	Cat# 344849; RRID:AB_2814272
rat monoclonal anti-CD3	Abcam	Cat# ab11089; RRID:AB_2889189
rabbit polyclonal anti-CD28	Sigma	Cat# HPA070003; RRID:AB_2686226
rabbit monoclonal anti-CD86	Cell Signaling	Cat# 91882S; RRID:AB_2797422
mouse monoclonal anti-CD80	R&D Systems	Cat# MAB140; RRID:AB_2244549
mouse monoclonal anti-CD207	Novocastra / Leica	Cat# NCL-L-Langerin; RRID:AB_563850
rabbit polyclonal anti-CD207	Sigma	Cat# HPA011216; RRID:AB_1078453
Cy3-conjugated goat anti-Rat IgG (H+L)	Jackson Immunoresearch	Cat# 112-165-003; RRID:AB_2338240
Alexa Fluor® 488-conjugated goat anti-rat IgG (H+L)	Thermo Fisher Scientific	Cat# A11006; RRID:AB_2534074
Alexa Fluor®488-conjugated goat anti-rabbit IgG (H+L)	Thermo Fisher Scientific	Cat# A11008; RRID:AB_143165
Alexa Fluor® 488-conjugated goat anti-mouse IgG1	Thermo Fisher Scientific	Cat# A21121; RRID:AB_2535764
Alexa Fluor® 647-conjugated donkey anti-mouse IgG (H+L)	Jackson Immunoresearch	Cat# 715-605-150; RRID:AB_2340862
Alexa Fluor® 594-conjugated donkey anti-rabbit IgG (H+L)	Jackson Immunoresearch	Cat# 711-585-152; RRID:AB_2340621
Anti-FLAG M2 antibody-conjugated agarose beads	Sigma-Aldrich	Cat# A2220; RRID:AB_10063035
Anti-FLAG M2 antibody	Sigma-Aldrich	Cat# F1804; RRID:AB_262044
Brilliant Violet 421 anti-human CD197 (CCR7) Antibody	Biolegend	Cat# 353208; RRID:AB_11203894
APC/Cyanine7 anti-human CD1c Antibody	Biolegend	Cat# 331520; RRID:AB_10644008
BV786 Mouse Anti-Human CD3 Clone UCHT1	BD Biosciences	Cat# 565491; RRID:AB_2739260
FITC Mouse Anti-Human CD3 Clone UCHT1	BD Biosciences	Cat# 555916; RRID:AB_396217
CD3-VioBlue, human monoclonal (BW264/56)	Miltenyi Biotec	Cat# 130-094-363; RRID:AB_10831672
CD3d Monoclonal Antibody (7D6), PE	Thermo Fisher Scientific	Cat# MHCD0304; RRID:AB_10376004
CD3 Monoclonal Antibody (OKT3), Functional Grade, eBioscience	Thermo Fisher Scientific	Cat# 16-0037-85; RRID:AB_468855
BV711 Mouse Anti-Human CD4 Clone RPA-T4	BD Biosciences	Cat# 740769; RRID:AB_2740432
CD4 Antibody, anti-human, APC-Vio 770 (M-T321)	Miltenyi Biotec	Cat# 130-100-355; RRID:AB_2657995
BV650 Mouse Anti-Human CD8 Clone RPA-T8	BD Biosciences	Cat# 563821; RRID:AB_2744462
CD8 (BW135/80)-FITC, human (clone: BW135/80)	Miltenyi Biotec	Cat# 130-080-601; RRID:AB_244336
PE Mouse Anti-Human CD4 Clone RPA-T4	BD Biosciences	Cat# 555347; RRID:AB_395752
CD11c APC Clone S-HCL-3	BD Biosciences	Cat# 333144; RRID:AB_2868645
FITC Mouse Anti-Human CD14 Clone M5E2	BD Biosciences	Cat# 555397; RRID:AB_395798
FITC Mouse Anti-Human CD16 Clone 3G8	BD Biosciences	Cat# 555406; RRID:AB_395806
FITC Mouse Anti-Human CD19 Clone 4G7	BD Biosciences	Cat# 345776; RRID:AB_2868804
APC-H7 Mouse Anti-Human CD19 Clone HIB19	BD Biosciences	Cat# 560727; RRID:AB_1727437
CD20 Antibody, anti-human, FITC	Miltenyi Biotec	Cat# 130-091-108; RRID:AB_244317
FITC Mouse anti-Human CD56 Clone B159	BD Biosciences	Cat# 562794; RRID:AB_2737799
BV421 Mouse Anti-Human CD25 Clone M-A251	BD Biosciences	Cat# 562442; RRID:AB_11154578

REAGENT or RESOURCE	SOURCE	IDENTIFIER
Brilliant Violet 421 anti-human CD27	Sony	Cat# 2114120
FITC Mouse Anti-Human CD27 Clone L128	BD Biosciences	Cat# 340424; RRID:AB_400031
CD28 Antibody, anti-human, APC	Miltenyi Biotec	Cat# 130-092-923; RRID:AB_871654
PE Mouse Anti-Human CD28 Clone CD28.2	BD Biosciences	Cat# 555729; RRID:AB_396072
BV421 Mouse Anti-Human CD28 Clone CD28.2	BD Biosciences	Cat# 562613; RRID:AB_2737676
CD28 Monoclonal Antibody (CD28.2), eBioscience	Thermo Fisher Scientific	Cat# 14-0289-82; RRID:AB_467194
PE-CF594 Mouse Anti-Human CD31 Clone WM59	BD Biosciences	Cat# 563652; RRID:AB_2738349
PE-CF594 Mouse Anti-Human CD45RA Clone HI100	BD Biosciences	Cat# 562298; RRID:AB_11154413
PE Mouse Anti-Human CD54 Clone HA58	BD Biosciences	Cat# 555511; RRID:AB_395901
PE-CF594 Mouse Anti-Human CD56 Clone B159	BD Biosciences	Cat# 562289; RRID:AB_11152080
CD56 FITC Clone NCAM16.2	BD Biosciences	Cat# 345811; RRID:AB_2868832
BV711 Mouse Anti-Human Invariant NK T Cell	BD Biosciences	Cat# 747720; RRID:AB_2872199
Alexa Fluor® 488 Mouse anti-Human FoxP3 Clone 259D/C7	BD Biosciences	Cat# 560047; RRID:AB_1645349
PE/Cyanine7 anti-human CD123 Antibody	Biolegend	Cat# 306010; RRID:AB_493576
PE Mouse Anti-Human CD134 Clone L106	BD Biosciences	Cat# 340420; RRID:AB_400027
BV711 Mouse Anti-Human CD141 Clone 1A4	BD Biosciences	Cat# 563155; RRID:AB_2738033
PE Mouse Anti-Human CD152 Clone BNI3	BD Biosciences	Cat# 555853; RRID:AB_396176
PE anti-human CD154 Antibody	Biolegend	Cat# 310806; RRID:AB_314829
BV711 Mouse Anti-Human CD161 Clone DX12	BD Biosciences	Cat# 563865; RRID:AB_2738457
FITC anti-human/mouse/rat CD278 (ICOS) Antibody	Biolegend	Cat# 313506; RRID:AB_416330
PE Mouse Anti-Human CD25 Clone M-A251	BD Biosciences	Cat# 555432; RRID:AB_395826
Alexa Fluor® 700 Mouse Anti-Human IFN-γ Clone B27	BD Biosciences	Cat# 557995; RRID:AB_396977
Vioblue TCRγ/δ Antibody, anti-human	Miltenyi Biotec	Cat# 130-113-507; RRID:AB_2733977
APC-Vio770 TCR Vα7.2 Antibody, anti-human, REAfinity	Miltenyi Biotec	Cat# 130-100-179; RRID:AB_2653673
CD183 (CXCR3)-VioBright FITC, human (clone: REA232)	Miltenyi Biotec	Cat# 130-118-545; RRID:AB_2734058
CD196 (CCR6)-APC, human (clone: REA190)	Miltenyi Biotec	Cat# 130-100-373; RRID:AB_2655933
CD194 (CCR4)-PE, human (clone: REA279)	Miltenyi Biotec	Cat# 130-103-812; RRID:AB_2655905
CD185 (CXCR5)-PE-Vio770, human (clone: REA103)	Miltenyi Biotec	Cat# 130-105-459; RRID:AB_2655788
PE Mouse anti-NF-κB p65 (pS529)	BD Biosciences	Cat# 558423; RRID:AB_647222
CD159a (NKG2A)-APC, human	Miltenyi Biotec	Cat# 130-098-812; RRID:AB_2655386
CD159c (NKG2C)-PE, human (clone: REA205)	Miltenyi Biotec	Cat# 130-103-635; RRID:AB_2655394
CD158a,h PC7	Beckman Coulter	Cat# A66899
CD158b1,b2,j PC5.5	Beckman Coulter	Cat# A66900; RRID:AB_2857331
Alexa Fluor 700 anti-human CD158e1 (KIR3DL1, NKB1) Antibody	Biolegend	Cat# 312712; RRID:AB_2130824
Anti-IgM-APC, human	Miltenyi Biotec	Cat# 130-093-076; RRID:AB_1036084
PE-CF594 Mouse Anti-Human IgG Clone G18-145	BD Biosciences	Cat# 562538; RRID:AB_2737640
FITC IgA Antibody, anti-human	Miltenyi Biotec	Cat# 130-114-001; RRID:AB_2726443
Pacific Blue anti-human HLA-DR	Biolegend	Cat# 980404; RRID:AB_2632616
CD279 (PD-1) Monoclonal Antibody (MIH4), PE, eBioscience	Thermo Fisher Scientific	Cat# 12-9969-42; RRID:AB_10736473
CD366 (TIM3) Monoclonal Antibody (F38-2E2), PE, eBioscience	Thermo Fisher Scientific	Cat# 12-3109-42; RRID:AB_2572605

REAGENT or RESOURCE	SOURCE	IDENTIFIER
CD223 (LAG-3) Monoclonal Antibody (3DS223H), PE, eBioscience	Thermo Fisher Scientific	Cat# 12-2239-42; RRID:AB_2572597
TIGIT Monoclonal Antibody (MBSA43), PE, eBioscience	Thermo Fisher Scientific	Cat# 12-9500-42; RRID:AB_10714831
PE anti-human CD272 (BTLA) Antibody	Biolegend	Cat# 344506; RRID:AB_2065761
HPV Monoclonal Antibody (K1H8)	Thermo Fisher Scientific	Cat# MA5-12446; RRID:AB_10978662
PE Mouse Anti-Human CD15 Clone HI98	BD Biosciences	Cat# 555402; RRID:AB_395802
PE-Cy7 Mouse Anti-Human CD16 Clone 3G8	BD Biosciences	Cat# 560918; RRID:AB_10563252
Polyclonal Goat Anti-Mouse Ig Clone Polyclonal	BD Biosciences	Cat# 553998; RRID:AB_395195
PE Mouse IgG2b κ Isotype Control Clone 27–35	BD Biosciences	Cat# 555743; RRID:AB_396086
Anti-TNF-α-APC, human	Miltenyi Biotec	Cat# 130-091-649; RRID:AB_244201
PE/Cy7 anti-human IL-2	Sony	Cat# 3101630
V5 Tag Monoclonal Antibody, HRP	Thermo Fisher Scientific	Cat# R961-25; RRID:AB_2556565
GAPDH Antibody (0411) HRP	Santa Cruz Biotechnology	Cat# sc-47724 HRP; RRID:AB_627678
Antibody against mouse papillomavirus E4	in house	Rabbit serum
Antibody against mouse papillomavirus L1	in house	MPV.B9
Rabbit polyclonal HPVE2 serum	John Doorbar Lab.	N/A
Mouse MCM7 antibody	Thermo Fisher Scientific	Cat# MA5-14291; RRID:AB_11009501
Goat anti-rabbit IgG (H+L)Alexa 594	Thermo Fisher Scientific	Cat# A11012; RRID:AB_141359
Immpress anti-mouse IgG HRP	Vector Labs	Cat# 30026; RRID:AB_2336532
monoclonal mouse IgG1 anti-tag (supernatant from KT3 hybridoma cell line)	(MacArthur and Walter, 1984)	N/A
Biotin-SP-conjugated AffiniPure Goat Anti-Mouse IgG + IgM (H +L)	Jackson ImmunoResearch Labs	Cat# 115-065-068; RRID:AB_2338563
Biotin-SP-conjugated AffiniPure Goat Anti-Human IgA + IgG + IgM (H+L)	Jackson ImmunoResearch Labs	Cat# 109-065-064; RRID:AB_2337627
Bacterial and virus strains		
expanded T7 Virscan phage library	S. Elledge (Brigham and Women's Hospital and Harvard University Medical School, Boston, MA, USA)	VirScan Phage Library, version 3
One Shot TOP10 Chemically Competent *E. coli*	Thermo Fisher Scientific	Cat# C404003
NEB Stable Competent *E. coli* (High Efficiency)	New England Biolabs	Cat# C3040H
Mouse papillomavirus	HSD:NU mouse tail lesions	MmuPV1
E.coli BL21	Sehr et al., 2001	N/A
E.coli Rosetta	Michael et al., 2008	N/A
Biological samples		
Peripheral blood mononuclear cells from indicated individuals	This manuscript	N/A
Plasma from indicated individuals	This manuscript	N/A
Skin scraps of warts	This manuscript	N/A
Skin biopsies of patient and control warts	This manuscript	N/A
Chemicals, peptides, and recombinant proteins		

REAGENT or RESOURCE	SOURCE	IDENTIFIER
Polyethylenimine	Polysciences	Cat# 23966
Opti-MEM	Thermo Fisher scientific	Cat# 31985070
Dulbecco's Modified Eagle Medium	Nacalai	Cat# 08459-64
DMEM, high glucose, GlutaMAX(TM)	Thermo Fisher scientific	Cat# 61-965-026
RPMI 1640 Medium, GlutaMAX Supplement	Thermo Fisher scientific	Cat# 61870010
X-VIVO 20 Serum-free Hematopoietic Cell Medium	Lonza	Cat# BE04-448Q
Protease inhibitor cocktail	Sigma-Aldrich	Cat# P8340
FLAG peptide	Sigma-Aldrich	Cat# F3290
Lys48-linked polyubiquitin chains	Boston Biochem	Cat# UC-230-100
1 M Tris-HCl	Invitrogen	Cat# 15567-027
0.1 M DTT (dithiothreitol)	Affymetrix	Cat# 70726 150 UL
HL-dsDNase	ArcticZymes	Cat# 70800-201
20 mM Nuclease-free MgCl2	Thermo Scientific	Cat# AB-0359
EvaGreen for qPCR	Biotium	Cat# 31000
intravenous immunoglobulin (IVIg)	CSL Behring	Privigen
IgG-depleted human serum	Molecular Innovations, Inc.	Cat# HPLASERGFA5ML
Protein Transport Inhibitor (Containing Brefeldin A)	BD Biosciences	Cat# 555029
Protein Transport Inhibitor (Containing Monensin)	BD Biosciences	Cat# 554724
Tuberculin/PPD	STATEN SERUM INSTITUT	N/A
Sephadex G-50 Superfine, Cytiva	Merck	Cat# GE17-0041-01
Phytohemagglutinin PHA-M, lyophilized powder	Sigma	Cat# L2646-10MG
Phorbol 12-myristate 13-acetate	Sigma aldrich	Cat# P8139-1MG
Ionomycin calcium salt from Streptomyces conglobatus	Sigma aldrich	Cat# I0634-5MG
Human IL-2 Recombinant Protein	Thermo Fisher Scientific	Cat# RP-8605
Ficoll® Paque Plus, Cytiva	Merck	Cat# GE17-1440-03
Fetal Bovine serum	Thermo Fisher Scientific	Cat# 16000036
Protamine sulfate	Merck	Cat# P3369-10G
Human Serum from human male AB plasma, USA origin, sterile-filtered	Merck	Cat# H4522
PepMix HCMVA (pp65) (> 70%)	JPT technologies	Cat# PM-PP65-1
Proleukin	Novartis	N/A
HPV-2E6 overlapping peptides	JPT technologies	Custom order
HPV-4L1 overlapping peptides	JPT technologies	Custom order
Mouse papillomavirus E4 peptide	https://Chinapeptides.net	PKTTPPRRELFPPTPLTQPP
Mouse papillomavirus L1 virus like particles (produced in HEK293T)	In house	MmuPV1-L1-VLPs
Tyramide CF 488	Biotium	Cat# 92171
Dapi: 4',6-Diamidino-2-phenylindol dihydrochloride	Thermo Fisher Scientific	Cat# 11926621
PE-Streptavidin Conjugate	Moss,Inc.	Cat# SAPE-001
HPV 2, 4, 6, 11, 16, 18 L1 antigens for multiplex serology	(Michael et al., 2008)	N/A

REAGENT or RESOURCE	SOURCE	IDENTIFIER
SeroMap Microspheres	Luminex (Austin, TX, USA)	Cat# L100-Sxxx-04
Critical commercial assays		
LIVE/DEAD Viability kit	Thermo Fisher Scientific	Cat# L3224
Chromium Single Cell 3′ Reagent Kits (v3.1)	10X Genomics	Cat# 120237
Chromium Single Cell 5′ Library & Gel Bead kit (V1)	10X Genomics	Cat# 1000014
Chromium Single Cell 5′ Feature Barcode Library Kit	10X Genomics	Cat# 1000080
Memory CD4+ T Cell Isolation Kit, human	Miltenyi	Cat# 130-091-893
Dead Cell Removal Kit	Miltenyi	Cat# 130-090-101
Taqman Universal PCR Master Mix for qPCR	Thermo Fisher Scientific	Cat# 4304437
Taqman Gene Expression Assays – CD28-FAM (Probe 1: Hs00174796_m1 and probe 2: Hs01007422_m1) and GUSB	Thermo Fisher Scientific	Cat# 4331182, Cat# 4326320E
QIAprep Spin Miniprep Kit	QIAGEN	Cat# 27106
RNeasy Fibrous Tissue Mini Kit	QIAGEN	Cat# 74704
RNeasy Plus Mini Kit	QIAGEN	Cat# 74136
RNeasy Plus Micro Kit	QIAGEN	Cat# 74034
HiSpeed Plasmid Maxi Kit	QIAGEN	Cat# 12663
SuperSignal West Femto Maximum Sensitivity Substrate	Thermo Fisher Scientific	Cat# 34096
LIVE/DEAD Fixable Aqua Dead Cell Stain Kit	Thermo Fisher Scientific	Cat# L34966
Foxp3 / Transcription Factor Staining Buffer Set	Thermo Fisher Scientific	*Cat# 00-5523-00*
T Cell Activation/Expansion Kit, human	Miltenyi Biotec	Cat# 130-091-441
MasterMix Multiplex Kit	QIAGEN	Cat# 206145
Specific Primer mix (βHPV, γHPV, or warts specific HPV)	International Agency for research on Cancer	N/A
Color-coded beads, coupled with specific probe for each HPV	International Agency for research on Cancer	N/A
Streptavidin, R-Phycoerythrin Conjugate	Molecular ProbesTM	Cat# S866
Silver Stain Kit	Wako	Cat# 299-58901
Agilent High Sensitivity DNA Kit	Agilent Technologies	Cat# 5067-4626
RNA ScreenTape Analysis	Agilent Technologies	Cat# 5067-5576
RNA ScreenTape Sample buffer	Agilent Technologies	Cat# 5067-5577
QuikChange II XL Site-Directed Mutagenesis Kit	Agilent Technologies	Cat# 200521
SureSelect Human All Exon V6	Agilent Technologies	Cat# 5190-8863
Ovation Universal RNA-Seq System 1–16	TECAN (NuGen)	Cat# 0343
CloneAmp HiFi PCR Premix	Takara Bio	Cat# 639298
SMART-Seq® v4 Ultra® Low Input RNA Kit for Sequencing	Takara Bio	Cat# 634891
In-Fusion® Snap Assembly Master Mix	Takara Bio	Cat# 638948
Nextera XT DNA Library Preparation Kit	Ilumina	Cat# FC-131-1096
Nextera XT Index Kit v2 set A	Ilumina	Cat# TG-131-2001
Protein A Dynabeads	Thermo Fisher Scientific	Cat# 10002D
Protein G Dynabeads	Thermo Fisher Scientific	Cat# 10004D
QIAquick PCR purification kit (50)	QIAGEN	Cat# 28104

REAGENT or RESOURCE	SOURCE	IDENTIFIER
Human IgG TOTAL ELISA	Thermo Fisher Scientific	Cat# 501128669
QIAquick Gel Extraction Kit	QIAGEN	Cat# 28704
Hiseq4000 (300 cycles), paired end kit	Illumina	Cat# FC-410-1003
Nextseq 500 High-output Kit v2 (75 cycles)	Illumina	Cat# FC-4044-2005
Perm Buffer III	BD Biosciences	Cat# 558050
Fix Buffer I	BD Biosciences	Cat# 557870
Bond Polymer Refine Detection	Leica	Cat# DS9800
Invitrogen iPrep PureLink gDNA Blood Kit	Thermo Fisher Scientific	Cat# 10552894
Genome-Wide Human SNP Array 6.0	Thermo Fisher Scientific	Cat# 901153
BigDye Terminator v3.1 Cycle Sequencing Kit	Thermo Fisher Scientific	Cat# 4337457
Oligo(dT)12-18 Primer	Thermo Fisher Scientific	Cat# 18418012
Reverse Transcriptase SuperScript II	Thermo Fisher Scientific	Cat# 18044-014
Taq DNA polymerase	Thermo Fisher Scientific	Cat# 10342053
TOPO TA Cloning Kit for Sequencing	Thermo Fisher Scientific	Cat# 450030
pcDNA3.1/V5-His TOPO TA Expression Kit	Thermo Fisher Scientific	Cat# K480001
X-tremeGENE 9 DNA Transfection Reagent	Merck	Cat# 6365779001
Calcium Phosphate Transfection Kit	Thermo Fisher Scientific	Cat# K278001
Acrodisc Syringe Filters with Supor Membrane, Sterile - 0.2 μm	Pall	Cat# 4612
CellTrace CFSE Cell Proliferation Kit, for flow cytometry	Thermo Fisher Scientific	Cat# C34570
M.O.M. (Mouse on Mouse) ImmPRESS HRP (Peroxidase) Polymer Kit	Vector	Cat# MP-2400
ImmPRESS anti-rabbit IgG polymer system	Vector	Cat# MP-7801
ImmPACT NovaRED Substrate	Vector	Cat# SK-4805
50% hematoxylin Gill's No. 1 solution	Sigma-Aldrich	Cat# GHS132-1L
Nuclear Fast Red	American MasterTech, Inc.	Cat# SSKC398
RNAscope® 2.5 VS Probe- V-MusPV-E4	Advanced Cell Diagnostics, Inc.	Cat# 473289
RNAscope 2.5 HD Assay – BROWN	Advanced Cell Diagnostics, Inc.	Cat# 322300
Megaprime DNA Labeling System	Amersham	Cat# RPN1604
The Brilliant III qPCR kit	Agilent	Cat# 600880
The RevertAid First Strand cDNA synthesis kit	Thermo-Fisher	Cat# K1622
RNAScope 2.5 HD Assay Brown	ACD/Bio-Techne	Cat# 322310
HPV 2 E6/E7 C1 RNAScope probe	ACD/Bio-Techne	Cat# 80660
Human PPIB RNAScope probe	ACD/Bio-Techne	Cat# 313901
Deposited Data		
3′ Single-cell RNA-seq of the patient PBMC or healthy controls	This manuscript	EGA: EGAS00001004837
CITE-seq (5′) single-cell RNA-seq of P1 and P2 PBMC and 1 healthy control	This manuscript	EGA: EGAS00001004837
High-throughput sequencing (HTS) of T cell receptor β (TRB) and T cell receptor α (TRA) dataset (control and patients)	Adaptive Biotechnologies	http://clients.adaptivebiotech.com/login Email: beziat-review@adaptivebiotech.com

REAGENT or RESOURCE	SOURCE	IDENTIFIER
		Password: beziat2021review
Whole-Exome and genome Sequencing of the patients (whole blood DNA and warts)	This manuscript	Sequence Read Archive (SRA: PRJNA715377)
Primary CD4+ naive T cell RNA-Seq data from the patient and heathy controls	This manuscript	gene expression omnibus (GEO: GSE139299)
RNA-Seq of the lesions of P1 and control common warts	This manuscript	gene expression omnibus (GEO: GSE139259)
Full HPV2 genome from P1	This manuscript	GenBank: MN605988
Full HPV4 genome from P2 and P3	This manuscript	GenBank: MN605989
Experimental models: cell lines		
HEK293T cells	ATCC	Cat# CRL-11268, RRID:CVCL_1926
Expanded CD4+ T cells from healthy controls or Patients' family	This manuscript	N/A
P815	ATCC	*Cat# ATCC TIB-64*
Jurkat	In House	N/A
Experimental models: mouse strains		
C57BL/6 mice	https://www.jax.org	https://www.jax.org/strain/000664
CD28ko mice	https://www.jax.org	002666 - B6.129S2-Cd28tm1Mak/J
Rag1ko mice	https://www.jax.org	https://www.jax.org/strain/002216
Oligonucleotides		
IS7_HsORF5_2	IDT Integrated DNA technologies	ACACTCTTTCCCTACACGACTCCAGTC AGGTGTGATGCTC
IS8_HsORF3_2	IDT Integrated DNA technologies	GTGACTGGAGTTCAGACGTGTGCTC TTCCGATCCGAGCTTATCGTCGTCAT CC
IS4_HsORF5_2	IDT Integrated DNA technologies	AATGATACGGCGACCACCGAGATCT A CACTCTTTCCCTACACGACTCCAGT
T7-Pep2.2_SP_subA	IDT Integrated DNA technologies	CTCGGGGATCCAGGAATTCCGCTGC GT
T7-Pep2.2_SP_subB	IDT Integrated DNA technologies	CTCGGGGATCCAGGAATTCGGAGCG GT
CD28-gDNA-FOR (sequencing gDNA)	Thermo Fisher Scientific	GCGTCTTTCAGTTCCCCTCA
CD28-gDNA-REV (sequencing gDNA)	Thermo Fisher Scientific	ACACATTGCCCTATTACAGCAAAA
CD28-cDNA-5UTR-FOR (sequencing cDNA + Exon trapping)	Thermo Fisher Scientific	TGGAACCCTAGCCCATCGTCA
CD28-cDNA-3UTR-REV (sequencing cDNA)	Thermo Fisher Scientific	AGCCGGCTGGCTTCTGGATA
ACTB-cDNA-FOR	Thermo Fisher Scientific	CCTTCCTGGGCATGGAGTCCT
ACTB-cDNA-REV	Thermo Fisher Scientific	AATCTCATCTTGTTTTCTGCG
pCMV6-FOR (sequencing insertion in pCMV6)	Thermo Fisher Scientific	ATTCGTCGACTGGATCCGGTA
pCMV6-REV (sequencing insertion in pCMV6 + Exon trapping)	Thermo Fisher Scientific	CATTTGCTGCCAGATCCTCTT
pLVX-mCherry-CD28-FOR (Cloning in pLVX)	Thermo Fisher Scientific	TATTTCCGGTGAATTATGC TCAGGCTGCTCTTGGC
pLVX-mCherry-CD28-REV (Cloning in pLVX)	Thermo Fisher Scientific	GAGAGGGGCGGGATCTCA GGAGCGATAGGCTGCG

REAGENT or RESOURCE	SOURCE	IDENTIFIER
ExonTrap-CD28-UTR-FOR (Cloning in pCMV6)	Thermo Fisher Scientific	CGAGGAGATCTGCCGCCGCG GCGTCTTTCAGTTCCCCTCAC
ExonTrap-CD28-Int1-REV (Cloning in pCMV6)	Thermo Fisher Scientific	TTATCTCTCTCTGCCACC TGTACATCCTTGG
ExonTrap-CD28-Int1-FOR (Cloning in pCMV6)	Thermo Fisher Scientific	CAGGTGGCAGAGAGAGAT AACTCCCCTCTGGAGTC
ExonTrap-CD28-ex2 -REV (Cloning in pCMV6)	Thermo Fisher Scientific	CTCGAGCGGCCGCGTACGCGTTTC ACATGGATAATGGTTCCATTG
CD28-cDNA-ATG-directional-FOR (Cloning in pcDNA3.1)	Thermo Fisher Scientific	CACCATGCTCAGGCTGCT CTTGGCTCTCA
CD28-cDNA-3′w/o.stop-REV (Cloning in pcDNA3.1)	Thermo Fisher Scientific	GGAGCGATAGGCTGCGAAGT
MUTsplice-CD28-ExonTrap-FOR (Mutagenesis c.52G>A Exon Trapping)	Thermo Fisher Scientific	CAATTCAAGTAACAAGTAAACAATG
MUTsplice-CD28-ExonTrap-REV (Mutagenesis c.52G>A Exon Trapping)	Thermo Fisher Scientific	CATTGTTTACTTGTTACTTGAATTG
MUTsplice-CD28-ExonTrap-FOR (Mutagenesis c.52G>A +5A>G Exon Trapping)	Thermo Fisher Scientific	GTAACAAGTAAGCAATGTTAATG
MUTsplice-CD28-ExonTrap-REV (Mutagenesis c.52G>A +5A>G Exon Trapping)	Thermo Fisher Scientific	CATTAACATTGCTTACTTGTTAC
MUT CD28 Gly18Arg For (Mutagenesis Gly18Arg)	Thermo Fisher Scientific	ATTCAAGTAACAAGAAACAAGAT
MUT CD28 Gly18Arg Rev (Mutagenesis Gly18Arg)	Thermo Fisher Scientific	ATCTTGTTTCTTGTTACTTGAAT
HPV-2 F1 (Primer for whole-HPV genome sequencing)	Thermo Fisher Scientific	5′-AACCGCTCAGGATGACGAAG-3′
HPV-2 R1 (Primer for whole-HPV genome sequencing)	Thermo Fisher Scientific	5′-TCTAAGCGGGACCACGACCT-3′
HPV-2 F2 (Primer for whole-HPV genome sequencing)	Thermo Fisher Scientific	5′-CCCTAATGATAACAACCAACAC-3′
HPV-2 R2 (Primer for whole-HPV genome sequencing)	Thermo Fisher Scientific	5′-TACGCTGTTCAACGCTGGT-3′
HPV-2 F2 (Primer for whole-HPV genome sequencing)	Thermo Fisher Scientific	5′-GCAGCCTCAGCAGAATCAA-3′
HPV-2 R3 (Primer for whole-HPV genome sequencing)	Thermo Fisher Scientific	5′-TCAACTACAGTGGTGGGTCGC-3′
HPV-2 F4 (Primer for whole-HPV genome sequencing)	Thermo Fisher Scientific	5′-GTGGAACAGAACACTTTAGCAG-3′
HPV-2 R4 (Primer for whole-HPV genome sequencing)	Thermo Fisher Scientific	5′-GCGGGTAACTCATCAAGCAAT-3′
HPV-2 F5 (Primer for whole-HPV genome sequencing)	Thermo Fisher Scientific	5′-GTTTTAGTAGGTTGGGACGC-3′
HPV-2 R5 (Primer for whole-HPV genome sequencing)	Thermo Fisher Scientific	5′-TACGCAGCGAGAAGAACATAG-3′
HPV-2 F6 (Primer for whole-HPV genome sequencing)	Thermo Fisher Scientific	5′-TAACACAACTATTGAGGACGGG-3′
HPV-2 R6 (Primer for whole-HPV genome sequencing)	Thermo Fisher Scientific	5′-TTCATACGGGAGGGGATAC-3′
HPV-2 F7 (Primer for whole-HPV genome sequencing)	Thermo Fisher Scientific	5′-GTATCCCCTCCCGTATGAAT-3′
HPV-2 R7 (Primer for whole-HPV genome sequencing)	Thermo Fisher Scientific	5′-TTCGTCATCCTGAGCGGTTT-3′
HPV-2 F8 (Primer for whole-HPV genome sequencing)	Thermo Fisher Scientific	5′-GCTGGGGCAATAGGGTCTTT-3′
HPV-2 R8 (Primer for whole-HPV genome sequencing)	Thermo Fisher Scientific	5′-AGTTGGCTGCAAAAACGACG-3′
HPV-2 F9 (Primer for whole-HPV genome sequencing)	Thermo Fisher Scientific	5′-TAAGTGTGGCAGAACCGTCC-3′
HPV-2 R9 (Primer for whole-HPV genome sequencing)	Thermo Fisher Scientific	5′-TTACTCAGCAACGTCGCCTT-3′
HPV-4 F1 (Primer for whole-HPV genome sequencing)	Thermo Fisher Scientific	5′-AAAAGGGACAGTGCATTTCTACT-3′
HPV-4 R1 (Primer for whole-HPV genome sequencing)	Thermo Fisher Scientific	5′-GTGCAGCAAAACGTCAGCTT-3′
HPV-4 F2 (Primer for whole-HPV genome sequencing)	Thermo Fisher Scientific	5′-GAGGAGTCGGTGGTTCCATT-3′
HPV-4 R2 (Primer for whole-HPV genome sequencing)	Thermo Fisher Scientific	5′-TGTATGAGACCCCATACCATTC-3′
HPV-4 F2 (Primer for whole-HPV genome sequencing)	Thermo Fisher Scientific	5′-GGCTGGACCTTCTAGCCAAG-3′

REAGENT or RESOURCE	SOURCE	IDENTIFIER
HPV-4 R3 (Primer for whole-HPV genome sequencing)	Thermo Fisher Scientific	5′-TGGCTTCCAATCTCCTTCTTCA-3′
HPV-4 F4 (Primer for whole-HPV genome sequencing)	Thermo Fisher Scientific	5′-GTACGCAGAGGAGGATGCAA-3′
HPV-4 R4 (Primer for whole-HPV genome sequencing)	Thermo Fisher Scientific	5′-AAACGTGCGACTAGGGACTC-3′
HPV-4 F5 (Primer for whole-HPV genome sequencing)	Thermo Fisher Scientific	5′-TACTGACGGTACTTGGAAATCTT-3′
HPV-4 R5 (Primer for whole-HPV genome sequencing)	Thermo Fisher Scientific	5′-CCTCAGTGTCGAAGGAGGAG-3′
HPV-4 F6 (Primer for whole-HPV genome sequencing)	Thermo Fisher Scientific	5′-CAGACCATACGGGAGAAAGAGC-3′
HPV-4 R6 (Primer for whole-HPV genome sequencing)	Thermo Fisher Scientific	5′-TTCCTTCTACTCAAGCTTTGCAT-3′
HPV-4 F7 (Primer for whole-HPV genome sequencing)	Thermo Fisher Scientific	5′-GCACTGACCAAAGAGACGCT-3′
HPV-4 R7 (Primer for whole-HPV genome sequencing)	Thermo Fisher Scientific	5′-CTCCCCTAGTTGCCAATGCT-3′
HPV-4 F8 (Primer for whole-HPV genome sequencing)	Thermo Fisher Scientific	5′-GCTAGCAGCCACCCTACAAT-3′
HPV-4 R8 (Primer for whole-HPV genome sequencing)	Thermo Fisher Scientific	5′-TGCTTTGTTCTCCTGAATGTTGAC-3′
HPV-4 F9 (Primer for whole-HPV genome sequencing)	Thermo Fisher Scientific	5′-AAGTGGTGTGCAAATTGGGC-3′
HPV-4 R9 (Primer for whole-HPV genome sequencing)	Thermo Fisher Scientific	5′-CAAATCTGTTTGGGTCTGGCA-3′
HPV-4 F10 (Primer for whole-HPV genome sequencing)	Thermo Fisher Scientific	5′-TTCCACGCTGGTACAGAAAGG-3′
HPV-4 R10 (Primer for whole-HPV genome sequencing)	Thermo Fisher Scientific	5′-TAGAGCATCTCCCATGGTGC-3′
HPV-4 F11 (Primer for whole-HPV genome sequencing)	Thermo Fisher Scientific	5′-TGCTCCTTTGGATGTCATTGC-3′
HPV-4 R11 (Primer for whole-HPV genome sequencing)	Thermo Fisher Scientific	5′-AAACCGCCTGCCTAAGGAAA-3′
HPV-4 F12 (Primer for whole-HPV genome sequencing)	Thermo Fisher Scientific	5′-CCTACACAGACCCCTGCAAC-3′
HPV-4 R12 (Primer for whole-HPV genome sequencing)	Thermo Fisher Scientific	5′-TGCAGAAGTCGTCCAAGGTT-3′
USP37-MUT-FOR (Mutagenesis Glu459Lys)	Thermo Fisher Scientific	GAACCTGTTTCTGGAAAAGAAAATTCAC
USP37-MUT-REV (Mutagenesis Glu459Lys)	Thermo Fisher Scientific	GTGAATTTTCTTTTCCAGAAACAGGTTC
KANSL1L-MUT-FOR (Mutagenesis Ser577Thr)	Thermo Fisher Scientific	GTACAGATTGACCCCTACTTTTTATTGGAC
KANSL1L-MUT-REV (Mutagenesis Ser577Thr)	Thermo Fisher Scientific	GTCCAATAAAAAGTAGGGGTCAATCTGTAC
Primers for mouse papillomavirus	IDT	5′-TAGCTTTGTCTGCCCGCACT-3′
Primers for mouse papillomavirus	IDT	5′-GTCAGTGGTGTCGGTGGGAA-3′
Probe for mouse papillomavirus	IDT	5′FAM-CGGCCCGAAGACAACACCGCCACG-3′TAMRA
Recombinant DNA		
pCMV6-Empty vector	Origene	*Cat# PS100001*
pcDNA3.1/V5-His-Empty vector	Thermo Fisher Scientific	Cat# V81020
pCMV6-CD28_WT-Myc-DDK	Origene	Cat# RC211318
pCMV6-CD28_Gly18Arg-V5-His	This manuscript	N/A
pCMV6-CD28_Val16fs-V5-His	This manuscript	N/A
pCMV6-CD28_I1-Ret-V5-His	This manuscript	N/A
pcDNA3.1-CD28_WT-V5-His	This manuscript	N/A
pcDNA3.1-CD28_Gly18Arg-V5-His	This manuscript	N/A

REAGENT or RESOURCE	SOURCE	IDENTIFIER
pcDNA3.1-CD28_Val16fs-V5-His	This manuscript	N/A
pcDNA3.1-CD28_I1-Ret-V5-His	This manuscript	N/A
pCMV6-KANSL1L_WT-Myc-DDK	Origene	Cat# RC215502
pCMV6-KANSL1L_Ser577Thr-Myc-DDK	This manuscript	N/A
pCMV6-USP37_WT-Myc-DDK	Origene	Cat# RC223407
pCMV6-USP37_Glu459Lys -Myc-DDK	This manuscript	N/A
pLVX-EF1α-IRES-mCherry	Clontech	Cat# 631987
pLVX-EF1α- CD28_WT-IRES-mCherry	This manuscript	N/A
pLVX-EF1α-CD28_Gly18Arg-IRES-mCherry	This manuscript	N/A
psPAX2	Addgene	Cat# 12260
pCMV-VSV-G	Addgene	Cat# 8454
pHXB2-Env	NIH-AIDS Reagent Program	Cat# 1069
pCMV6-CD28_WT-ExonTrapping	This manuscript	N/A
pCMV6-CD28_c.52G>A-ExonTrapping	This manuscript	N/A
pCMV6-CD28_c.52+5A>G-ExonTrapping	This manuscript	N/A
Software and algorithms		
Cell Ranger	10X Genomics	v5.0.1
DoubletFinder	McGinnis et al., 2019	v2.0.3
Seurat R package	Stuart et al., 2019	V4.0.0
Uniform Manifold Approximation and Projection (UMAP)	Becht et al., 2018	v.0.3.5
MAST	Finak et al., 2015	v1.16.0
BWA	Li and Durbin, 2010	https://github.com/lh3/bwa
RSeQC	Wang et al., 2012	http://rseqc.sourceforge.net
DESeq2	Love et al., 2014)	https://bioconductor.org/packages/release/bioc/html/DESeq2.html
HPVDetector	Chandrani et al., 2015	N/A
HTSeq	Anders et al., 2015	https://github.com/htseq/htseq
IGV	Robinson et al., 2011	https://software.broadinstitute.org/software/igv/
R	The R Project for Statistical Computing	https://www.r-project.org
STAR aligner	Dobin et al., 2013	https://github.com/alexdobin/STAR
VarScan	Koboldt et al., 2012	http://dkoboldt.github.io/varscan/
Fiji Software	Schindelin et al., 2012	https://fiji.sc/
ImmunoSEQ ANALYZER	Adaptive Biotechnologies	http://clients.adaptivebiotech.com/login
ComplexHeatmap	Gu et al., 2016	http://www.bioconductor.org/packages/devel/bioc/html/ComplexHeatmap.html
phip-stat	Mohan et al., 2019	https://github.com/lasersonlab/phip-stat
Bowtie for alignment of PhIP-Seq raw reads	Mohan et al., 2019	http://bowtie-bio.sourceforge.net/index.shtml
MERLIN 1.1.2 software	Abecasis et al., 2002	http://csg.sph.umich.edu/abecasis/merlin/download/
GATK HaplotypeCaller	McKenna et al., 2010	https://www.broadinstitute.org/gatk

REAGENT or RESOURCE	SOURCE	IDENTIFIER
SAMtools	Li et al., 2009	http://samtools.sourceforge.net/
Picard	http://broadinstitute.github.io/picard/	http://broadinstitute.github.io/picard/
Alamut Visual 2.15	https://www.interactive-biosoftware.com/alamut-visual/	N/A
BioRender	https://biorender.com/	N/A